A Study of Asymptotic Behaviour in the Truncated Conformal Space Approach

Dermot Mc Ateer

Submitted for the degree of
Doctor of Philosophy

Heriot-Watt University

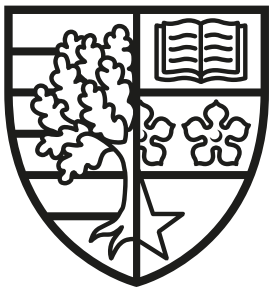

Department of Mathematics,
School of Mathematical and Computer Sciences.

February, 2020

Abstract

The Truncated Conformal Space Approach (TCSA) is a numerical technique for calculating the spectrum of Hamiltonian operators in Quantum Field Theory which are described as perturbations of Conformal Field Theories. The truncation errors of the method have been systematically studied near the UV fixed point (when the characteristic energy related to the coupling is less than the truncation cut-off) where a good theoretical understanding has been achieved. However, numerically the method has also demonstrated a good agreement with other results for much larger values of the coupling, when the RG flow approaches a new fixed point in the infrared. We investigate this regime for a number of boundary RG flows, testing the leading exponent and truncation errors.

We study the 'flows beyond' the first fixed point which have been observed numerically but yet lack a theoretical understanding. We show that while in some models such flows approximate reversed physical RG flows, in others, the spectrum approaches a stable regime that does not correspond to any local boundary condition. In certain examples, multiple fixed points are passed as we increase the coupling.

We consider perturbations by irrelevant operators in an effort to control the qualitative behaviour of these flows and offer an explanation for their origin.

Furthermore we find that in general the flows beyond the first fixed point are very sensitive to modifications of the truncation scheme. We consider modified truncation schemes both within and outwith the Truncated Conformal Space Approach to investigate these effects.

For family and friends.

"Curiouser and curiouser!"
Alice in Wonderland,
Lewis Carroll.

"It would be so nice if something made sense for a change."

Alice in Wonderland,

Lewis Carroll.

Acknowledgements

I'd like to thank my supervisor, Anatoly Konechny, for introducing me to a wonderfully rich and interesting area of physics, for tirelessly and patiently answering all of my questions and for supporting me and providing encouragement when things became 'non-linear'. His enthusiasm for physics is infectious. I have learned an incredible amount from him over these past few years. I am also indebted to him for his extensive feedback on this thesis.

Thank you to those that helped with the proof reeding; Calum and Iain for their critiques of the early chapters; Dad, Matt, Mary and Philipp for reviews of many sections throughout. The blame for all remaining typos lies squarely on your shoulders[1].

I'd like to thank my parents who have always supported me and have always fostered in me an eagerness to learn. Much to the detriment of their own stress levels, I am inspired by them to look for new and exciting challenges.

My friends, who support me through everything, thank you (III).

To my fellow PhD students, thank you for making my studies so enjoyable, filled with interesting conversations in physics, politics and thankfully, a lot of sport.

Thank you to Artisan roast, who's delicious coffee and lack of wi-fi ensured that this thesis didn't take another ten years to write.

Finally, Mary, my love, who left a job and moved city to have an adventure. You'll never quite know what that meant to me. A life lived like this can only be a rich one. Thank you for your continued love and support through everything. This process has not always been easy. I'm incredibly lucky to have you by my side through it all.

[1]Including the one in this paragraph.

Research Thesis Submission

Please note this form should be bound into the submitted thesis.

Name*:*	Dermot Mc Ateer		
School:	MACS		
Version: *(i.e. First, Resubmission, Final)*	First	Degree Sought:	PhD

Declaration

In accordance with the appropriate regulations I hereby submit my thesis and I declare that:

1. The thesis embodies the results of my own work and has been composed by myself
2. Where appropriate, I have made acknowledgement of the work of others
3. The thesis is the correct version for submission and is the same version as any electronic versions submitted*.
4. My thesis for the award referred to, deposited in the Heriot-Watt University Library, should be made available for loan or photocopying and be available via the Institutional Repository, subject to such conditions as the Librarian may require
5. I understand that as a student of the University I am required to abide by the Regulations of the University and to conform to its discipline.
6. I confirm that the thesis has been verified against plagiarism via an approved plagiarism detection application e.g. Turnitin.

ONLY for submissions including published works

Please note you are only required to complete the Inclusion of Published Works Form (page 2) if your thesis contains published works)

7. Where the thesis contains published outputs under Regulation 6 (9.1.2) or Regulation 43 (9) these are accompanied by a critical review which accurately describes my contribution to the research and, for multi-author outputs, a signed declaration indicating the contribution of each author (complete)
8. Inclusion of published outputs under Regulation 6 (9.1.2) or Regulation 43 (9) shall not constitute plagiarism.

* *Please note that it is the responsibility of the candidate to ensure that the correct version of the thesis is submitted.*

Signature of Candidate*:*		Date:	

Submission

Submitted By *(name in capitals):*	DERMOT MC ATEER
Signature of Individual Submitting:	
Date Submitted:	

For Completion in the Student Service Centre (SSC)

Limited Access	Requested	Yes		No		Approved	Yes		No	
E-thesis Submitted ***(mandatory for final theses)***										
Received in the SSC by *(name in capitals):*						Date:				

Inclusion of Published Works

Please note you are only required to complete the Inclusion of Published Works Form if your thesis contains published works under Regulation 6 (9.1.2)

Declaration

This thesis contains one or more multi-author published works. In accordance with Regulation 6 (9.1.2) I hereby declare that the contributions of each author to these publications is as follows:

Citation details	Konechny, A. & McAteer, D. J. High Energ. Phys. (2019) 2019: 44. https://doi.org/10.1007/JHEP09(2019)044
Anatoly Konechny	Contributed an equal share of the ideas, writing, and proof-reading.
Dermot Mc Ateer	Contributed an equal share of the ideas, writing, and proof-reading.
Signature:	
Date:	

Please included additional citations as required.

Contents

Chapter 1

Introduction

Symmetry has always been a powerful and central tool in the study of the physical world. Ancient civilisations built theories of the cosmos around the 'perfect' geometry of the circle whilst modern mathematicians and physicists are driven by a notion of beauty in their search for understanding. Indeed, using symmetry to simplify a difficult problem may seem an obvious route towards progress. However, in the 20th Century, in particular, the role of symmetry became elevated, almost, to the level of principle. This is largely due to Emmy Noether [1],[2] whose contribution to modern theoretical and mathematical physics is still grossly unheralded outside of academic circles. Noether's theorem relating continuous symmetries and conserved quantities placed the study of symmetry at the centre of efforts in theoretical physics for the last century and a wealth of success has resulted in this approach: we can think of our best descriptions of the fundamental particle interactions in which gauge symmetry plays a central role or the unification of the fundamental forces which have historically arisen when some (usually broken) symmetry is restored at large enough energies, suggesting that there may indeed be a unified description of physics containing a large symmetry group.

Conformal symmetry has proven to be an incredibly rich hunting ground for mathematicians and physicists alike, combining a variety of interesting mathematical ideas with a wide range of applicability in describing physical phenomena. Indeed, Conformal Field Theory has been successful in describing a large array of physics with applications in Statistical Physics, Condensed Matter, String Theory and more

recently, via the AdS/CFT conjecture.

Conformal Field Theory really comes into its own in two dimensions, where the local symmetry algebra is infinite placing many restrictions on the theory. Here it is used to describe critical phenomena and is important in the theory of second order phase transitions. An important development in describing such phenomena was the discovery of universality (see for example [3], [4] and [5]): many different physical systems are described by the same critical point. At these critical points, knowledge of the underlying microscopic behaviour of the system is somehow forgotten by nature and the large scale behaviour is not dependent on the microscopic description. This is an incredibly powerful statement and the type of simplification that theoretical physicists dream of. If two systems are described by the same critical point, then they belong to the same *universality class*. Can CFT be used to classify all universality classes of two-dimensional critical systems?

Any overview of CFT would be remiss if they did not mention the seminal paper of Belavin, Polyakov and Zamolodchikov [6] which laid the foundations for much of the modern study of the subject. Here, the authors combined the representation theory of the Virasoro Algebra, defined by Kac [7] and Feigin and Fuchs [8] with a local operator algebra and constructed a class of exactly solvable Conformal Field Theories, the famous *minimal models*. (The representation theory These minimal models were subsequently identified with various two dimensional statistical models and their critical points. That Conformal Field Theories may be exactly solvable realisations of Quantum Field Theory is an incredibly important point as finding solutions to strongly coupled Quantum Field Theories is a notoriously difficult problem. Often-times, these exact solutions exist with little or no knowledge of a Hamiltonian or a Lagrangian providing an alternative route into study which is not available in more general Quantum Field Theories. The underlying principle of this approach is the *bootstrap* hypothesis (see [9], [10] and [6] ,[11] for application to Conformal Field Theory) where physicists try to solve a CFT using only the symmetries of the theory itself, without perturbation theory or other tools, using instead, the associativity of the operator algebra of local fields. In recent years, this method

has had tremendous success, for example, in calculating the most precise numerical estimations of scaling dimensions of primary operators in the three dimensional Ising model [31]. This is particularly impressive as other numerical methods such as Monte Carlo simulations have been used for decades whilst this bootstrap approach has only been implemented relatively recently.

Indeed, numeric approaches have had success elsewhere in Quantum Field Theory in recent years. Hamiltonian Truncation, and the Truncated Conformal Space Approach in particular have had great success in studying Renormalisation Group flows from conformal fixed points. Introduced by Yurov and Zamolodchikov in their seminal work [42] (see [61] and references therein for a review of the method and applications) TCSA provides a method for analysing the spectrum of perturbed Conformal Field Theories and has the advantage over other methods of being light on resources. It is possible to run a TCSA programme and achieve accurate results on any standard laptop. However, whilst TCSA has proven to be successful, outside of the weak coupling limit there is little understanding as to why it works well. Understanding the TCSA spectrum at strong coupling may contribute to our understanding of strong coupling physics and improve our 'tool-kit' for tackling problems in this regime.

Should the reader still needed convincing, another reason for studying CFT is the view that a general Quantum Field Theory may be considered as a conformal fixed point of an RG Flow, plus a perturbing direction. In other words, understanding Conformal Field Theory and renormalisation theory ([12], [13], [14], [15], [16], [17]) amounts to understanding Quantum Field Theory more fully. Being able to probe the Renormalisation Group using CFT and associated analytic and numeric techniques is of great benefit. Indeed, the Renormalisation Group and effective field theory descriptions of physics are active fields of research. Conformal Field Theories are fixed points in the Renormalisation Group flow [30], thus punctuating theory space, providing points of reference from which physicists may gain sure footing in their explorations of physical phenomena. Conformal Field Theory can then help to answer questions such as 'what is the space of QFTs or CFTs?' and 'can we fully map out this theory space?' The Truncated Conformal Space Approach allows us

to analyse not just these conformal fixed points, but the entire RG flow.

The thesis is laid out as follows. Chapter 2 contains an overview of some relevant theory for the work contained in future chapters. Working predominantly in two dimensions, we introduce the main ideas of Conformal Field Theory and boundary Conformal Field Theory. We briefly introduce the Ising and tricritical Ising models in which the main work of this thesis is carried out and discuss the Renormalisation Group including the Hamiltonian approach to renormalisation.

In chapter 3 the Truncated Conformal Space Approach is introduced. A detailed algorithm is constructed here with some technical notes on its implementation. To build a working programme for TCSA, one needs to build a basis of states and calculate the matrix elements of the perturbed Hamiltonian. We detail explicitly how such a programme may be constructed and provide some general guidance on its implementation, including some helpful tips on optimisation.

In chapter 4, we discuss some generalities of the large coupling regime of the TCSA spectrum, setting out our theoretical expectations for its asymptotic behaviour. We lay the analytic groundwork for much of what follows in the subsequent chapters. In particular, the behaviour of the spectrum around the IR fixed point is discussed where we consider both the approach to the fixed point and describe a mechanism which subsequently drives the RG flow away from this point. Both these features will be considered in greater detail in chapters 5 and 6.

In chapter 5 we present the first application of the preceding work. The perturbed boundary Ising and tricritical Ising models are introduced in detail. We use a free fermion description for the Ising model and in the absence of such a description in the tricritical Ising model, the Virasoro algebra is used. We analyse the RG flow on approach to the infrared fixed point determining the exponent corresponding to the leading irrelevant operator along which this approach occurs, in line with our theoretical expectations as set out in chapter 4.

In chapter 6, we investigate the 'flows beyond' the IR fixed point. In TCSA the IR fixed point is reached at finite coupling. Extending the coupling beyond this, the spectrum remarkably rearranges itself again to approximate that of another fixed point. We study these flows, testing the theoretical explanation provided in chapter 4. Understanding this asymptotic behaviour is an intriguing problem: even the 'simplest' of examples of these flows is curious. For the boundary magnetic field perturbation of the Ising model, we find an example flow beyond that seems to violate locality.

There are examples where this pattern of rearrangement continues, resulting in a sequence of flows beyond. However, this sequence does not repeat ad infinitum: it always has a definitive endpoint. We investigate this by considering irrelevant perturbations of IR fixed points in an effort to control the qualitative behaviour of the flow beyond and to produce a 'no flow' situation which may correspond to the end of a sequence of flows arriving from the UV.

Of course, the flows, being unphysical, are an artefact of the truncation. Finally then, we study how different truncation schemes may affect them. We present analytic solutions to two models in a mode truncation scheme and consider modified truncation schemes with TCSA in an effort to gain further understanding into truncation effects and IR regularisation schemes.

We present our conclusions and some closing remarks in chapter 7.

Chapter 2

Introductory Material

In this chapter, we present a brief overview of some foundational subjects relevant for this thesis. We begin with an introduction to Conformal Field Theory (CFT) and boundary Conformal Field Theory (BCFT). A full review of these subjects is beyond the scope of this thesis. Also, there exist many excellent reviews in the literature of which a small selection are listed here:

- *Conformal Field Theory*, P. di Francesco and D. Sénéchal [18]: The 'Yellow book' covers an astonishing amount of ground, introducing the foundational theory and some more advanced applications. It has become the de facto reference for the material.
- *Applied Conformal Field Theory*, P. Ginsparg [22]: An excellent and clear introduction to the subject covering the foundational theory with some applications to statistical models.
- *Conformal Invariance And Statistical Mechanics*, J.L. Cardy [23]. A brief introduction to CFT covering some of the main ideas of boundary CFT from one of the masters of the subject.
- *Lectures on CFT*, J.Qualls [24]. A very readable introduction to the subject which includes some more modern ideas including an introduction to the bootstrap approach.

We discuss the models which we will work with in this thesis: the Ising and tricritical Ising models. We introduce the unperturbed Quantum Field Theory (QFT) descriptions leaving a more detailed presentation of the perturbed models until later in chapters 5 and 6.

The final idea we introduce is that of the Renormalisation Group (RG) and the Renormalisation Group flow. We discuss the space of field theories, conformal fixed points and briefly outline the renormalisation procedure, introducing the beta function of the coupling and discussing the Schrieffer-Wolff method in the Hamiltonian picture.

2.1 Conformal Field Theory

2.1.1 Conformal invariance in d-dimensions

As with many good stories in physics, we start with the spacetime metric tensor, $g_{\mu\nu}(x)$, in d-dimensions. We will assume that our metric is Euclidean unless we state otherwise. The conformal transformations that we study are those coordinate transformations which leave the metric invariant up to a scale:

$$g_{\mu\nu}(x) \to g'_{\mu\nu}(x') = \Omega(x) g_{\mu\nu}(x). \tag{2.1}$$

The group of such conformal transformations are those that preserve angles but not necessarily lengths of two arbitrary curves which cross each other at some point. It contains the Poincaré group along with dilatations and special conformal transformations. Consider an infinitesimal coordinate transformation in d dimensions, of the form

$$x'^{\mu} = x^{\mu} + \epsilon^{\mu}(x) + \mathcal{O}(\epsilon^2) \tag{2.2}$$

where $\epsilon \ll 1$. Such a transformation is conformal if it satisfies condition (2.1) which is true provided the following relation is satisfied:

$$\partial_\mu \epsilon_\nu + \partial_\nu \epsilon_\mu = \frac{2}{d}(\partial \cdot \epsilon) g_{\mu\nu} \tag{2.3}$$

where $\partial \cdot \epsilon = \partial^\mu \epsilon_\mu$.

We assume, for simplicity that the metric $g_{\mu\nu} = \eta_{\mu\nu}$ where $\eta_{\mu\nu}$ is the flat Euclidean metric.

From equation (2.3), we can derive the explicit form of a conformal transformation:

$$\epsilon_\mu = a_\mu + b_{\mu\nu}x^\nu + c_{\mu\nu\rho}x^\nu x^\rho \tag{2.4}$$

where $c_{\mu\nu\rho}$ is symmetric in the last two indices.

The constant term in equation (2.4) is unconstrained by equation (2.3). It describes infinitesimal translations of the form (c.f. equation (2.2)) $x'^\mu = x^\mu + a^\mu$ for which the generator is the momentum operator $P_\mu = -i\partial_\mu$.
In order to study constraints on the linear term, we substitute (2.4) into (2.3) to find

$$b_{\mu\nu} + b_{\nu\mu} = \frac{2}{d}(\eta^{\rho\sigma}b_{\rho\sigma})\eta_{\mu\nu}. \tag{2.5}$$

From this, we see that $b_{\mu\nu}$ may be split into symmetric and anti-symmetric parts:

$$b_{\mu\nu} = \alpha\eta_{\mu\nu} + m_{\mu\nu} \tag{2.6}$$

where $m_{\mu\nu} = -m_{\nu\mu}$. The symmetric term describes infintesimal scale transformations $x'^\mu = (1+\alpha)x^\mu$ with generator $D = -ix^\mu\partial_\mu$ whilst the anti-symmetric part describes infinitesimal rotations $x'^\mu = (\delta^\mu_\nu + m^\mu_\nu)x^\nu$ with generator $L_{\mu\nu} = i(x_\mu\partial_\nu - x_\nu\partial_\mu)$, the angular momentum operator.

Finally, we may consider the quadratic term in (2.4). Before proceeding, we need to look at equation (2.3) again. By applying an additional derivative ∂_ρ and permuting indices we obtain the following equations:

$$\begin{aligned}
\partial_\rho\partial_\mu\epsilon_\nu + \partial_\rho\partial_\nu\epsilon_\mu &= \frac{2}{d}\eta_{\mu\nu}\partial_\rho(\partial\cdot\epsilon) \\
\partial_\nu\partial_\rho\epsilon_\mu + \partial_\mu\partial_\rho\epsilon_\nu &= \frac{2}{d}\eta_{\rho\mu}\partial_\nu(\partial\cdot\epsilon) \\
\partial_\mu\partial_\nu\epsilon_\rho + \partial_\nu\partial_\mu\epsilon_\rho &= \frac{2}{d}\eta_{\nu\rho}\partial_\mu(\partial\cdot\epsilon)
\end{aligned} \tag{2.7}$$

Taking the sum of the last two equations and subtracting the first equation from this we get the following

$$2\partial_\mu\partial_\nu\epsilon_\rho = \frac{2}{d}(-\eta_{\mu\nu}\partial_\rho + \eta_{\rho\mu}\partial_\nu + \eta_{\nu\rho}\partial_\mu)(\partial\cdot\epsilon). \tag{2.8}$$

We may now substitute (2.4) into (2.8) which yields

$$c_{\mu\nu\rho} = \eta_{\mu\rho}b_\nu + \eta_{\mu\nu}b_\rho - \eta_{\nu\rho}b_\mu \qquad \text{where} \qquad b_\mu = \frac{1}{d}c^\rho_{\rho\mu}. \tag{2.9}$$

The resulting transformation is the *Special Conformal Transformation (SCT)* $x'^\mu = x^\mu + 2(x\cdot b)x^\mu - (x^2)b^\mu$ which has the generator $K_\mu = -i(2x_\mu x^\nu\partial_\nu - (x^2)\partial_\mu)$.

The finite transformations contained in (2.4) and their associated generators are:

$$\begin{aligned}
&\text{Translations: } x'^\mu = x^\mu + a^\mu && \text{Generator: } P_\mu = -i\partial_\mu,\\
&\text{Rotations: } x'^\mu = \omega^\mu_\nu x^\nu && \text{Generator: } L_{\mu\nu} = i(x_\mu\partial_\nu - x_\nu\partial_\mu),\\
&\text{Dilations: } x'^\mu = \lambda x^\mu && \text{Generator: } D = -ix^\mu\partial_\mu,\\
&\text{SCT: } x'^\mu = \frac{x^\mu - b^\mu x^2}{1 - 2\vec{b}\cdot\vec{x} + b^2x^2} && \text{Generator: } K_\mu = -i(2x_\mu x^\nu\partial_\nu - x^2\partial_\mu).
\end{aligned} \tag{2.10}$$

Details of how these arise from $a_\mu, b_{\mu\nu}$ and $c_{\mu\nu\rho}$ may be found in [18]. The Poincaré group and the dilations form a subgroup of this full d-dimensional group meaning that a theory invariant under these transformations is not necessarily invariant under the special conformal transformations. The generators obey the commutation rules below, defining the conformal algebra.

$$
\begin{aligned}
[D, P_\mu] &= iP_\mu \\
[D, K_\mu] &= -iK_\mu \\
[K_\mu, P_\nu] &= 2i(\eta_{\mu\nu} D - L_{\mu\nu}) \\
[K_\rho, L_{\mu\nu}] &= i(\eta_{\rho\mu} K_\nu - \eta_{\rho\nu} K_\mu) \\
[P_\rho, L_{\mu\nu}] &= i(\eta_{\rho\mu} P_\nu - \eta_{\rho\nu} P_\mu) \\
[L_{\mu\nu}, L_{\rho\sigma}] &= i(\eta_{\nu\rho} L_{\mu\sigma} + \eta_{\mu\sigma} L_{\nu\rho} - \eta_{\mu\rho} L_{\nu\sigma} - \eta_{\nu\sigma} L_{\mu\rho})
\end{aligned}
\tag{2.11}
$$

The conformal group in d-dimensions is isomorphic to SO(d+1,1) with 1/2(d+2)(d+1) parameters [18].

2.1.2 Two-dimensional conformal invariance

The power of conformal invariance really comes into its own in two dimensions. Looking again at the condition for an arbitrary transformation to be conformal, (2.3), we see that in 2d it takes a special form, namely, that of the Cauchy-Riemann equations

$$\partial_1 \epsilon_1 = \partial_2 \epsilon_2, \qquad \partial_1 \epsilon_2 = -\partial_2 \epsilon_1. \tag{2.12}$$

This means that we have the full power of complex analysis at our disposal in two dimensions. We therefore identify two dimensional Cartesian space with the complex plane in the usual way, defining coordinates

$$z = x + iy, \qquad \bar{z} = x - iy. \tag{2.13}$$

Equation (2.12) implies that the 2d conformal transformations can be identified with analytic coordinate transformations

$$z \to f(z), \qquad \bar{z} \to \bar{f}(\bar{z}), \qquad f'(z) \neq 0. \tag{2.14}$$

We choose a basis for the infinitesimal conformal transformations $z \to \tilde{z} =$

$z + \epsilon(z)$ (and similarly for $\bar{z}$) to be

$$z \to z - a_n z^{n+1}, \qquad \bar{z} \to \bar{z} - \bar{a}_n \bar{z}^{n+1} \tag{2.15}$$

where $n \in \mathbb{Z}$. These are generated by the operators

$$l_n = -z^{n+1}\frac{d}{dz}, \qquad \bar{l}_n = -\bar{z}^{n+1}\frac{d}{d\bar{z}} \tag{2.16}$$

satisfying the algebra

$$\begin{gathered}[l_n, l_m] = (n-m)l_{n+m}, \qquad [\bar{l}_n, \bar{l}_m] = (n-m)\bar{l}_{n+m}, \\ \text{with } [l_n, \bar{l}_m] = 0.\end{gathered} \tag{2.17}$$

As l_n and $\bar{l}_m$ commute, the conformal algebra is a direct sum of two isomorphic subalgebras satisfying (2.17). This justifies the use of z and $\bar{z}$ as independent coordinates. For notational convenience, we will frequently discuss only the holomorphic dependence in what follows, dropping the anti-holomorphic contributions.

The conformal algebra is incredibly powerful in the context of 2d CFT where the infinite number of generators $l_n, \bar{l}_m$ place severe restrictions on the theory. The $l_n, \bar{l}_m$'s become the familiar $L_n, \bar{L}_m$'s of Virasoro fame, in a centrally extended algebra, once we take conformal anomalies into account in Quantum Field Theory.
It is important to note that the algebra (2.17) cannot be extended to a globally defined group of transformations[1]. It is a local symmetry algebra. A global well defined group of invertible transformations can be realised with the generators l_{-1}, l_0, l_1 and their anti-holomorphic counterparts, where in particular,

- $l_{-1}, \bar{l}_{-1}$ generate the translations.
- $(l_0 + \bar{l}_0), i(l_0 - \bar{l}_0)$ generate the dilatations and rotatations respectively.
- $l_1, \bar{l}_1$ generate the special conformal transformations.

[1] In Euclidean space, that is. In Minkowski space, an extension to a globally defined group is possible.

The corresponding finite transformations form a group, the complex Möbius group

$$f(z) = \frac{az+b}{cz+d}, \qquad ad-bc=1, \qquad a,b,c,d \in \mathbb{C} \tag{2.18}$$

which is isomorphic to the group $\mathrm{SL}(2,\mathbb{C})/\mathbb{Z}_2$ where the quotient comes from the fact that under a simultaneous sign change in a,b,c,d, the transformation is invariant.

2.1.3 Primary fields

Let's now consider fields $\phi : \mathcal{H} \to \mathcal{H}$, familiar to us from the world of Quantum field theory, which are operator valued distributions acting on some Hilbert space $\mathcal{H}$. When discussing field theory, the standard practice is to construct a suitable basis of states and build the Hilbert space from tensor products of representations built on this basis. We will discuss the structure of the Hilbert space in more detail later, when we have acquired some additional machinery, where we will see that in a Conformal Field Theory equipped with the Virasoro algebra, $\mathcal{H}$ may be decomposed into irreducible representations of $\mathrm{Vir}_c \otimes \overline{\mathrm{Vir}}_c$, the product of left and right movers of the Virasoro algebra with generators $L_n, \bar{L}_n, n \in \mathbb{Z}$. First, though, we consider the transformation properties of such a field under the conformal transformations.

We say that the field $\phi(z,\bar{z})$ has conformal dimensions $(h,\bar{h})$ if, under scaling it transforms as

$$\phi(z,\bar{z}) \to \phi'(z,\bar{z}) = \lambda^h \bar{\lambda}^{\bar{h}} \phi(\lambda z, \bar{\lambda}\bar{z}). \tag{2.19}$$

Such a field is called a primary field of dimension $(h,\bar{h})$ if under a conformal transformation it transforms as

$$\phi(z,\bar{z}) \to \phi'(z,\bar{z}) = \Big(\frac{\partial f}{\partial z}\Big)^h \Big(\frac{\partial \bar{f}}{\partial \bar{z}}\Big)^{\bar{h}} \phi(f(z), \bar{f}(\bar{z})). \tag{2.20}$$

If this transformation holds only for global conformal transformations, then the field is called quasi-primary.

Under the infinitesimal conformal transformation $z \to z + \epsilon(z), \bar{z} \to \bar{z} + \bar{\epsilon}(\bar{z})$, the transformation law (2.20) takes the form

$$\delta_{\epsilon,\bar{\epsilon}}\phi(z,\bar{z}) = ((h\partial\epsilon + \epsilon\partial) + (\bar{h}\bar{\partial}\bar{\epsilon} + \bar{\epsilon}\bar{\partial}))\phi(z,\bar{z}) \tag{2.21}$$

where $\partial = \partial_z, \bar{\partial} = \partial_{\bar{z}}$.

2.1.4 The stress-energy tensor

In any Quantum Field Theory, we may define the stress-energy tensor as a measure of the susceptibility of the action to fluctuations in the metric:

$$T^{\mu\nu}(x) = -\frac{2}{g}\frac{\delta S}{\delta g_{\mu\nu}(x)}. \tag{2.22}$$

Of course, calculation of the above requires knowledge of the action in the first place. In a conformal field theory, however, we may make use of the large number of restrictions that conformal invariance places on the theory. Using the bootstrap approach, it may be possible to completely determine the fundamental data of a CFT (the spectrum of operators and their correlation functions) using only the symmetries of the theory, with no knowledge of this action.

What can we say about the stress-energy tensor from conformal invariance alone? On a Euclidean plane with metric $ds^2 = dzd\bar{z}$, conservation of the stress-energy tensor, $\partial^\mu T_{\mu\nu}$, takes the following form:

$$\begin{aligned} \partial_{\bar{z}}T_{zz} + \partial_z T_{\bar{z}z} = 0, \\ \partial_z T_{\bar{z}\bar{z}} + \partial_{\bar{z}} T_{z\bar{z}} = 0. \end{aligned} \tag{2.23}$$

On top of this, we have the scale invariance or traceless condition $T^\mu_\mu = 0$ [2], giving

$$T_{z\bar{z}} = T_{\bar{z}z} = 0. \tag{2.24}$$

Therefore, the stress-energy tensor splits into distinct holomorphic and anti-holomorphic parts

$$T(z) = T_{zz}, \qquad \bar{T}(\bar{z}) = T_{\bar{z}\bar{z}} \tag{2.25}$$

[2] See [18] for details on how this traceless condition arises from conservation of the current associated to global scale invariance of T.

where in Euclidean coordinates, these are related by complex conjugation. In Minkowski space, they correspond to left and right moving modes and are truly decoupled.

We may define a mode expansion for T(z) as the Laurent expansion

$$L_n = \int \frac{dz}{2\pi i} z^{n+1} T(z), \tag{2.26}$$

where the contour encircles the origin. Cauchy's theorem allows us to write the holomorphic stress tensor as

$$T(z) = \sum_{n\in\mathbb{Z}} z^{-n-2} L_n, \tag{2.27}$$

where we have a similar definition for $\bar{L}_n$ and $\bar{T}(\bar{z})$.

2.1.5 Radial quantisation

Consider the infinite cylinder with coordinates $w = \tau + i\sigma, \bar{w} = \tau - i\sigma$ and identify σ with $\sigma + 2\pi$ where τ and σ represent Euclidean time and space coordinates respectively. The conformal map from the cylinder to the plane is[3]:

$$z = \exp(\tau + i\sigma). \tag{2.28}$$

Past infinity is mapped to the point z=0 on the plane and future infinity on the cylinder is mapped to the point z=∞. Equal time surfaces are mapped to concentric circles on the plane. The dilatation operator generates translations in the radial time direction and as such acts as the Hamiltonian of the system. The dynamics are described by the operator equation of motion

$$\frac{d\Phi}{d\tau} = [H, \Phi]. \tag{2.29}$$

[3]For a general cylinder of circumference R, the map is $z = \exp(2\pi w/R)$.

where Φ is some field operator of the theory. We can write this infinitesimally as

$$\delta_\lambda \Phi = [\lambda H, \Phi] \qquad \text{where } H = \int \frac{dz}{2\pi i} zT(z) = L_0. \tag{2.30}$$

H is the charge associated with the scaling current zT(z) arising from the dilatation transformation with parameter $\epsilon(z) = \lambda z$. If we want to write a similar transformation law for a general conformal transformation, one should use

$$T_\epsilon = \int \frac{dz}{2\pi i} \epsilon(z) T(z). \tag{2.31}$$

Inserting this into a commutator as above, we get the general transformation law

$$\delta_{\epsilon,\bar{\epsilon}} \Phi(w, \bar{w}) = \frac{1}{2\pi i} \int_{\mathcal{C}} [dz \epsilon(z) T(z), \Phi(w, \bar{w})] + [d\bar{z}\bar{\epsilon}(\bar{z})\bar{T}(\bar{z}), \Phi(w, \bar{w})]. \tag{2.32}$$

There is some ambiguity here as we have to determine whether w and $\bar{w}$ are inside the contour $\mathcal{C}$. We will return to this expression later in section 2.1.7 once we have introduced the operator product expansion and address this ambiguity.

2.1.6 Correlation functions

In two dimensions, conformal symmetry places a large set of restrictions on the form of the correlation functions. Invariance under translations requires that the two point function of two holomorphic quasi-primary fields is of the form:

$$\langle \phi(z_1)\phi(z_2) \rangle = G(z_1, z_2) \sim g(z_1 - z_2). \tag{2.33}$$

Invariance under dilatations implies that

$$g(z_1, z_2) = \frac{C_{12}}{(z_1 - z_2)^{h_1 + h_2}} \tag{2.34}$$

where the constant C_{12} can be fixed by normalising the fields. Finally, invariance under the inversions adds a restriction on the conformal weights: $h_1 = h_2 = h$.
The two-point function of two arbitrary quasi-primary fields is therefore restricted

to be of the following form[4]

$$< \phi_1(z_1, \bar{z}_1)\phi_2(z_2, \bar{z}_2) >= \frac{C_{12}}{(z_1 - z_2)^{2h}(\bar{z}_1 - \bar{z}_2)^{2\bar{h}}} \tag{2.35}$$

which is zero if the conditions $h_1 = h_2 = h, \bar{h}_1 = \bar{h}_2 = \bar{h}$ are not satisfied.

Similarly, the form of the three point function is restricted to be of the form

$$< \phi_1(z_1, \bar{z}_1)\phi_2(z_2, \bar{z}_2)\phi_3(z_3, \bar{z}_3) >= \frac{C_{123}}{z_{12}^{h_{123}} z_{23}^{h_{231}} z_{13}^{h_{312}}} . \frac{1}{\bar{z}_{12}^{\bar{h}_{123}} \bar{z}_{23}^{\bar{h}_{231}} \bar{z}_{13}^{\bar{h}_{312}}} . \tag{2.36}$$

where $z_{ij} = z_i - z_j$, $h_{ijk} = h_i + h_j - h_k$ and similarly for $\bar{z}_{ij}$ and $\bar{h}_{ijk}$. Again, C_{123} is some constant which may be fixed by normalisation of the fields. However, these constants are non-trivial. They carry dynamical information about the operator algebra of the CFT and may be related to the structure constants which we will discuss in Chapter 5.

Unfortunately, correlation functions for four or more fields are not so simple and they can not be restricted so completely. However, conformal invariance means that we can write an arbitrary four point (and hence n-point via the OPE) function in terms of the two and three point functions but it will in general be some function of the cross ratio

$$\eta = \frac{z_{12} z_{34}}{z_{13} z_{24}} . \tag{2.37}$$

The transformations (2.18) involve three independent complex parameters. It is, therefore, always possible to conformally map three points z_1, z_2, z_3 to any points of our choosing. The best we can do then is to take, say $z_1, z_2, z_3, z_4 = \infty, 1, \eta, 0$ and the four point function will have a general dependence on the cross ratio [18], taking the form

$$G_{34}^{21}(\eta, \bar{\eta}) = \lim_{z_1, \bar{z}_1 \to \infty} z_1^{2h_1} \bar{z}_1^{2\bar{h}_1} \langle \phi_1(z_1, \bar{z}_1)\phi_2(1,1)\phi_3(\eta, \bar{\eta})\phi_4(0,0) \rangle \tag{2.38}$$

[4]See, [20] for more details.

where we have defined

$$G_{34}^{21}(\eta,\bar{\eta}) = \langle h_1, \bar{h}_1 |\, \phi_2(1,1)\phi_3(\eta,\bar{\eta})\, | h_4, \bar{h}_4 \rangle \tag{2.39}$$

It can be shown[5] that G_{34}^{21} may be written in terms of analytic functions (and their anti-analytic counterparts) known as *conformal blocks*.

$$G_{34}^{21}(\eta,\bar{\eta}) = \sum_p C_{p34} C_{p12} \mathcal{F}_{34}^{21}(p|\eta) \bar{\mathcal{F}}_{34}^{21}(p|\bar{\eta}) \tag{2.40}$$

Conformal blocks are important in modern applications of CFT, particularly in the Conformal Bootstrap where a symmetry relation between them is used to solve the theory. We use them only indirectly as part of a concrete method for calculating the so-called *fusion matrices* in chapter 5 and so leave a fuller discussion for another time.

2.1.7 The operator product expansion

We return our attention now to the general conformal transformation (2.32). In order to be understood formally, we need to address the ordering ambiguity in the operator product. This is nothing other than the usual ordering ambiguity that we are familiar with in Quantum Field Theory, which is circumvented using Schwinger's time ordering prescription. Here, with states radially ordered and constant time surfaces corresponding to concentric circles, we introduce a radial ordering on the product:

$$\begin{aligned} \mathcal{R}(A(z)B(w)) &= A(z)B(w), \qquad \text{if } |z| > |w| \\ \mathcal{R}(A(z)B(w)) &= \pm B(w)A(z), \qquad \text{if } |z| < |w| \end{aligned} \tag{2.41}$$

[5] For a more detailed presentation of the conformal blocks see, for example,[18].

where the negative sign in the second equation is only used when both A and B are fermionic operators. This allows us to write (2.32) as

$$\begin{aligned}\delta_{\epsilon,\bar{\epsilon}}\Phi(w,\bar{w}) &= [T_\epsilon(z),\Phi(w,\bar{w})] + \text{anti-chiral term} \\ &= \Big(\int_{|z|>|w|} - \int_{|z|<|w|}\Big)\frac{dz}{2\pi i}\epsilon(z)\mathcal{R}(T(z)\Phi(w,\bar{w})) + \text{a.c term} \\ &= \int_{\mathcal{C}(w)}\frac{dz}{2\pi i}\epsilon(z)\mathcal{R}(T(z)\Phi(w,\bar{w})) + \text{a.c term}\end{aligned} \tag{2.42}$$

where now the contour encircles the point w in the z-plane as shown in figure 2.1.

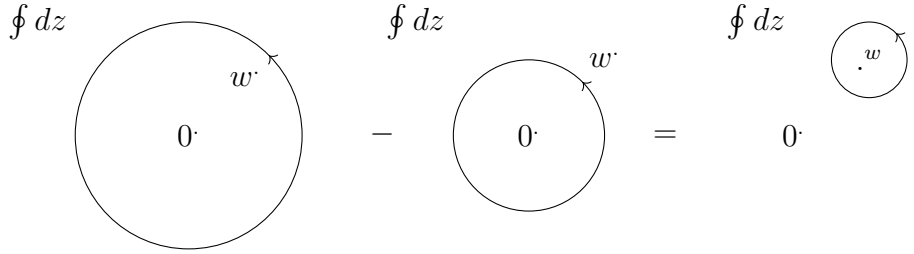

Figure 2.1: Evaluation of the contour integral for radially ordered products of operators.

The integral is only non-vanishing if there is a singularity in the operator product which by Cauchy's residue theorem contributes a value of the residue at the pole. We are led to define the operator product expansion (OPE) which allows us to write the radially ordered product of local fields as a sum over fields and their derivatives. It provides an algebraic product structure on the space of quantum fields. Wilson's general OPE takes the form [32]

$$A(z)B(w) \sim \sum_{\Delta} C_\Delta(z-w)O_\Delta(w) \tag{2.43}$$

where the operators $O_\Delta(w)$ form a complete set and due to translational invariance, the coefficients depend only on the separation of the two operators. Products of the form (2.43) are understood to be valid within the Green's function with other elementary operators of the theory:

$$\lim_{z\to\infty}\big\langle\mathcal{R}\big(A(z)B(w) - \sum_{\Delta} C_\Delta(z-w)O_\Delta(w)\big)\Phi_1(w_1)\cdots\Phi_n(w_n)\big\rangle = 0 \tag{2.44}$$

We can then use (2.32)/(2.42) and (2.21) to construct the OPE of the stress-energy tensor and a primary field. Indeed, equating these two expressions for the variation of a field, we have

$$((h\partial\epsilon + \epsilon\partial) + \text{a.c term})\Phi(w,\bar{w}) = \frac{1}{2\pi i}\int dz\epsilon(z)\mathcal{R}(T(z)\Phi(w,\bar{w})) + \text{a.c term.} \quad (2.45)$$

Using the contour integrals

$$\begin{aligned} h\partial_w\epsilon(w)\Phi(w,\bar{w}) &= \frac{1}{2\pi i}\oint_{\mathcal{C}(w)} dz\ \frac{h\epsilon(z)}{(z-w)^2}\Phi(w,\bar{w}), \\ \epsilon(w)\partial_w\Phi(w,\bar{w}) &= \frac{1}{2\pi i}\oint_{\mathcal{C}(w)} dz\ \frac{\epsilon(z)}{z-w}\partial_w\Phi(w,\bar{w}) \end{aligned} \quad (2.46)$$

we can infer the form of the radial product to be

$$\begin{aligned} \mathcal{R}(T(z)\Phi(w,\bar{w})) = \frac{h}{(z-w)^2}\Phi(w,\bar{w}) + \frac{\partial_w}{(z-w)}\Phi(w,\bar{w}) + \Phi^{(-2)}(w,\bar{w}) \\ + (z-w)\Phi^{(-3)}(w,\bar{w}) + \cdots \end{aligned} \quad (2.47)$$

where the ellipses denote an infinite number of other regular terms. In future, we drop the $\mathcal{R}$ symbol and consider the OPE as shorthand for a radially ordered product. We therefore write the OPE of a primary field of conformal dimension $(h,\bar{h})$ with the stress-energy tensor as

$$\begin{aligned} T(z)\Phi(w,\bar{w}) &= \frac{h}{(z-w)^2}\Phi(w,\bar{w}) + \frac{\partial_w}{(z-w)}\Phi(w,\bar{w}) + \cdots \\ \bar{T}(\bar{z})\Phi(w,\bar{w}) &= \frac{\bar{h}}{(\bar{z}-\bar{w})^2}\Phi(w,\bar{w}) + \frac{\partial_{\bar{w}}}{(\bar{z}-\bar{w})}\Phi(w,\bar{w}) + \cdots \end{aligned} \quad (2.48)$$

The non-singular terms occurring in (2.47) and (2.48) depend on local fields, called descendants. These fields can be defined through integration:

$$\Phi^{(-n)}(w,\bar{w}) = \hat{L}_{-n}(w)\Phi(w,\bar{w}) = \oint_w \frac{dz}{2\pi i}(z-w)^{-n+1}T(z)\Phi(w,\bar{w}). \quad (2.49)$$

The $\hat{L}_n(w)$'s that appear here are the operators which appear in the expansion of

the stress-energy tensor (2.27), this time, around the point w instead of the origin as was seen previously. In particular, we have

$$\begin{aligned} &\hat{L}_0(z)\Phi(z,\bar{z}) = h\Phi(z,\bar{z}), \qquad \hat{L}_{-1}(z)\Phi(z,\bar{z}) = \partial_z\Phi(z,\bar{z}) \\ &\hat{L}_n(z)\Phi(z,\bar{z}) = 0 \qquad n \geq 1. \end{aligned} \tag{2.50}$$

The argument of the $\hat{L}_n$ operators is always the same as the field it is acting on. It is therefore safe (and common practice) to omit the argument of this operator whilst keeping the argument of the field explicit. We can build an infinite set of such descendant fields by repeated application of the $\hat{L}_{-n}(z)$'s to the primary fields.

We see from expression (2.48) that we may determine the conformal weights $h, \bar{h}$, of a primary field from the OPE with the stress-energy tensor components $T, \bar{T}$, where they appear as the coefficient of the singular $\sim \frac{1}{z^2}$ term. The OPE of the stress tensor with itself is written in shorthand format as

$$T(z)T(w) = \frac{c/2}{(z-w)^4} + \frac{2T(w)}{(z-w)^2} + \frac{\partial_w T(w)}{(z-w)} + \cdots \tag{2.51}$$

where we do not show the regular terms. The stress-energy tensor is a quasi-primary field of weight h=2. The constant term, c, is the central charge or conformal anomaly. We will discuss this in more detail in section (2.1.8).

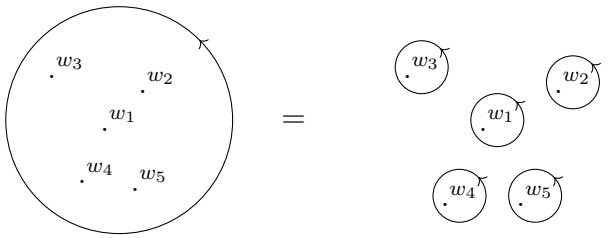

Figure 2.2: Deformation of contour in equation (2.52).

We can put all this together now and consider the correlator of the stress-energy tensor with any number of primary operators, where we deform the contour encircling all operator insertions into a sum of terms with contours encircling single

operator insertions at points w_i as shown in figure 2.2:

$$\begin{aligned}
&\Big\langle \oint_0 \frac{dz}{2\pi i}\epsilon(z)T(z)\Phi_1(w_1)\cdots\Phi_m(w_m)\Big\rangle \\
&= \sum_{j=1}^{m}\Big\langle \Phi_1(w_1)\cdots\Big(\oint_{w_j}\frac{dz}{2\pi i}\epsilon(z)T(z)\Phi_j(w_j)\Big)\cdots\Phi_m(w_m)\Big\rangle \\
&= \sum_{j=1}^{m}\Big\langle \Phi_1(w_1)\cdots\delta_\epsilon\Phi_j(w_j)\cdots\Phi_m(w_m)\Big\rangle. \\
&= \sum_{j=1}^{m}\Big\langle \Phi_1(w_1)\cdots[\epsilon(w_j)\partial + h\partial\epsilon(w_j)]\Phi(w_j)\cdots\Phi_m(w_m)\Big\rangle.
\end{aligned} \tag{2.52}$$

where we have used the known transformation laws of a primary field (2.21) and (2.42). Making use of equations (2.46) and noting that the RHS of the above equation is valid for arbitrary $\epsilon(z)$ and an arbitrary contour, we may now write down the conformal Ward identity:

$$\langle T(z)\Phi_1(w_1)\cdots\Phi_m(w_m)\rangle = \sum_{j=1}^{m}\Big[\frac{h_j}{(z-w_j)^2}+\frac{1}{z-w_j}\frac{\partial}{\partial w_j}\Big]\langle\Phi_1(w_1)\cdots\Phi_m(w_m)\rangle \tag{2.53}$$

From equations (2.53) and (2.49) we can derive an important relation for the correlators of descendant fields with a string of primary fields, thus determining the physical properties of the descendants from the associated primaries. Taking $X = \phi_1(w_1)\cdots\phi_N(w_N)$, we have

$$\begin{aligned}
\langle\Phi^{(-n)}(w)X\rangle &= \frac{1}{2\pi i}\oint_w dz(z-w)^{1-n}\langle T(z)\Phi(w)X\rangle \\
&= -\frac{1}{2\pi i}\oint_{\{w_i\}} dz(z-w)^{1-n}\sum_i\{\frac{1}{z-w_i}\partial_{w_i}\langle\Phi(w)X\rangle + \frac{h_i}{(z-w_i)^2}\langle\Phi(w)X\rangle\} \\
&\equiv \mathcal{L}_{-n}\langle\Phi(w)X\rangle \qquad \text{n } \geq 1,
\end{aligned} \tag{2.54}$$

where we define

$$\mathcal{L}_{-n} = \sum_i\{\frac{(n-1)h_i}{(w_i-w)^n} - \frac{1}{(w_i-w)^{n-1}}\partial_{w_i}\}. \tag{2.55}$$

We have reduced the calculation of correlation functions involving descendant fields to the application of the differential operator, $\mathcal{L}_{-n}$, to a correlation function involving only primary fields.

Of course, there are descendant fields which are more complicated than $\Phi^{(-n)}$, involving a number of Virasoro modes acting on our some state $|h\rangle$. These are defined recursively:

$$\begin{aligned}\Phi^{(-k,-n)}(w) &= (\hat{L}_{-k}\hat{L}_{-n}\Phi)(w) \\ &= \frac{1}{2\pi i}\oint_w dz(z-w)^{1-k}T(z)(\hat{L}_{-n}\Phi)(w).\end{aligned} \tag{2.56}$$

Likewise, we may of course consider correlators such as $\langle\Phi^{(-n)}(z)\Phi^{(-m)}(w)\rangle$ containing more than one descendant. However, the message remains the same: correlation functions involving descendant fields may be reduced to correlation functions of primary fields.

2.1.8 Virasoro algebra and the central charge

By considering the action of successive operators $\hat{L}_n$ to the field Φ [19], we can derive the Virasoro algebra

$$[\hat{L}_n, \hat{L}_m] = (n-m)\hat{L}_{n+m} + \frac{c}{12}n(n^2-1)\delta_{n+m,0} \tag{2.57}$$

Recalling that the operators L_n appearing in the mode expansion of the stress-energy tensor are simply the $\hat{L}_n$ operators at the origin $L_n = \hat{L}_n(0)$, we note that they also obey the Virasoro algebra. The second term is the central extension of the algebra, a term which commutes with all symmetry operators (and in this particular case, all operators in the theory). It is called the central charge of the theory and in some sense measures the number of degrees of freedom of the CFT. It shows up in the OPE of the stress tensor with itself. If we take an infinitesimal version of this OPE, we can look at how the stress tensor transforms under an arbitrary conformal

transformation.

$$\begin{aligned}\delta_\epsilon T(w) = [T_\epsilon, T(w)] &= \oint_w dz\epsilon(z)T(z)T(w) \\ &= [\epsilon(w)\partial_w + 2\partial_w\epsilon(w)]T(w) + \frac{c}{12}\partial_w^3\epsilon(w)\end{aligned} \tag{2.58}$$

which can be integrated to a finite transformation z=f(w) of the form:

$$T(z) \to T'(w) = \Big(\frac{dz}{dw}\Big)^2 T(z) + \frac{c}{12}S(z,w), \tag{2.59}$$

where S(z,w) is the Schwartzian derivative, $S(z,w) = [\partial_w z\partial_w^3 z - \frac{3}{2}(\partial_w^2 z)^2]/(\partial_w z)^2$. Under an arbitrary conformal transformation, the stress tensor picks up an anomalous term proportional to the Schwartzian derivative. Choosing the conformal transformation taking us from the cylinder to the plane, we find the following:

$$T_{\text{cyl}}(z) = z^2 T_{\text{pl}}(z) - c/24. \tag{2.60}$$

Substituting the mode expansion of T we find

$$T_{\text{cyl}}(z) = \sum_{n\in\mathbb{Z}} L_n z^{-n} - c/24 \tag{2.61}$$

and in particular

$$L_0^{\text{cyl}} = L_0^{\text{pl}} - c/24 \tag{2.62}$$

which will be important later when discussing TCSA on the strip. It also allows us to think of the central charge as representing the Casimir energy.

2.1.9 The state operator correspondence and highest weight representations

The conformal ('in'-)vacuum, which we define as $|0\rangle$ is always SL(2,$\mathbb{C}$) invariant. It must therefore be annihilated by the generators of the global conformal group L_{-1}, L_0, L_1 (and their anti-holomorphic counterparts). In fact, there are more con-

straints on the vacuum. In particular

$$L_n \left|0\right\rangle = 0, \qquad \bar{L}_n \left|0\right\rangle = 0, \qquad n \geq -1 \tag{2.63}$$

which also recovers the condition that $T(z),\ \bar{T}(\bar{z})$ are regular as $z, \bar{z} \to 0$ (c.f. eqn (2.27)). The vacuum state may be formally introduced as the insertion of the unit operator at the origin $z,\ \bar{z} = 0$ as this corresponds to the infinite past in the radially quantised picture, as discussed previously. It is then natural to define an asymptotic 'in-state' by applying the operators in the CFT to this vacuum state.

$$\left|A_{\text{in}}\right\rangle = \lim_{z,\bar{z}\to 0} A(z,\bar{z}) \left|0\right\rangle . \tag{2.64}$$

In order to introduce 'out-states', we can naturally define

$$\left\langle A_{\text{out}}\right| = \lim_{w,\bar{w}\to 0} \left\langle 0\right| A'(w,\bar{w}). \tag{2.65}$$

where we have defined the state in a coordinate system where $w \to 0$ corresponds to taking a point at infinity. We now relate A(z,$\bar{z}$) and A$'$(w,$\bar{w}$) via the conformal mapping $w \to z = 1/w$, which takes the point at infinity to the origin, under which, the field A transforms as

$$A'(w,\bar{w}) = (-w^{-2})^h (-\bar{w}^{-2})^{\bar{h}} A(1/w, 1/\bar{w}). \tag{2.66}$$

We may now define the CFT out-states as[6]

$$\left\langle A_{\text{out}}\right| = \lim_{z,\bar{z}\to\infty} \left\langle 0\right| A(z,\bar{z}) z^{2h} \bar{z}^{2\bar{h}}, \tag{2.67}$$

with $\left\langle A_{\text{out}}\right| = \left|A_{\text{in}}\right\rangle^\dagger$, the adjoint operator, defined as[7]

$$A(z,\bar{z})^\dagger = A(\frac{1}{z},\frac{1}{\bar{z}}) \frac{1}{z^{2h}} \frac{1}{\bar{z}^{2\bar{h}}}. \tag{2.68}$$

[6]There is a subtlety here. Writing $w = |w| e^{i\chi}$, the coefficient in (2.66) may be written as $(\frac{1}{|w|^2} e^{-2i\chi + i\pi})^h (\frac{1}{|\bar{w}|^2} e^{2i\chi - i\pi})^{\bar{h}} = (e^{-2i\chi + i\pi})^{(h-\bar{h})}$. Therefore, the out-states are defined as per eqn (2.67) up to a spin dependent phase. In the A-series minimal models that we consider, the primaries are spinless and this subtlety is avoided. This is also the case if the spin is integer or half-integer. In other scenarios however, this needs to be considered.

[7]This is true only for self-conjugate fields. The most general relation would be $A_\alpha(z,\bar{z})^\dagger = C_\alpha^\beta A_\beta(1/z, 1/\bar{z}) z^{-2h} \bar{z}^{-2\bar{h}}$.

The primary states may be defined as the application of the primary fields $\phi(z,\bar{z})$ to the vacuum in the natural way:

$$|h,\bar{h}\rangle = \lim_{z,\bar{z}\to 0} \phi_{h,\bar{h}}(z,\bar{z})\,|0\rangle \tag{2.69}$$

Application of the OPE between T(z) and the primary field ϕ (2.48) demonstrates that the primary states are eigenstates of the Hamiltonian:

$$\begin{aligned}
[L_n, \phi(w,\bar{w})] &= \oint \frac{dz}{2\pi i} z^{n+1} T(z)\phi(w,\bar{w}) \\
&= \oint \frac{dz}{2\pi i} z^{n+1}\Big[\frac{h\phi(w,\bar{w})}{(z-w)^2} + \frac{\partial\phi(w,\bar{w})}{z-w} + \cdots\Big] \\
&= h(n+1)w^n\phi(w,\bar{w}) + w^{n+1}\partial\phi(w,\bar{w})
\end{aligned} \tag{2.70}$$

where the dots represent further regular terms. From this, we see

$$\begin{aligned}
&L_0\,|h,\bar{h}\rangle = h\,|h,\bar{h}\rangle\,, \qquad && \bar{L}_0\,|h,\bar{h}\rangle = \bar{h}\,|h,\bar{h}\rangle\,, \\
&L_n\,|h,\bar{h}\rangle = 0, && \bar{L}_n\,|h,\bar{h}\rangle = 0, \qquad n>0.
\end{aligned} \tag{2.71}$$

These equations define the so-called *highest weight states*. Representations of the Virasoro algebra built on these highest weight states are called Verma modules. Verma modules are characterised by the central charge and the conformal dimensions of the highest weight state upon which it is built. The Virasoro operators, $L_{\pm n}$, act as raising and lowering operators familiar from Quantum Field Theory. Indeed, from the commutator

$$[L_0, L_{-n}] = nL_{-n} \tag{2.72}$$

we see that we can build excited states from $|h\rangle$ by successive application L_{-n}:

$$L_{-k_1}\cdots L_{-k_n}\,|h\rangle \tag{2.73}$$

where we order the modes such that $k_1 \le \cdots \le k_n$. These are the descendant states at level N. The weight of such a state is h+N where N=$k_1 + \cdots k_n$. The descendant

states may also be realised by the application of the descendant fields on the vacuum:

$$L_{-n}\left|h\right\rangle = L_{-n}(\phi(0,0)\left|0\right\rangle) = (\hat{L}_{-n}\phi(0,0))\left|0\right\rangle = \Phi^{(-n)}\left|0\right\rangle . \tag{2.74}$$

2.1.10 Hilbert space and representations

We now want to discuss the structure of the Hilbert space of the CFT in a little more detail. CFTs can be built on linear combinations of the primary fields and their descendants. In constructing Verma modules like this, it is possible that some linear combination of descendant states, say $|\chi\rangle$, satisfies the highest weight state condition:

$$L_{-n}\left|\chi\right\rangle = 0, \text{ for } n > 0. \tag{2.75}$$

The state $|\chi\rangle$ is then simultaneously a primary and a descendant. These states are known as *null states* or *singular vectors*. The state $|\chi\rangle$ is also a highest weight state. It forms a sub representation inside the original Verma module and is orthogonal to the entire Verma module. This is easily seen through Hermitian conjugation of the inner product of $|\chi\rangle$ with some basis state:

$$\left\langle\chi\right| L_{-k_1}\cdots L_{-k_n}\left|h\right\rangle = \left\langle h\right| L_{k_n}\cdots L_{k_1}\left|\chi\right\rangle^{\dagger} = 0. \tag{2.76}$$

This extends naturally to the descendants of null states also. To construct an irreducible representation of the Virasoro algebra, we remove all such states from the Verma module.

Other states of interest in CFTs are the negative normed states, the presence of which spoils unitarity[8] and violates the Hilbert space axioms. Inner products of the form

$$\left\langle h_1\right| L_{\tilde{k}_1}\cdots L_{\tilde{k}_m} L_{-k_1}\cdots L_{-k_n}\left|h_2\right\rangle \tag{2.77}$$

depend on the conformal weight h and the value of the central charge (occurring through the application of the Virasoro algebra during explicit calculation). Demanding the theory be unitary places large restrictions on the allowed values of h

[8]Representations of the Virasoro algebra are said to be unitary if they contain no negative norm states.

and c. Generally, in order to investigate unitarity, we can consider the Gram matrix, G, of inner products between all basis states. This matrix is block diagonal with the inner product of states at different Virasoro level vanishing. As G is Hermitian, it can be diagonalised. Therefore, we can learn something about the structure of the state space via the determinant of this matrix, which equals the product of its eigenvalues. In particular:

- If the determinant is zero, there are null vectors in the basis.
- If the determinant is negative, there are (an odd number of) states of negative norm in the basis and the theory is non-unitary.
- If the determinant is positive, more work is needed to determine whether unitarity is violated.

There exist a general formula, due to Kac [29], for the calculation of this determinant:

$$\det G^{(l)} = \alpha_l \prod_{r,s\geq 1 rs\leq l} [h - h_{r,s}(c)]^{p(l-rs)} \tag{2.78}$$

where $G^{(l)}$ is the Gram matrix of inner products of states at level l, $p(l-rs)$ is the number of integer partitions of $l-rs$ and

$$\begin{aligned} \alpha_l &= \prod_{r,s\geq 1, rs\leq l} [(2r)^s 2!]^{m(r,s)} \\ m(r,s) &= p(l-rs) - p(l-r(s+1)). \end{aligned} \tag{2.79}$$

We choose the following representation (of which there are many) for the functions $h_{r,s}(c)$

$$\begin{aligned} h_{r,s}(c) &= h_0 + \frac{1}{4}(r\alpha_+ + s\alpha_-)^2, \\ h_0 &= \frac{1}{24}(c-1), \\ \alpha_\pm &= \frac{\sqrt{1-c} \pm \sqrt{25-c}}{\sqrt{24}}. \end{aligned} \tag{2.80}$$

The Minimal Models

If $\frac{\alpha_-}{\alpha_+}$ is rational, we may write

$$p\alpha_- + q\alpha_+ = 0 \tag{2.81}$$

where p and q are two coprime integers. In such theories the Verma module includes an infinite number of null states [18]. If we remove all submodules associated with such states, we are left with a *finite* set of operators. These theories are known as Rational Conformal Field Theories, of which, a special class of such theories are the famous minimal models. These models have a finite number of local fields with well-defined scaling behaviour and contain only the conformal symmetries. The finite set of conformal families (the set consisting of a primary field and all its descendants) can be labelled by the Kac indices r, s where

$$1 \leq r \leq q, \qquad\qquad 1 \leq s \leq p. \tag{2.82}$$

We shall denote a minimal model with integers p,q as $\mathcal{M}(p, q)$ and take $p > q$.
The Ising and Tricritical Ising models which are studied in this thesis are both minimal models.

2.1.11 Fusion rules

We briefly introduce the idea of fusion in a CFT. The fusion rules determine which conformal families, along with their multiplicities, have their primaries or descendants appearing in the OPE of the other conformal families.

$$[\phi_i] \times [\phi_j] \approx \sum_k [\phi_k] \tag{2.83}$$

where $[\phi_i]$ represents the operators contained in the conformal family built on the primary operator ϕ_i. The minimal models have a commutative and associative fusion algebra taking the form

$$[\phi_i] \times [\phi_j] = \sum_k \mathcal{N}_{ij}^k [\phi_k] \tag{2.84}$$

where $\mathcal{N}_{ij}^{k} \in \mathbb{Z}_{>0}$ are the fusion numbers and are equal to 0 or 1 for primary fields in the minimal models. We may write the fusion rules for the minimal models as

$$\phi_{(r,s)} \times \phi_{(m,n)} = \sum_{\substack{k=1+|r-m| \\ k+r+m=1 \bmod 2}}^{k_{max}} \sum_{\substack{l=1+|s-n| \\ l+s+n=1 \bmod 2}}^{l_{max}} \phi_{(k,l)} \tag{2.85}$$

where

$$\begin{aligned} k_{max} &= \min(r+m-1, 2p'-1-r-m), \\ l_{max} &= \min(s+n-1, 2p-1-s-n). \end{aligned} \tag{2.86}$$

and k and l are incremented by 2. We will see these again when calculating the three point functions for the tricritical Ising model.

2.2 Boundary Conformal Field Theory

We turn our attention now to Conformal Field Theories on bounded geometries. Working first on the upper half plane (UHP), we place an arbitrary boundary condition α along the real axis. That local conformal invariance must be preserved along this boundary translates into a condition on the algebra of the Virasoro generators. In particular, for the transformations $z \to z + \epsilon(z)$ to be real on the boundary, $\epsilon(z)$ must be real there ($\epsilon(\bar{z}) = \bar{\epsilon}(z)$) meaning that we have a single copy of the Virasoro modes instead of the usual two distinct copies.

In order to derive the Ward Identities on the UHP, we begin with the analogue of those on the plane:

$$\delta_{\epsilon,\bar{\epsilon}}\langle X \rangle = \frac{1}{2\pi i}\oint_C dz\epsilon(z)\langle T(z)X\rangle - \frac{1}{2\pi i}\oint_C d\bar{z}\bar{\epsilon}(\bar{z})\langle \bar{T}(\bar{z})X\rangle. \tag{2.87}$$

where the contour C encircles the origin and $X = \phi_{h_1\bar{h}_1}(z_1,\bar{z}_1)\cdots\phi_{h_n\bar{h}_n}(z_n,\bar{z}_n)$, a product of local primary fields. In the full plane, $\epsilon(z)$ and $\bar{\epsilon}(\bar{z})$ are independent and we in fact have two equations giving the independent variations δ_ϵ and $\delta_{\bar{\epsilon}}$. On the UHP, the variations are related by complex conjugation and we have a single identity. We take C to be a sufficiently large contour encompassing all points at which the correlation functions are to be evaluated, usually a large semi-circle in

the UHP which runs along a portion of the real axis.

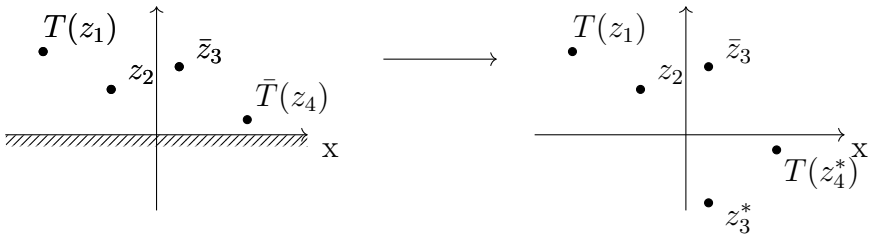

Figure 2.3: Cardy's doubling trick showing how points and operators in the UHP are represented in the full plane.

To proceed, we use the 'doubling' trick of Cardy [27] (see Fig. 2.3). We consider the dependence of the correlators in the UHP on coordinates $\bar{z}_i$ as a dependence on holomorphic coordinates $z_i^* = \bar{z}_i$ on the lower half plane (LHP). In effect, we are introducing a mirror image of the system in the LHP via a parity transformation. Moving across the boundary the tensors change accordingly, switching holomorphic indices into anti-holomorphic ones and vice-versa: $T(z^*) = \bar{T}(z), \bar{T}(z^*) = T(z)$, etc. This is true provided that the *gluing condition*

$$T(z, \bar{z}) = \bar{T}(z, \bar{z}), \qquad z = \bar{z} \ \in \mathbb{R} \tag{2.88}$$

is satisfied along the boundary which is the statement that there is no energy or momentum transfer across the boundary[9]. Indeed, if this boundary condition is true, then the above statement concerning holomorphic indices of tensors is true by analytic continuation.

With this machinery, we can write the conformal Ward identity as:

$$\delta_\epsilon \langle X \rangle = \frac{1}{2\pi i} \oint_C dz \epsilon(z) \langle T(z) X' \rangle \tag{2.89}$$

where now we have $X' = \phi_{h_1}(z_1)\bar{\phi}_{\bar{h}_1}(\bar{z}_1) \cdots \phi_{h_n}(z_n)\bar{\phi}_{\bar{h}_n}(\bar{z}_n)$ with the fields split into holomorphic and anti-holomorphic constituent parts $\phi_h, \bar{\phi}_{\bar{h}}$ respectively. The correlator of X on the UHP satisfies the same equation as the correlator of X' on the whole plane, seen as a function of the holomorphic coordinates $z_1, \cdots, z_n, z_1^*, \cdots, z_n^*$.

[9] As can be seen by writing the condition $T(x) = \bar{T}(x)$ in Cartesian coordinates: $T_{xy} = 0$.

We move now, to the infinite strip of width L with coordinates σ, τ running across and along the strip respectively. We place boundary conditions α, β on each side of the strip at $\sigma = 0, \sigma = L$ respectively and label the corresponding Hamiltonian $H_{\alpha\beta}$. Eigenstates of $H_{\alpha\beta}$ fall into irreducible representations of the Virasoro algebra. We define $n^i_{\alpha\beta}$ as the number of times the irreducible highest weight representation labelled by i occurs in the spectrum of $H_{\alpha\beta}$.

As shown in figure 2.4 we can map the strip to the UHP via the conformal mapping w=$\frac{L}{\pi} \ln z$, where $w = \tau + i\sigma$ is the coordinate on the strip and z, the coordinate on the UHP. When we do this, we will have a discontinuity at the origin, where the boundary condition changes from α to β, corresponding to the insertion of a boundary operator $\phi^{(\alpha\beta)}(0)\,|0\rangle$ acting on the vacuum. By the state-operator correspondence, this is a boundary state with weight $h_{\alpha\beta}$ equal to the lowest value of i with non-zero value of $n^i_{\alpha\beta}$. By acting on such a state by other local operators we get states in representations which have non-zero $n^i_{\alpha\beta}$.

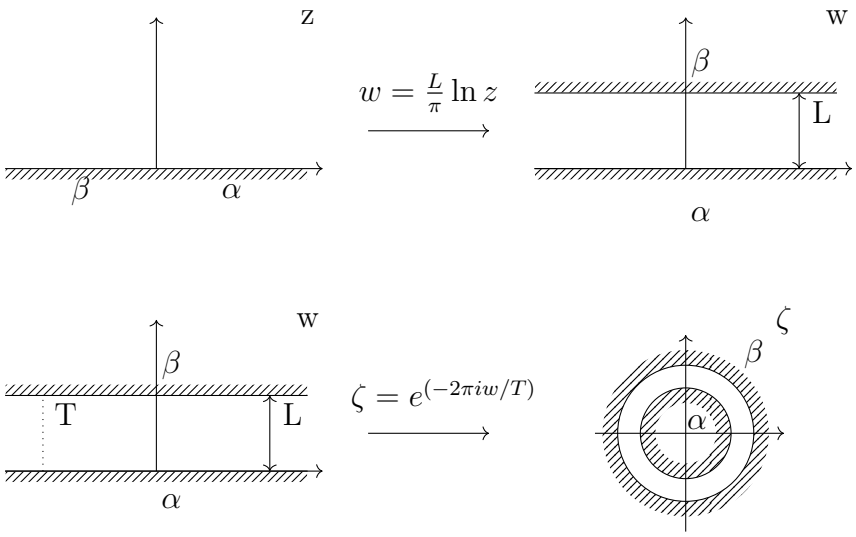

Figure 2.4: Maps between geometries.

Returning to the strip, we consider two different quantisation schemes to elucidate the above interpretation of boundary operators. We make the time direction of the strip periodic and work on the geometry of the finite cylinder, of circumference T and length L, with the inherited boundary conditions from the strip. We can then construct the Hamiltonian generating translations in the time direction. This

scheme is familiar in string theory as the open string channel. The second scheme for quantisation relates to the closed string channel in which the boundary conditions are encoded in the propagation of boundary states $|\alpha\rangle$, $|\beta\rangle$.

Z from H^τ

Let's first consider the quantisation in the time direction. We introduce the partition function for the cylinder:

$$Z_{\alpha\beta} = Tr(q^{H_{\alpha\beta}}) \qquad q = e^{2\pi i\rho}, \tag{2.90}$$

where $\rho = iT/2L$ is the modular parameter, the ratio of the two fundamental circles on the torus. It is often labelled by τ in standard references, which we instead reserve for the time coordinate on the strip.

We may write the partition function as

$$Z_{\alpha\beta} = \sum_i n^i_{\alpha\beta}\chi_i(q) \tag{2.91}$$

where $\chi_i(q)$ is the Virasoro character of the representation i: $\chi_i(q) = q^{-c/24}Tr_i q^{L_0}$. It is known that in the Rational Conformal Field Theories under the modular transformation $\rho \to -1/\rho$ the character of a representation transforms as

$$\chi_i(q) = \sum_j S_{ij}\chi_j(\tilde{q}), \tag{2.92}$$

where $\tilde{q} = e^{-2\pi i/\rho}$ and S_{ij} is the modular S-matrix. In this case, the partition function may then be written as

$$Z_{\alpha\beta}(q) = \sum_{ij} n^i_{\alpha\beta}S_{ij}\chi_j(\tilde{q}). \tag{2.93}$$

Z from H^σ

We now consider the second quantisation scheme. The modular transformation discussed above interchanges the roles of T and L making it possible to change the axes and consider the Hamiltonian generating translations in the σ direction. To proceed, we map the cylinder to the plane. However, not the z-plane that we are

used to, rather, the ζ-plane as shown in figure 2.4 via the conformal mapping:

$$\zeta = \exp\left(-2\pi i w/T\right). \tag{2.94}$$

The associated Hamiltonian is (c.f eqn (2.30) and the transformation (2.21))

$$H^{\sigma} = \frac{2\pi}{T}(L_0^{\zeta} + \bar{L}_0^{\zeta} - \frac{c}{12}) \tag{2.95}$$

where we have labelled the Hamiltonian with the σ index to differentiate it from the previous Hamiltonians generating translations in the time direction and we have labelled the Virasoro modes by the ζ index to make clear that these modes are in the ζ-plane geometry.

In this ζ-plane, the boundary conditions are realised through the propagation of boundary states, themselves realised by concentric circles. The propagation of the boundary state $|\alpha\rangle$ at the inner boundary, towards some final boundary state $|\beta\rangle$, can be written using the partition function as

$$\begin{aligned} Z_{\alpha\beta}(q) &= \langle\alpha| \, e^{LH^{\sigma}} \, |\beta\rangle \\ &= \langle\alpha| \, (\tilde{q}^{1/2})^{L_0^{\zeta}+\bar{L}_0^{\zeta}-c/12} \, |\beta\rangle \, . \end{aligned} \tag{2.96}$$

Earlier, we detailed the condition for a conformal transformation to remain conformal on a bounded geometry: no energy can flow across the boundary. On the cylinder, this condition becomes:

$$T^{\mathrm{cyl}}(0,t) = \bar{T}^{\mathrm{cyl}}(0,t), \qquad T^{\mathrm{cyl}}(L,t) = \bar{T}^{\mathrm{cyl}}(L,t). \tag{2.97}$$

Mapping this condition to the ζ-plane using (2.20) implies that

$$T^{\zeta}(\zeta)\zeta^2 = \bar{T}^{\zeta}(\bar{\zeta})\bar{\zeta}^2 \tag{2.98}$$

leading to a constraint on the Virasoro modes acting on the boundary states $|\alpha\rangle$, $|\beta\rangle$:

$$(L_n^{\zeta} - \bar{L}_{-n}^{\zeta}) \, |\alpha\rangle = 0 \tag{2.99}$$

with a similar condition on $|\beta\rangle$. This is an important and restrictive constraint. The general solution due to Ishibashi [28] is

$$|j\rangle\rangle = \sum_n |j;N\rangle \otimes U\overline{|j;N\rangle} \tag{2.100}$$

where $|j;N\rangle$ is a holomorphic state belonging to the verma module labelled by j, with N representing the different states within the module and U is an anti-unitary operator satisfying

$$U\,|j;0\rangle = \overline{|j;0\rangle}^*, \qquad U\bar{L}_n^\zeta = \bar{L}_n^\zeta U. \tag{2.101}$$

The physical boundary states satisfying (2.91) are the Cardy states. They are linear combinations of the Ishibashi states, each associated with some Verma module

$$|\alpha\rangle = \sum_n \langle j\,|\alpha\rangle\,|j\rangle\rangle. \tag{2.102}$$

With these states in our arsenal, we may rewrite the partition function as[10]

$$\begin{aligned} Z_{\alpha\beta}(q) &= \sum_{i,j} \langle\alpha|\,i\rangle\rangle\langle\langle i|(\tilde{q}^{1/2})^{L_0^\zeta+\bar{L}_0^\zeta-c/12}|j\rangle\rangle\langle\langle j\,|\beta\rangle \\ &= \sum_j \langle\alpha|\,j\rangle\rangle\langle\langle j\,|\beta\rangle\,\chi_j(\tilde{q}). \end{aligned} \tag{2.103}$$

Comparing this equation with (2.93) we find

$$\sum_i S_{ij} n_{\alpha\beta}^i = \langle\alpha|\,j\rangle\rangle\langle\langle j\,|\beta\rangle\,. \tag{2.104}$$

From this equation we can identify the states

$$\begin{aligned} |\tilde{0}\rangle &= \sum_j \sqrt{S_{0j}}|j\rangle\rangle, \\ |\tilde{l}\rangle &= \sum_j \frac{S_{lj}}{\sqrt{S_{0j}}}|j\rangle\rangle. \end{aligned} \tag{2.105}$$

[10]Here, we restrict ourselves to diagonal theories where the partition function on the torus is a diagonal combination the Virasoro characters $Z = \sum_i \chi_i(\rho)\chi_i(\bar{\rho})$ - see [18] for further details.

We can again apply (2.103) to find

$$\begin{aligned}\sum_i S_{ij} n^i_{\tilde{k}\tilde{l}} &= \langle \tilde{k}|\, j\rangle\rangle\langle\langle j\,|\tilde{l}\rangle \\ &= \frac{S_{ki}S_{lj}}{S_{0j}}.\end{aligned} \tag{2.106}$$

This is equivalent to the Verlinde formula relating the fusion numbers to the modular S matrix [25]:

$$\sum_i S_{ij}\mathcal{N}^i_{kl} = \frac{S_{kj}S_{lj}}{S_{0j}}. \tag{2.107}$$

We therefore draw the conclusion that

$$n^i_{\tilde{k}\tilde{l}} = \mathcal{N}^i_{kl}. \tag{2.108}$$

The number of times the representation i appears in the spectrum of the Hamiltonian $H_{\tilde{k}\tilde{l}}$ is exactly the fusion coefficient $\mathcal{N}^i_{kl}$.

Let's consider this more closely. Initially, we have the Hamiltonian $H_{\tilde{l}\tilde{0}}$ and the only

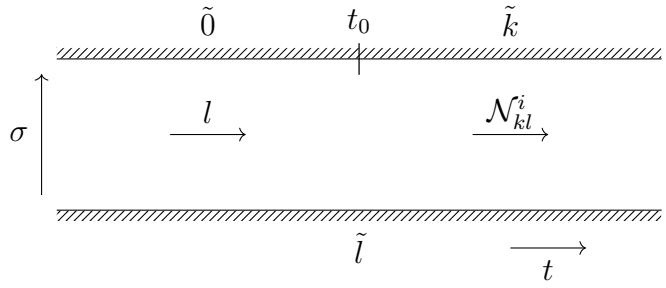

Figure 2.5: Propagating modes on the infinite strip.

propagating states belong to the representation l. Let's say at some time t_0 then, we change the boundary condition from $(\tilde{0},\tilde{l})$ to $(\tilde{k},\tilde{l})$. The propagating states are now in the representation i of which there are $\mathcal{N}^i_{kl}$ copies. We can simultaneously think of this scenario in the boundary operator language where at time t_0, a boundary operator $\phi_{\tilde{0}\tilde{k}}$ has been applied to the states in the initial l representation. $\phi_{\tilde{0}\tilde{k}}$ transforms in the representation k of the Virasoro algebra. Its action on states in the l representation is to produce states in a variety of other representations of which representation i will occur $n^i_{kl} = \mathcal{N}^i_{kl}$ times according to the fusion rules.

2.3 The Ising model

In these next sections, we introduce two applications of the above technology that are well established in the literature: The Ising and tricritical Ising models.

The simplest non-trivial minimal model is the Ising model. It is the continuum limit of the lattice spin model with lattice sites taking spin value $\sigma_i = \pm 1$. It is the $\mathcal{M}(4,3)$ minimal model with central charge c=1/2 containing three primary fields: the identity $\mathbb{I}$, the Ising spin σ and the energy density ϵ, of conformal weights (0,0), (1/16,1/16), (1/2,1/2) respectively. Denoting by $\phi_{(r,s)}$ the field of weight $h_{r,s}$, the fields may be labelled by their Kac indices (see section 2.1.10) as:

$$\begin{aligned} \mathbb{I} &\iff \phi_{(1,1)}, \\ \sigma &\iff \phi_{(2,2)}, \\ \epsilon &\iff \phi_{(2,1)}. \end{aligned} \tag{2.109}$$

We label the conformal families for the primary operators as $[\sigma], [\epsilon]$ and $[\mathbb{I}]$. Then, as the non-vanishing operator products for members of a conformal family are determined by the associated primaries, we may write down the following non-trivial fusion rules (c.f. eqn (2.85)):

$$\begin{aligned} [\sigma] \times [\sigma] &= [\mathbb{I}] + [\epsilon], \\ [\sigma] \times [\epsilon] &= [\sigma], \\ [\epsilon] \times [\epsilon] &= [\mathbb{I}]. \end{aligned} \tag{2.110}$$

Of course, the Ising model is a model of the Virasoro algebra and hence has a representation in terms of the Virasoro modes L_n. However, we may also recognise it as the c=1/2 free fermion model which we outline here[11].

The action describing free Majorana fermions in two dimensional Euclidean space is

$$S = \frac{1}{2\pi} \int d^2x (\bar{\psi}\partial\bar{\psi} + \psi\bar{\partial}\psi) \tag{2.111}$$

[11] More information on the relationship between the two descriptions is contained in section 5.1.1. See also, e.g. [18].

with classical equations of motion $\partial\bar{\psi} = \bar{\partial}\psi = 0$ whose solutions are any holomorphic and anti-holomorphic functions $\psi(z), \bar{\psi}(\bar{z})$.
Defining the stress-energy tensor $T(z) = -2\pi T_{zz} = -\frac{1}{2} : \psi(z)\partial\psi(z) :$, the OPE of ψ with T(z) is given by

$$T(z)\psi(w) = \frac{1/2\psi(w)}{(z-w)^2} + \frac{\partial\psi(w)}{z-w} + \cdots \tag{2.112}$$

meaning that the fermion field has conformal weight 1/2.
The OPEs of ψ and T with themselves are

$$\begin{aligned} \psi(z)\psi(w) &= \frac{1}{z-w} + \cdots \\ T(z)T(w) &= \frac{1/4}{(z-w)^4} + \frac{2T(w)}{(z-w)^2} + \frac{\partial T(w)}{(z-w)} + \cdots \end{aligned} \tag{2.113}$$

where we see that the stress-energy tensor is a quasi-primary field of weight 2.

2.3.1 The boundary Ising model

The Ising Model on a Cylinder

If we place the theory on the cylinder with circumference L, we can take a mode expansion of the field provided we account for the boundary conditions:

$$\psi(x) = \sqrt{\frac{2\pi}{L}} \sum_k b_k e^{-2\pi i k x/L} \tag{2.114}$$

where the b_k's satisfy the usual canonical anti-commutation relations:

$$\{b_j^\dagger, b_k\} = \delta_{j,k}, \qquad \{b_j^\dagger, b_k^\dagger\} = \{b_j, b_k\} = 0. \tag{2.115}$$

There are two possibilities for the boundary conditions with the field being either periodic or anti-periodic on the boundary:

$$\begin{aligned} \psi(x + 2\pi L) &= \psi(x) \\ \psi(x + 2\pi L) &= -\psi(x). \end{aligned} \tag{2.116}$$

The periodic case describes Ramond fermions with integer index in (2.114) and the anti-periodic case describes Neveu-Schwarz (NS) fermions with half integer index. The mode expansion in the Heisenberg picture may be written

$$\psi(x,\tau) = \sqrt{\frac{2\pi}{L}} \sum_k b_k e^{-2\pi k w/L}, \qquad w = \tau + ix \tag{2.117}$$

where $b_k = b_k(0)$ and τ is Euclidean time.

Ising Model on the Plane

The cylinder is mapped to the plane by the map

$$z = e^{2\pi w/L} \tag{2.118}$$

where z,w are the coordinates on the plane and cylinder respectively. Under this mapping the field transforms as

$$\psi_{\rm cyl}(w) = \sqrt{\frac{2\pi z}{L}} \psi_{\rm pl}(z). \tag{2.119}$$

The mode expansion on the plane, therefore, is

$$\psi_{pl}(z) = \sum_k b_k z^{-k-1/2}. \tag{2.120}$$

The extra factor of -1/2 in equation (2.120) when compared with equation (2.117) means that the meanings of the boundary conditions (2.116) have been interchanged: Ramond fermions are now described by the anti-periodic case and NS fermions by the periodic case.

2.4 The tricritical Ising model

The next simplest minimal model is the tricritical Ising model. As there is no simple free field representation of the theory, we can use the Virasoro algebra. The tricritical Ising model (TIM) is the A-type[12] M(5,4) minimal model with central

[12]See [70] for details on the classification of the field content of the bulk minimal models.

charge $c = 7/10$. It is the continuum limit of the lattice spin model with lattice spins taking values -1, 0 and 1. The model has 6 primary bulk fields ψ_i with 6 associated conformal boundary conditions given by the Cardy construction. The weights of the primary fields take values in the Kac table (with $p = 5$, $p' = 4$):

$$h_{(r,s)} = \frac{1}{4t}(d^2 - (t-1)^2) \qquad \text{with } d = r \cdot t - s, \qquad t = p/p'. \tag{2.121}$$

Table 2.1 contains the notation for the primary states, their weights, common notations for the corresponding boundary conditions (inspired by the boundary spin interpretation) and the boundary primary fields that live on these boundary conditions. Appendix B.1 contains the non-trivial fusion rules for the TIM. We often label the weight of state h_{rs} as (rs) or (r,s). Each may be used interchangeably in what follows.

Primary Operator	$\mathbb{I}$	ϵ	ϵ'	ϵ''	σ	σ'
Virasoro Label	(11)	(12)	(13)	(31)	(22)	(21)
Conformal Weight Δ	0	1/10	3/5	3/2	3/80	7/16
Notation for Cardy b.c.	(-)	(-0)	(0+)	(+)	(d)	(0)
Boundary Fields	$\mathbb{I}$	$\mathbb{I}$,ϵ'	$\mathbb{I}$,ϵ'	$\mathbb{I}$	$\mathbb{I}$,ϵ,ϵ',ϵ''	$\mathbb{I}$, ϵ''

Table 2.1: Table of notation for the tricritical Ising model.

As detailed before, the L_0 operator generates dilations in the radial direction and hence acts as the Hamiltonian of the system, which, on the strip is given by:

$$H = \frac{\pi}{L}(L_0 - c/24). \tag{2.122}$$

For TCSA on the strip the representation of L_0 that is realised depends on the boundary conditions on either side of the strip. Labelling the boundary conditions s, s$'$ at $\sigma = 0,\ \sigma = L$, the Hilbert space consists of states

$$\mathcal{H}^{(s,s')} = \bigoplus_i \mathcal{N}^i_{s,s'} \mathcal{H}_i. \tag{2.123}$$

States in $\mathcal{H}_i$ are obtained as Virasoro descendants of the primary field ψ_i through the application of Virasoro modes L_{-n}:

$$L_{-k_1} \dots L_{-k_n} |\psi_i\rangle \qquad k_i > 0.$$

2.5 Perturbed Conformal Field Theory and the Renormalisation Group

Imagine a space of Quantum Field Theories, with each point in theory space corresponding to some description of physics. What structure may we place on such a space? Are there theories or classes of theories which are related to each other? Can we find quantities which are related across these classes? Perhaps it is possible to find new descriptions of physics from some known point of understanding?

We can begin to answer such questions by considering the Renormalisation Group. The theory of renormalisation is now standard material and there are many excellent resources (see, for example, [34], [35]). We present a short introduction to the key ideas, mirroring the argument presented in [36].

Let's say we have a Quantum Field Theory defined by the following action

$$S_{\Lambda_0}[\varphi] = \int d^d x \left[\frac{1}{2} \partial^\mu \varphi \partial_\mu \varphi + \sum_i \Lambda_0^{d-d_i} g_{i0} \mathcal{O}_i(x) \right] \tag{2.124}$$

where the operators $\mathcal{O}_i$ are made up of powers of the field φ and its derivatives. We have put explicit reference to some energy scale Λ_0 in the equation such that the couplings g_{i0} are dimensionless. We can define a regularised partition function

$$\mathcal{Z}_{\Lambda_0}(g_{i0}) = \int_{\mathcal{F}_{\leq \Lambda_0}} \mathcal{D}\varphi e^{-S_{\Lambda_0}[\varphi]/\hbar}. \tag{2.125}$$

where $\hbar$ is the reduced Planck's constant and we take the integral over the space $\mathcal{F}_{\leq \Lambda_0}$ of smooth functions with energy $\leq \Lambda_0$. At this point, we look to lower the energy scale to some $\Lambda < \Lambda_0$.

First, we split the fields into low energy and high energy pieces:

$$\begin{aligned}\varphi(x) &= \int_{|p|\leq\Lambda_0} \frac{d^dp}{(2\pi)^d} e^{ip\cdot x}\tilde{\varphi}(p) \\ &= \int_{|p|\leq\Lambda} \frac{d^dp}{(2\pi)^d} e^{ip\cdot x}\tilde{\varphi}(p) + \int_{\Lambda<|p|\leq\Lambda_0} \frac{d^dp}{(2\pi)^d} e^{ip\cdot x}\tilde{\varphi}(p) \\ &:= \phi(x) + \chi(x)\end{aligned} \tag{2.126}$$

where the low energy modes ϕ now take values in $\mathcal{F}_{\leq\Lambda}$ and the high energy modes χ take values in $\mathcal{F}_{(\Lambda,\Lambda_0]}$. The path integral measure may also be split over these high and low energy modes:

$$\mathcal{D}\varphi = \mathcal{D}\phi\mathcal{D}\chi. \tag{2.127}$$

We can now perform the integral over χ, integrating out the high energy modes. Writing

$$\mathcal{Z}_{\Lambda_0}(g_{i0}) = \int_{\mathcal{F}_{\leq\Lambda}} \mathcal{D}\phi \int_{\mathcal{F}_{(\Lambda,\Lambda_0]}} \mathcal{D}\chi e^{-S_{\Lambda_0}[\phi+\chi]/\hbar} \tag{2.128}$$

and comparing with (2.125) we write down the *effective action at scale* Λ involving only the lower energy modes:

$$S^{\text{eff}}_{\Lambda}[\phi] = -\hbar\log\left[\int_{\mathcal{F}_{(\Lambda,\Lambda_0]}} \mathcal{D}\chi \exp(-S_{\Lambda_0}[\phi+\chi]/\hbar)\right]. \tag{2.129}$$

If the initial action takes the general form (2.124), then the effective action will take the form

$$S^{\text{eff}}_{\Lambda}[\phi] = \int d^dx \left[\frac{\zeta_\Lambda}{2}\partial^\mu\phi\partial_\mu\phi + \sum_i \Lambda^{d-d_i}\zeta_\Lambda^{n_i/2} g_i(\Lambda)\mathcal{O}_i(x)\right] \tag{2.130}$$

where ζ_Λ is a renormalisation factor, which accounts for quantum corrections to the coefficient of the kinetic term that may arise from the integrating out process. In order to compare equations (2.130) and (2.124), we can define a renormalised field by a simple rescaling, $\varphi = \sqrt{\zeta_\Lambda}\phi$, and rescale the momenta of the fields.

This is the essential idea of the renormalisation process:

- Integrate out the high momentum modes
- Rescale the momenta
- Rescale the fields such that the kinetic term is canonically normalised

This leaves us with an effective field theory describing physics in the IR regime. Equation (2.129) is the Renormalisation Group equation for the effective action. This process can be applied iteratively to obtain a new effective action at lower and lower energy scales.

The partition function, $\mathcal{Z}_\Lambda(g_i(\Lambda))$, obtained from this effective action is the same as that defined originally in (2.125): $\mathcal{Z}_\Lambda(g_i(\Lambda)) = \mathcal{Z}_{\Lambda_0}(g_{i0}(\Lambda_0))$. Lowering the energy scale infinitesimally, we get the following differential equation

$$\Lambda \frac{d\mathcal{Z}_\Lambda(g)}{d\Lambda} = \left(\Lambda \frac{\partial}{\partial \Lambda}\Big|_{g_i} + \Lambda \frac{\partial g_i(\Lambda)}{d\Lambda} \frac{\partial}{\partial g_i}\Big|_{\Lambda} \right) \mathcal{Z}_\Lambda(g) = 0. \tag{2.131}$$

This is the Renormalisation Group Equation for the partition function and is a Callan-Symanzik equation [40],[41]. It tells us that as we change the energy scale of the system by integrating out the high energy modes, the couplings in the effective action vary, taking into account the change in degrees of freedom in the fields over which we take the path integral. We call this variation in the couplings, *running the coupling*. That the couplings run is important and is captured by the beta function which describes the RG flow. It is defined as the derivative of the coupling with respect to the logarithm of the energy scale:

$$\beta(g) = \frac{\partial g}{\partial \log(\Lambda)}. \tag{2.132}$$

In the models that we consider, the beta function is constant and running the coupling is equivalent to following this flow.

Points with vanishing beta-function are *fixed points* of the RG flow which in 2 dimensions coincide with Conformal Field Theories [33]. RG flow then gives structure to our space of QFTs, punctuating it with conformal fixed points. In section 2.1.8, we introduced the central charge of a Theory. Whilst introduced there in the context of a Conformal Field Theory, the central charge is not unique to theories with

conformal symmetry. It is also defined away from these conformal fixed points. In 2 dimensions, Zamolodchikov's famous c-theorem [37] details how the central charge is monotonically decreasing along RG flow meaning that RG flows are directed and therefore irreversible. The direction of the flow is determined by the dimension of the perturbing operator.

If we start at some fixed point of the RG flow and turn on the coupling of an operator ψ of dimension Δ_ψ, then:

- If $\Delta_\psi < d$, the operator is *relevant* and drives the RG flow away from the fixed point. The coupling of relevant operators grows as the scale is lowered.
- If $\Delta_\psi > d$, the operator is *irrelevant* and drives the RG flow towards the fixed point. The coupling of an irrelevant operator becomes smaller as the scale is lowered towards the IR.
- If $\Delta_\psi = d$, the operator is *marginal*. These operators neither increase nor decrease on RG flow.

In this thesis we consider boundary perturbations of Conformal Field Theories and investigate the resulting RG flow. Placing a theory on a bounded geometry such as the strip or cylinder provides an IR regulator, removing the IR divergences. Divergences in the UV may be subtracted using counterterms in the usual way. More information on regularisation and divergences in QFT may be found in the referenced texts.

2.5.1 The Schrieffer-Wolff transformation

In TCSA, we work in the Hamiltonian formalism of QFT. Here, the process of integrating out high energy degrees of freedom in order to find a low energy description of the dynamics is captured in the Schrieffer-Wolff (SW) method [38] (see also [39] for a nice review of the method) in which we apply a sequence of unitary transformations to the Hilbert space to decouple the high and low energy subspaces. The

perturbed Hamiltonian is transformed into block form

$$H = \left[\begin{array}{ccc|c} ll & \cdots & \cdots & lh \\ \vdots & \ddots & & \vdots \\ \hline \vdots & & \ddots & \vdots \\ hl & \cdots & \cdots & hh \end{array}\right] \tag{2.133}$$

where l represents the low energy interactions and h the high energy ones. Applying SW to the Hamiltonian makes the off diagonal mixing terms smaller and smaller, pushing interactions to higher and higher orders of the coupling λ. The effective Hamiltonian is the restriction of the rotated Hamiltonian to the low energy subspace and this restriction acts as the 'integrating out' process of Hamiltonian Renormalisation.

Let H_0 be an operator on the finite dimensional Hilbert space $\mathcal{H}$ and define $\mathcal{P}_0$ as the subspace spanned by eigenvectors of H_0 whose eigenvalues lie in some interval $\mathcal{I}_0 \subseteq \mathbb{R}$. Similarly, we take a slightly larger subset $\mathcal{I}$ and take $\mathcal{P}$ as the subspace spanned by eigenvectors of the *perturbed* Hamiltonian $H = H_0 + \lambda V$ which have eigenvalue lying in $\mathcal{I}$. We also define P and P_0 as the orthogonal projections onto the subspaces $\mathcal{P}$ and $\mathcal{P}_0$ respectively.

The goal now is to construct an effective Hamiltonian which acts only on $\mathcal{P}_0$ and reproduces the low lying spectrum of H. This is achieved via the direct rotation between $\mathcal{P}$ and $\mathcal{P}_0$ [39]. The direct rotation of two non-orthogonal v_i, v_j states in the Hilbert space is defined as the unitary operator

$$U_{v_i \to v_j} = \sqrt{R_{v_i} R_{v_j}} \tag{2.134}$$

where R is the reflection operator $R_{v_i} = \mathbb{I} - 2\left|v_i\right\rangle\left\langle v_i\right|$.
The Schrieffer-Wolff transformation for the unperturbed Hamiltonian H_0, the perturbation λV and the low energy subspace $\mathcal{P}_0$ then gives the effective Hamiltonian operator

$$H_{eff} = P_0 U (H_0 + \lambda V) U^\dagger P_0. \tag{2.135}$$

Chapter 3

TCSA

3.1 General introduction

The Truncated Conformal Space Approach (TCSA) of Yurov and Zamolodchikov [42], [43] is a numerical technique for finding finite size spectrum of Hamiltonians in Quantum Field Theory described as perturbations of Conformal Field Theories. In this approach one considers an ultraviolet fixed point, described by a two-dimensional Conformal Field Theory, that is perturbed by a local operator ϕ with scaling dimension Δ. TCSA proved to be a reliable numerical method for studying the strong-coupling physics of such Quantum Field Theories. We refer the reader to a recent review [61] where the basics as well as many applications are reviewed. Indeed, much work has been done on TCSA with early work on the analysis of truncation errors and the TCSA Renormalisation Group carried out in [52], [53], [55]. It has had great success in the study of RG flows, for example in [44], [56] and [57] and in recent years, more progress has been made with TCSA undergoing a further period of development including work in higher dimensions (see [58], [59], [60]).
For the majority of these perturbed theories, the large coupling limit is described by a trivial theory in which only a vacuum (possibly degenerate) state survives in the low energy sector. Examples of RG flows ending in a non-trivial infrared fixed point studied by TCSA are relatively scarce. The situation is different for boundary RG flows which always end up in a non-trivial fixed point.
TCSA was adopted to boundary RG flows in [45] and has been used extensively to study perturbations of boundary theories (see, for example, [46], [47], [48], [49],

[50], [51]). In this case we consider a 2d CFT on a strip of width L with a choice of conformal boundary condition at each end. Let $0 \leq \sigma \leq L$ be the coordinate across the strip and $-\infty < \tau < \infty$ be the coordinate along the strip and let s and s' be the boundary condition labels for the $\sigma = 0$ and $\sigma = L$ ends respectively. Choosing τ to be a Euclidean time gives a quantisation scheme in which the Hilbert space $\mathcal{H}^{(s,s')}$ for a theory on an interval of length L splits into Virasoro irreducible representations $\mathcal{H}_i$. For a diagonal Virasoro minimal model s and s' are just primary state labels and the state space decomposition has the form [26]

$$\mathcal{H}^{(s,s')} = \bigoplus_i \mathcal{N}^i_{s,s'} \mathcal{H}_i \tag{3.1}$$

where $\mathcal{N}^i_{s,s'}$ are the fusion coefficients. Perturbing the boundary condition on the $\sigma = 0$ end with a boundary operator ψ is described by a Hamiltonian

$$H = \frac{\pi}{L}[L_0 - \frac{c}{24} + L\mu\psi(0,0)] \tag{3.2}$$

where μ is a dimensionful coupling.
States in $\mathcal{H}_i$ are obtained as Virasoro descendants of the primary field $|\psi_i\rangle$. They are spanned by states of the form

$$L_{-k_1} \dots L_{-k_n} |\psi_i\rangle \qquad k_j > 0 \tag{3.3}$$

where L_{-k_j} are Virasoro modes. In practice it is convenient to work with a linear basis of states of the form (3.3) which are not necessarily orthonormal. For minimal models, where we have null states, we choose such a basis for a subspace on which the Gram matrix is non-degenerate. We will discuss the Gram matrix more shortly.

In TCSA we truncate the state space (3.1) keeping only linear combinations of states whose conformal weight is smaller than some maximal weight set by a truncation parameter $\Delta_{\max}$. In the simplest form we can take all weights that satisfy

$$\Delta \leq \Delta_{\max} \,. \tag{3.4}$$

Here the Virasoro weights Δ are the eigenvalues of L_0 and are of the form $\Delta = h_i + N$ where h_i is the value of the primary weight in the given Virasoro irreducible

representation and N is a non-negative integer that gives the weight of the Virasoro descendants. For a state of the form (3.3) $N = \sum_{j=1}^{n} k_j$.

We assume for simplicity that we have finitely many primaries labelled by $i = 1, \ldots, p$. Depending on the value of $\Delta_{\max}$ the prescription (3.4) sets the maximum descendant level N for each conformal tower labelled by the primary weight h_i. Thus, given $\Delta_{\max}$ we get a number of bounds $N_{\max}(h_i, \Delta_{\max})$. A more general truncation scheme, still based only on conformal weights, is specified by setting independent maximal descendant levels $(N_{\max}^{(1)}, \ldots, N_{\max}^{(p)})$ so that we keep states with weights $\Delta = h_i + N_i$ in the corresponding conformal towers satisfying

$$N_1 \leq N_{\max}^{(1)}\,, \quad N_2 \leq N_{\max}^{(2)}\,, \ldots\,, N_p \leq N_{\max}^{(p)}\,. \tag{3.5}$$

The perturbed Hamiltonian (3.2) is restricted to the truncated state space. The main TCSA observables are energy levels e_i of the dimensionless Hamiltonian $\tilde{H} = LH/\pi$. We look to find the spectrum of the truncated Hamiltonian by solving the eigenvalue problem:

$$\tilde{H}\,|\psi\rangle = e\,|\psi\rangle\,. \tag{3.6}$$

Expanding the field in some basis of states $|\psi\rangle = \lambda^j\,|j\rangle$, we can write the simple eigenvalue problem:

$$\tilde{H}^i_j \lambda^j = e\lambda^i, \tag{3.7}$$

where the Hamiltonian in the expanded basis is given by

$$\tilde{H}\,|j\rangle = \tilde{H}^i_j\,|i\rangle\,. \tag{3.8}$$

The matrix $\tilde{H}^i_j$ here is not hermitian. In order to convert this problem to hermitian form, we consider matrix elements

$$\tilde{H}_{ij} = \langle i|\,\tilde{H}\,|j\rangle\,. \tag{3.9}$$

The two pictures are related by $\tilde{H}_{ij} = G_{ik}\tilde{H}^k_j$ where G_{ik} is the Gram matrix of inner products of basis states. Both G_{ij} and $\tilde{H}_{ij}$ are hermitian if the Hamiltonian is hermitian. We can then frame the problem in terms of the generalised eigenvalue

problem

$$\tilde{H}_{ij}\lambda^j = eG_{ij}\lambda^j. \tag{3.10}$$

We can easily move between the two pictures (3.7) and (3.10). In the TCSA algorithm described below, we work in the generalised picture.

We return now to the Hamiltonian (3.2). For a primary field $\psi(0,0)$ of conformal dimension Δ^{UV} the matrix elements between states of the form (3.3) can be calculated in the truncated Hilbert space using three point functions and standard commutation relations

$$[L_n - L_0, \psi(0,0)] = \Delta^{\mathrm{UV}} n\psi(0,0)\,. \tag{3.11}$$

The resulting finite matrix is then diagonalised numerically.

These are the two key steps in TCSA: Calculation of the basis and the matrix elements. In the following sections, we construct an algorithm for TCSA. All routines are written using Wolfram Mathematica 11.

3.2 Programming TCSA: basis generation

In what follows, we construct a recursive algorithm for the generation of a truncated basis of Virasoro states, which with some model specific alterations, may be applied to any theory of the Virasoro algebra.
The goal is to create a basis of vectors $v_i^{(N)}$ at level N. These basis vectors consist of a set of Virasoro raising operators acting on one of the Virasoro primary fields of the theory. This basis is neither normalised nor orthogonal by supposition.
We assume an order on our Virasoro modes and define our states to be of the form

$$|\underline{v}_i^N\rangle = L_{-n_1}L_{-n_2}...L_{-n_l}\,|\phi_i\rangle\,, \qquad\qquad N = n_1 + n_2 + ... + n_l, \tag{3.12}$$

where N indicates the Virasoro level of the state, $n_1 \geq n_2 \geq ... \geq n_l$ and $|\phi_i\rangle$ is a Virasoro primary. In what follows, we drop the primary label i and write the above state as $|\underline{v}^N\rangle$ for notational convenience. However, it is understood that inner

products will ultimately depend on the primary that the state is built on.

We look to construct a basis of such states. We will define the set of basis states at some level N by $\mathcal{V}_N$. At level zero of the recursion, we take the primary fields as our basis. Note that these states are chosen to be orthonormal.
At level N of the recursion, we suppose that we have calculated all basis states, as described above and inner products between them. We presume also, that we have calculated all overlaps between basis states and a single Virasoro mode - the relevance of this step is explained below. Details on how best to store this information is included in section 3.5.

At level N+1, the single generator states $L_{-n}\left|\underline{v}^{N+1-n}\right\rangle$ (where $\left|\underline{v}^{N+1-n}\right\rangle \in \mathcal{V}_{N+1-n}$) act as our candidate basis elements. It is in calculating inner products of candidate states, that the overlaps between basis states and a single Virasoro mode become important. We create a routine for calculating such overlaps in section 3.2.1 but continue here assuming we have this technology.

The main idea of the algorithm is to iteratively consider such additional states in the basis and calculate the associated Gram matrix of inner products. Calculating the determinant of this matrix will determine whether the basis contains any linearly dependant states: if this determinant is non-zero, then the added candidate is linearly independent from the others in the basis and can therefore be used as a basis state. If the determinant is zero, then the matrix is degenerate and the candidate state is linearly dependent on the other states previously included in the basis. This candidate state will then be dropped from the basis and the next candidate will be considered.
We proceed to calculate the matrix of overlaps of all such candidates:

$$\left\langle \underline{u}^{N+1-m}\right| L_m L_{-n}\left|\underline{v}^{N+1-n}\right\rangle \tag{3.13}$$

for $\left|\underline{u}^{N+1-m}\right\rangle, \left|\underline{v}^{N+1-m}\right\rangle \in \mathcal{V}_{N+1-m}$.

Note:

Candidate states which are discarded consist of a single Virasoro mode acting on a basis state. Should the additional Virasoro mode not satisfy the ordering condition (3.12) we term the state 'ordered-but-one'. When we discard the candidate basis vector, we stop calculating its inner product with 'new' basis vectors i.e. basis vectors which are determined and stored at some later stage in the recursion. This is of course fine for basis generation. However, in calculating the inner products, we need to be able to calculate the matrix elements for a single L_m mode, thus coming across inner products of basis vectors with ordered-but-one states. It will, therefore, be helpful to store the inner product of the discarded candidates with 'new' basis vectors. We will store two matrices: the true Gram matrix for the basis states and a larger matrix of inner products which will also include inner products with the discarded candidates. This second matrix will have the following block structure

$$G = \left[\begin{array}{c|c} A & B \\ \hline B & C \end{array}\right] \tag{3.14}$$

where A is a block containing inner products of the form $\langle$ordered$|$ordered$\rangle$, B of the form $\langle$ordered$|$ordered-but-one$\rangle$ and C is a block containing products of the form $\langle$ordered-but-one$|$ordered-but-one$\rangle$.

In order to calculate the overlaps (3.13) we use the Virasoro algebra:

$$[L_m, L_n] = (m-n)L_{m+n} + \frac{c}{12}(m^3 - m)\delta_{m+n,0} \tag{3.15}$$

giving us:

$$\begin{aligned} \langle \underline{u}^{N+1-m} | L_m L_{-n} | \underline{v}^{N+1-n} \rangle = \\ \langle \underline{u}^{N+1-m} | \, (m+n) L_{m-n} \, | \underline{v}^{N+1-n} \rangle + \langle \underline{u}^{N+1-m} | \, L_{-n} L_m \, | \underline{v}^{N+1-n} \rangle \\ + \frac{c}{12}(m^3 - m)\delta_{m-n,0} \, \langle \underline{u}^{N+1-m} | \underline{v}^{N+1-n} \rangle \, . \end{aligned} \tag{3.16}$$

To proceed, we use a partition of unity (POU) at level p=N+1-m-n, inserting it

between the Virasoro modes in the second term. The POU we will use is of the form:

$$\sum_{\underline{k},\underline{l}\in\mathcal{V}_p} |\underline{k}\rangle \langle\underline{l}| \, (G^p_{kl})^{-1}. \tag{3.17}$$

where we are summing over basis states at level p and G^p_{kl} is the Gram matrix at level p. The action of the POU on a state $|\underline{v}^p\rangle$ is

$$\sum_{\underline{k},\underline{l}\in\mathcal{V}_p} |\underline{k}\rangle \langle\underline{l}| \, (G^p_{kl})^{-1} \, |\underline{v}^p\rangle = \sum_{\underline{k},\underline{l}\in\mathcal{V}_p} |\underline{k}\rangle \, (G^p_{kl})^{-1} G^p_{lv} = \sum_{\underline{k},\underline{l}\in\mathcal{V}_p} |\underline{k}^p\rangle \, \delta_{kv} = |\underline{v}^p\rangle \, . \tag{3.18}$$

We note that this POU exists in the quotient space with all null vectors removed.

Putting this all together, we find the following formula which is key for our basis generation:

$$\begin{aligned} \langle\underline{u}^{N+1-m}|L_m L_{-n} \, |\underline{v}^{N+1-n}\rangle &= \langle\underline{u}^{N+1-m}| \, (m+n) L_{m-n} \, |\underline{v}^{N+1-n}\rangle + \\ &\sum_{\underline{k},\underline{l}\in\mathcal{V}_p} \langle\underline{v}^{N+1-m}| \, L_{-n} \, |\underline{k}^p\rangle \, (G^p_{kl})^{-1} \, \langle\underline{l}^p| \, L_m \, |\underline{v}^{(N+1-n)}\rangle \\ &+ \frac{c}{12}(m^3 - m)\delta_{m-n,0} \, \langle\underline{v}^{(N+1-m)}|\underline{v}^{(N+1-n)}\rangle \, . \end{aligned} \tag{3.19}$$

with p=N+1-m-n.

This formula calculates new overlaps from old, known overlaps and determines our basis states at level N+1 thus completing the recursive algorithm. As detailed before, within the above routine, we are required to calculate the matrix elements of a single Virasoro mode. For example, if both $\langle\underline{u}^{N+1-m}|$ and $|\underline{v}_i^{N+1-n}\rangle$ are basis states then the first term of (3.19) may be of this type as opposed to the inner product of two basis vectors. We calculate these now.

3.2.1 Matrix elements of a single Virasoro mode

Here we construct the matrix elements for single Virasoro modes which are used in the above basis generation routine[1]:

$$\langle \underline{u}^{N+1-m}| \, L_m \, |\underline{\tilde{v}}^{N+1}\rangle \, . \tag{3.20}$$

We proceed as before, using a partition of unity to write this in terms of products of lower level overlaps. We cannot insert the POU immediately as it will not lower the level. First, we lower the level of the ket state:

$$\langle \underline{u}^{N+1-m}| \, L_m \, |\underline{\tilde{v}}_i^{N+1}\rangle = \langle \underline{u}^{N+1-m}| \, L_m L_{-k} \, |\underline{v}^{N+1-k}\rangle \, . \tag{3.21}$$

where $|\underline{\tilde{v}}^{N+1}\rangle = L_{-k} \, |\underline{v}^{N+1-k}\rangle$ with $|\underline{v}^{N+1-k}\rangle \in \mathcal{V}_{N+1-k}$.

At this point we use the Virasoro Algebra to write this as:

$$\begin{aligned}\langle \underline{u}^{N+1-m}| \, L_m \, |\underline{\tilde{v}}^{N+1}\rangle = \langle \underline{u}^{N+1-m}| \, L_{-k} L_m \, |\underline{v}^{N+1-k}\rangle + \langle \underline{u}^{N+1-m}| \, (m+k) L_{m-k} \, |\underline{v}^{N+1-k}\rangle \\ + \frac{c}{12}(m^3 - m)\delta_{m-k,0} \, \langle \underline{u}^{N+1-m}|\underline{v}^{N+1-k}\rangle \, .\end{aligned} \tag{3.22}$$

Labelling these terms, in order, 1,2,3 we discuss how to calculate them as part of the recursion.

In the first term, we insert a partition of unity at level q=N+1-m-k between the Virasoro modes, giving the following:

$$\sum_{\underline{l},\underline{r}\in\mathcal{V}_q} \langle \underline{u}^{N+1-m}| \, L_{-k} \, |\underline{l}^q\rangle \, (G^q_{lr})^{-1} \, \langle \underline{r}^q| \, L_m \, |\underline{v}^{N+1-k}\rangle \, . \tag{3.23}$$

This product contains inner products of basis states and terms of the form

$$\langle \text{ordered basis element}|\text{ordered-but-one basis element}\rangle \, . \tag{3.24}$$

[1]The ˜ notation will become clear shortly.

We can simply calculate this using the stored data from previous levels in the recursion.

In the second term, we have two scenarios to consider:

If m-k > 0, we absorb L_{m-k} into the bra state:

$$\begin{aligned}\langle \underline{u}^{N+1-m}| \, (m+k) L_{m-k} \, |\underline{v}^{N+1-k}\rangle &= (m+k) \, \langle \tilde{\underline{u}}^{N+1-m+m-k} | \underline{v}^{N+1-k}\rangle \\ &= (m+k) \, \langle \tilde{\underline{u}}^{N+1-k} | \underline{v}^{N+1-k}\rangle \, .\end{aligned} \tag{3.25}$$

where $|\tilde{\underline{u}}^{N+1-k}\rangle = L_{m-k} \, |\underline{u}^{N+1-m}\rangle$.

If m-k < 0, we absorb L_{m-k} into the ket state:

$$\langle \underline{u}^{N+1-m}| \, (m+k) L_{m-k} \, |\underline{v}^{N+1-k}\rangle = (m+k) \, \langle \underline{u}^{N+1-m} | \tilde{\underline{v}}^{N+1-m}\rangle \, . \tag{3.26}$$

where $|\tilde{\underline{v}}^{N+1-m}\rangle = L_{m-k} \, |\underline{v}^{N+1-k}\rangle$.[2]

Both of these quantities are known.

Finally, the third term is simply some constant times the overlap of two basis elements at some lower level in the recursion. As such, it is already known.

We now have a complete routine for basis generation in a Virasoro model.

3.3 Programming TCSA: the perturbing operator

Now that we have calculated a basis, we calculate the matrix elements (3.9)

$$H_{ij} = \langle \underline{i}| \, \frac{\pi}{L} [(L_0 - c/24) + L\mu\psi_k] \, |\underline{j}\rangle \, . \tag{3.27}$$

[2]Note: $|\tilde{\underline{v}}^{N+1-m}\rangle$ is not the same state as in eqns (3.20)/(3.21). We are simply using the ˜ notation to denote that an existing basis state has had a mode added (eqn (3.26)) or removed (eqns (3.20)/(3.21)).

where $|\underline{i}\rangle, |\underline{j}\rangle$ are arbitrary basis elements. The matrix elements of the free Hamiltonian are straightforward, involving only inner products on basis states:

$$\langle \underline{i}| \frac{\pi}{L}(L_0 - c/24) |\underline{j}\rangle = \frac{\pi}{L}(\Delta_j - c/24) \langle \underline{i}|\underline{j}\rangle \tag{3.28}$$

where Δ_j is the conformal weight of the state $|\underline{j}\rangle$ and $\Delta_j = \Delta_i$ for contributing elements.

The matrix elements of the perturbing field $\psi_k(z)$ are more involved. We construct a recursive algorithm for their calculation. The level zero components are the normalised structure constants determined by the three point functions of ψ_k with the primary fields of the theory which have been previously calculated in [69]:

$$\langle \phi_i^{(ab)}| \psi_k^{(bc)}(z) |\phi_k^{(ca)}\rangle = C_{ij}^{(abc)k}. \tag{3.29}$$

More details of their calculation in the tricritical Ising model are contained in Chapter 5 where the notation $\psi^{(ab)}$ is also explained.

At level N of the recursion, we assume that we have calculated all matrix elements with ψ: $\langle \underline{u}^N| \psi_k(z) |\underline{v}^N\rangle$ where $|\underline{v}^N\rangle \in \mathcal{V}_N$ are basis states at level N. Now we construct a procedure for calculating this information at level N+1. We bear in mind that we are using half-plane operators to represent the Hamiltonian on a strip. Under the relevant mapping (see chapter 2), we evaluate the field and its derivatives at z=1.

At level N+1, we calculate the matrix elements between two arbitrary basis states $|\tilde{\underline{u}}^{N+1}\rangle, |\tilde{\underline{v}}^{N+1}\rangle$

$$\langle \tilde{\underline{u}}^{N+1}| \psi_k(1) |\tilde{\underline{v}}^{N+1}\rangle . \tag{3.30}$$

We first lower the bra state and then we will proceed to lower the ket:

$$\begin{aligned}
\langle \tilde{\underline{u}}^{N+1}| \psi_k(1) |\tilde{\underline{v}}^{N+1}\rangle &= \langle \underline{u}^{N+1-m}| L_m \psi_k(1) |\tilde{\underline{v}}^{N+1}\rangle \\
&= (m h_{\psi_k} + h_{\underline{u}^{N+1-m}} - h_{\tilde{\underline{v}}^{N+1}}) \langle \underline{u}^{N+1-m}| \psi_k(1) |\tilde{\underline{v}}^{N+1}\rangle \\
&+ \langle \underline{u}^{N+1-m}| \psi_k(1) L_m |\tilde{\underline{v}}^{N+1}\rangle .
\end{aligned} \tag{3.31}$$

Where $|\tilde{\underline{u}}^{N+1}\rangle = L_{-m}\,|\underline{u}^{N+1-m}\rangle$. In the above calculation, we have used the following formula for the commutator involving the Virasoro modes and a primary field ϕ of weight h:

$$[L_n, \phi(w)] = h(n+1)w^n\phi(w) + w^{n+1}\partial\phi(w). \tag{3.32}$$

Therefore, at w=1 (on the strip),

$$[L_n - L_0, \phi(1)] = hn\phi(1). \tag{3.33}$$

We insert a partition of unity at level t=N+1-m in the second term giving:

$$\begin{aligned}\langle\tilde{\underline{u}}^{N+1}|\psi_k(1)\,|\tilde{\underline{v}}^{N+1}\rangle &= (mh_{\psi_k} + h_{\underline{u}^{N+1-m}} - h_{\tilde{\underline{v}}^{N+1}})\,\langle\underline{u}^{N+1-m}|\,\psi_k(1)\,|\tilde{\underline{v}}^{N+1}\rangle \\ &+ \sum_{\underline{r},\underline{s}\in\mathcal{V}_t}\langle\underline{u}^{N+1-m}|\,\psi_k(1)\,|\underline{r}^t\rangle\,(G^t_{rs})^{-1}\,\langle\underline{s}^t|\,L_m\,|\tilde{\underline{v}}^{N+1}\rangle\,.\end{aligned} \tag{3.34}$$

In lowering the level of the bra state, we have reduced the second term in the above to something calculable. It involves the product of three objects which are known from some previous stage of the recursion: matrix elements of ψ_k at level N+1-m, the inner product of basis states at level N+1-m and the inner product of the basis state $\langle\underline{s}^t|$ with the state $L_m\,|\underline{v}^{N+1}\rangle$ which we have previously named an 'ordered-but-one' state - a basis state with an additional L_m mode acting on it. To finish off the calculation, we must lower the level of the ket state in the first term.
Proceeding as before, we find the following formulae for the matrix elements of the perturbing operator at level N+1:

$$\begin{aligned}&\langle\tilde{\underline{u}}^{N+1}|\psi_k(1)\,|\tilde{\underline{v}}^{N+1}\rangle = \\ &\sum_{\underline{g},\underline{h}\in\mathcal{V}_{t-n}} A\,\langle\underline{u}^{N+1-m}|\underline{g}^{t-n}\rangle\,(G^{t-n}_{gh})^{-1}\,\langle\underline{h}^{t-n}|\,\psi_k(1)\,|\underline{v}^{N+1-n}\rangle \\ &+ \sum_{r,s}\langle\underline{u}^{N+1-m}|\,\psi_k(1)\,|\underline{r}^t\rangle\,(G^t_{rs})^{-1}\,\langle\underline{s}^t|\,L_m\,|\tilde{\underline{v}}^{N+1}\rangle\end{aligned} \tag{3.35}$$

where t= N+1-m and we have set $A = (mh_{\psi_k} + h_{\underline{u}^{N+1-m}} - h_{\tilde{\underline{v}}^{N+1}})(nh_{\psi_k} + h_{\underline{v}^{N+1-n}} - h_{\underline{u}^{N+1-m}})$.

We now have a working algorithm for TCSA - calculation of basis states and matrix elements of the perturbed Hamiltonian. In the following section, we note some technical details of the programme and some information on storage and optimisation.

3.4 A short note on the free fermion basis

As detailed in section 2.3, the Ising model can be described using either a Virasoro basis or a free fermion basis. The free fermion basis is introduced in more detail in chapter 5 and the interested reader may wish to return to this note once they have completed section 5.1. Building a TCSA algorithm in this basis is much simpler than doing so in the Virasoro basis. States are modelled as either an even or odd number of creation operators acting on the Fock space vacuum. These can be modelled in TCSA using ordered partitions of integers with no repeats.
The matrix elements of the free Hamiltonian and the perturbing operator are then calculated using standard anti-commutation relations between the fermionic modes.

3.5 Technical details of the programme

We discuss some technical details of the programme using the basis generation routine as a framework to illustrate the ideas. We take the tricritical Ising model as an example. Here, the level 0 basis states are the six primary operators.
To implement the routine detailed in section (3.2), we model the primary states by numbers $1, \cdots, 6$ and store the associated conformal weights as variables $\Delta_1, \cdots, \Delta_6$ as shown in table 3.1.

Primary State	$\|\mathbb{I}\rangle$	$\|\epsilon\rangle$	$\|\epsilon'\rangle$	$\|\epsilon''\rangle$	$\|\sigma\rangle$	$\|\sigma''\rangle$
Representation	1	2	3	4	5	6

Table 3.1: Programmatic representation of primary states

We represent higher level states as partitions of the Virasoro level. For example, the state $|\underline{v}^N\rangle = L_{-k_1}L_{-k_2}...L_{-k_n}|\phi\rangle$ is represented by the partition

$$\{\#\phi, h_{\underline{v}}, \{k_1, k_2, ..., k_n\}\}, \tag{3.36}$$

where $\#\phi$ represents the appropriate numerical representation of the given primary operator ϕ as detailed above and $h_{\underline{v}}$ represents the Virasoro level of the state. For example, the state $L_{-3}L_{-2}\left|\epsilon\right\rangle$ is represented by $\{2, 5, \{3, 2\}\}$.

The ordering on our states will need to be taken into account when constructing such candidate basis elements. We do so by constructing ordered partitions of integers (corresponding to the level).

We can then perform Virasoro operations on our states, such as acting by L_0. For example, $L_0\left|\epsilon\right\rangle$ gives the weight of the state $\left|\epsilon\right\rangle$ which is represented by the partition $\{2, 0, \{\}\}$. Labelling this partition by P, say, this weight is stored in the variable Δ_2 which is accessed via the partition as $\Delta_{P[[1]]} = \Delta_2$ where P[[1]] gives the first element of the partition P. When acting L_0 on the higher level partition $Q = \{2, 5, \{3, 1, 1\}\}$ (which represents the state $|L_{-3}L_{-1}L_{-1}\epsilon\rangle$), we add the Virasoro level of the state to the weight of the associated primary. We access the level directly from the second element of the partition and use the stored variable for the weight as before. As a result, $L_0\left|\epsilon\right\rangle$ will equal $Q[[2]] + \Delta_{Q[[1]]} = 5 + 2$.

At each stage of the algorithm, we pass in two states and calculate the inner products as per our routine. We may do so naively and sequentially using nested loops. However, such loops essentially create a matrix and where possible it is recommended that analytic matrix operations are used for as long as possible throughout the routine to increase performance. For example, matrix multiplication in place of a nested loop multiplication operation. It is also much more efficient, where possible, to construct a function which may be applied to a matrix of states, for example, than to create a routine which carries out the same functionality iteratively using nested loops. Built in functions should of course be used where possible. Doing so can improve performance by a significant amount.

In Appendix C we provide some details of runtimes for the TCSA algorithm in the Ising and tricritical Ising models.

An aside on associations

At this point, we need to consider storage. Instead of using lists to store inner products and overlaps, or assigning values to some nominal function, we will instead use a dictionary or what is known as an association in Mathematica where we assign a key-value pair to each object. It is a way of storing information which can be accessed quickly and easily and is useful for data which is not naturally ordered within a matrix or array.

Associations in Mathematica are based on the Hash Array Map Trie (HAMT), an associative array combining the characteristics of a hash table and a mapped trie. Data is provided in the form of a key-value pair consisting of an expression and associated value. An example Mathematica command is:

$$\text{AssociateTo[innerProductMatrix,}\{\{x,y\}\to 2,\{y,x\}\to 2\}]; \tag{3.37}$$

which may be interpreted as adding the inner products $\langle x|y\rangle = \langle y|x\rangle = 2$ to the association named innerProductMatrix by assigning a value of 2 to the keys $\{x, y\}$ and $\{y, x\}$.

For the purposes of TCSA, speed is a valuable commodity. Here associations have many benefits over more naive ways of data storage with speed of insertion and deletion of order $\mathcal{O}(\log(N))$ and speed of lookup of order $\mathcal{O}(1)$.

However, all this does not come for free. Although scalable to arbitrary size one should bear in mind that associations are rather heavy on memory usage, something which must be considered for TCSA where for example, a basis of order 10,000 can quickly generate a relatively dense association of order $\mathcal{O}(10^8)$ for inner products. In particular, importing large stored associations is very heavy on memory usage.

Chapter 4

General Considerations

In the following chapters, we discuss applications of TCSA to perturbed Conformal Field Theories and present the main body of work of this thesis. First, though, we discuss some general theoretical considerations of the large coupling asymptotics of the TCSA spectrum. Our considerations here are mostly analytic, though they include a dose of heuristics inspired by numerical data.

As described in chapter 3, the main observables in TCSA are the energy levels e_i of the dimensionless Hamiltonian (3.2). These levels are functions of the dimensionless coupling

$$\lambda = \mu L^{1-\Delta^{\mathrm{UV}}}. \tag{4.1}$$

The ground state energy e_0 is divergent in the continuum theory when $\Delta^{\mathrm{UV}} \geq 1/2$ and if we work with raw TCSA data, we focus on the energy gaps $e_i - e_0$ that are independent of this divergence. The values of the gaps $e_i - e_0$ interpolate between the (approximations to) scaling dimensions of the UV and IR fixed points. While in the continuum theory the IR fixed point is located at an infinite value of the coupling, in TCSA we get the closest approach to the IR BCFT at some finite value which depends on Δ_{max}. The main signature of this approach is the near crossing of the gaps $e_i - e_0$ that can be matched with the Virasoro multiplicities in the IR BCFT.

In a continuum renormalised theory, if we start out in the UV by perturbing a boundary CFT by a boundary field of dimension Δ^{UV} the corresponding coupling

μ of dimension $(\text{mass})^{1-\Delta^{\text{UV}}}$ sets an energy scale

$$E_\mu = (\mu)^{\frac{1}{1-\Delta^{\text{UV}}}} . \tag{4.1}$$

Near the infrared fixed point described by a BCFT with the Virasoro dilation operator L_0^{IR} we expect the theory to be described by an effective Hamiltonian of the form

$$h^{\text{IR}} = L_0^{\text{IR}} + C_1 \mu^{-t_1} L\phi_1^{\text{IR}}(0) + C_2 \mu^{-t_2} L\phi_2^{\text{IR}}(0) + \dots \tag{4.2}$$

where ϕ_i^{IR} stand for irrelevant operators with scaling dimensions $\Delta_1^{\text{IR}} < \Delta_2^{\text{IR}} < \dots$ inserted at $\sigma = 0, \tau = 0$. The operator ϕ_1^{IR} is the leading irrelevant operator. Matching the dimensions implies

$$t_i = \frac{\Delta_i^{\text{IR}} - 1}{1 - \Delta^{\text{UV}}} . \tag{4.3}$$

We can also rewrite (4.2) in terms of the dimensionless coupling:

$$h^{\text{IR}} = L_0^{\text{IR}} + C_1 \lambda^{-t_1} V_1^{\text{IR}} + C_2 \lambda^{-t_2} V_2^{\text{IR}} + \dots \tag{4.4}$$

where $V_i^{\text{IR}} = \phi_i(0) L^{\Delta_i^{\text{IR}}}$ are dimensionless operators. It should be said that in the subleading terms starting with V_2 the simple power functions λ^{-t_i} can be decorated by logarithms (see e.g. [73]) but we do not expect this to happen at the leading irrelevant term.

It follows from (4.4), using perturbation theory, that for large λ the energy gaps should behave as

$$e_i - e_0 = \Delta_i^{\text{IR}} + A_i \lambda^{-t_1} + \dots \tag{4.5}$$

where A_i are some constants and the ellipsis stands for subleading terms suppressed by larger inverse powers of λ.

Consider now the same perturbed BCFT regulated by level truncation. Numerical results show that the energy levels approach the dimensions of the IR fixed point in a neighbourhood of some finite reference value of the coupling λ^*. This value depends both on the truncation parameter $\Delta_{\max}$ and on the energy level. We assume that we focus on some particular band of low lying energies which all approach the

dimensions of the IR fixed point in a neighbourhood of λ^*. We expect truncation errors to modify (4.5). Heuristically we can assume that (4.5) is replaced by

$$e_i - e_0 = \Delta_i^{\mathrm{IR}} + (\lambda - \lambda^*)A_i^{(-1)} + A_i\lambda^{-t_1} + \dots \tag{4.6}$$

Here the first term is small when λ is near λ^* but is linearly growing when λ deviates from that value. The linearity of this correction is motivated by the fact that in the truncated Hamiltonian both the unperturbed Hamiltonian and the perturbation are finite matrices and for large λ the perturbed eigenvalues become approximately linear in λ. The numerical coefficients $A_i^{(-1)}$ and A_i can be expected to depend on $\Delta_{\max}$. In particular $A_i^{(-1)}$ should be suppressed by inverse powers of $\Delta_{\max}$.

To describe the above corrections at the Hamiltonian level we assume that the following relation holds for matrices on the truncated Hilbert space

$$h = L_0^{\mathrm{UV}} + \lambda V^{UV} = e^{T(\lambda)}(L_0^{\mathrm{IR}} + f_1(\lambda)V_1^{\mathrm{IR}} + f_2(\lambda)V_2^{\mathrm{IR}} + \dots)e^{-T(\lambda)} \tag{4.7}$$

where, as in (4.4), the matrices V_i come from local irrelevant operators of the IR fixed point and $T(\lambda)$ is an anti-hermitian matrix so that $e^{T(\lambda)}$ is a unitary operator (for each λ). Furthermore the functions $f_i(\lambda)$ are expected to be small whenever $|\lambda - \lambda^*| < \rho$ for some ρ. It should be stressed that we consider only a number of low energy eigenvalues and treat the representation in (4.7) above only as an effective Hamiltonian for the low lying energy levels.

Assuming that in the $\Delta_{\max} \to \infty$ limit we recover the field theory expansion (4.4) we can write

$$f_i(\lambda) = \tilde{f}_i(\lambda - \lambda^*) + C_i\lambda^{-t_i} \tag{4.8}$$

where the functions $\tilde{f}_i(\lambda - \lambda^*)$ are small for $|\lambda - \lambda^*| < \rho$ and are suppressed by inverse powers of $\Delta_{\max}$. In this picture whenever f_i are small enough the eigenvalues of h can be approximated by first order perturbation theory around the eigenvalues of L_0^{IR} and thus will have approximately the same functional form as (4.8). In particular they may have a linearly growing term as in (4.6). If we are outside the infrared fixed point dominance region, given by $|\lambda - \lambda^*| < \rho$, perturbation theory will no longer work and the energy curves $e_i(\lambda)$ may significantly deviate from the IR fixed

point values. If the function $\tilde{f}_1(\lambda - \lambda^*)$ is positive and growing while $C_i < 0$ then[1] for some $\lambda = \lambda^{**}$ the function f_1 will vanish and then change sign. If near λ^{**} the leading irrelevant coupling f_1 changes faster than the subleading ones and the latter remain small then this regime can be *perturbatively* described as a reflected RG flow where we perturb the IR fixed point by V_1 with the opposite sign of the coupling which grows in magnitude with λ.

We have argued above that the linearity of the leading truncation correction in (4.6) could be explained from the asymptotic linearity of the eigenvalues at large λ. The slopes $A_i^{(-1)}$ would then be given by the differences of the corresponding eigenvalues of the interaction matrix $V^{\rm UV}$. This is certainly true for very large values of λ. However, in numerical data to be presented later in the paper, we observe several approximately linear regimes past the vicinity of the physical IR fixed point at $\lambda = \lambda^*$, before the linear regime described by the domination of $V^{\rm UV}$ is reached. Each of these approximately linear regimes has its own set of slopes. We will discuss these regimes, related to what we call flows beyond, in detail, in chapter 6. Here we would like to refine our simple explanation for the linearity, using relation (4.7) between the effective Hamiltonians. We will argue that, under certain additional assumptions to be spelled out shortly, the functions $e_i(\lambda)$ are approximately linear near λ^{**}. To that end differentiate both sides of (4.7) and set $\lambda = \lambda^{**}$. This gives us

$$V^{\rm UV} = e^{T(\lambda^{**})}([T'(\lambda^{**}), L_0^{\rm IR} + f_1(\lambda^{**})V_1^{\rm IR} + \dots] + f_1'(\lambda^{**})V_1^{\rm IR} + \dots)e^{-T(\lambda^{**})} \quad (4.9)$$

where ellipses stand for contributions of subleading irrelevant operators. Substituting this back into the left hand side of (4.7) we rewrite the Hamiltonian as

$$\begin{aligned} h &= L_0^{\rm UV} + \lambda V^{UV} = (L_0^{\rm UV} + \lambda^{**} V^{UV}) + (\lambda - \lambda^{**})V^{\rm UV} \\ &= e^{T(\lambda^{**})}(L_0^{IR} + g_1(\lambda)V_1^{\rm IR} + g_2(\lambda)V_2^{\rm IR} + \dots \\ &+ (\lambda - \lambda^{**})[T'(\lambda^{**}), L_0^{\rm IR} + f_1(\lambda^{**})V_1^{\rm IR} + f_2(\lambda^{**})V_2^{\rm IR} \dots])e^{-T(\lambda^{**})} \end{aligned} \quad (4.10)$$

[1] $C_i < 0$ is the case when the energies approach the fixed point values from below as in the Ising and tricritical Ising boundary flows to be discussed later in chapter 5.

where

$$g_1(\lambda) = (\lambda - \lambda^{**}) f_1'(\lambda^{**}) \,, \quad g_i(\lambda) = f_i(\lambda^{**}) + (\lambda - \lambda^{**}) f_i'(\lambda^{**}) \,, \;\; i > 1 \,. \tag{4.11}$$

Here we used the assumption that $f_1(\lambda^{**}) = 0$.

If the generator of unitary rotations, $T(\lambda)$, can be expanded in local operators then the commutator term can also be expanded in local operators and we get a local expansion in operators[2] V_i^{IR} with modified functions $g_i(\lambda)$ that are again linear in λ. Alternatively the commutator term may be negligibly small in the vicinity of λ^{**} if the functions $g_i(\lambda)$ change more rapidly than $T(\lambda)$. We will assume that one of these two scenarios is realised and we can neglect the commutator terms. This implies that we have linear trajectories in the space of IR Hamiltonians parametrised by the IR couplings g_i given by (4.11) where g_1 vanishes at λ^{**}.

Assuming that near λ^{**} all irrelevant couplings g_i are small with g_1 still dominating we have the second perturbative regime described by a reflected flow with g_1 of the opposite sign to that of the physical approach to the fixed point, and changing linearly with λ. In that region the energy gaps $e_i - e_0$ are also changing linearly with the coupling[3]. We offer this scenario as a tentative explanation of the approximately linear regime of $e_i - e_0$ that we find in the numerical results immediately past the point of closest approach to the IR fixed point. The above discussion is illustrated on Fig. 4.1. It should be noted in regard to this picture that although in the space of g_i couplings the point λ^* appears to be far from the obvious fixed point $g_i = 0$, due to the action of unitary transformations it is actually close to it.

[2]Also we should mention that there is a possibility of switching on a relevant operator with a coupling suppressed by $\Delta_{\max}$. For the $\psi_{1,3}$ flows we consider in the tricritical and in the critical Ising models the IR fixed points do not have any relevant operators so, for simplicity, in our general discussion we assume they are absent.

[3]Unless there is some symmetry that forces the diagonal matrix elements of V_1 to vanish in which case the perturbative expansion starts with some power λ^n with $n > 1$.

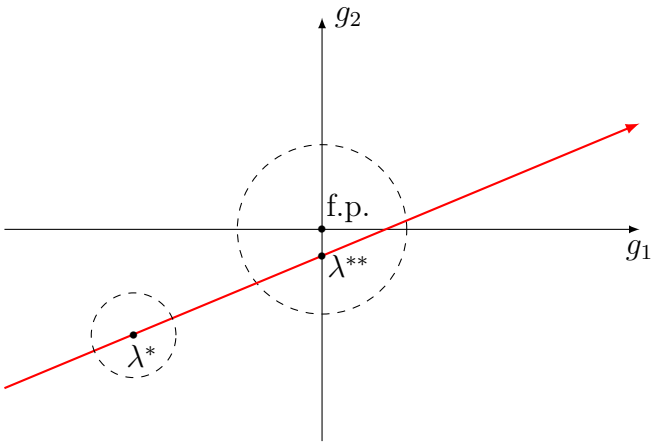

Figure 4.1: A sample TCSA trajectory in $\{g_i\}$-space. Two perturbative regimes are marked by circles.

It is important to note that the effective IR Hamiltonians appearing on the right hand sides of (4.7) and (4.10) are finite matrices defined in the truncated Hilbert space of the UV fixed point. At the IR fixed point this truncation is representable by some *different*, complicated truncation prescription. Thus if we were to write (4.7) or (4.10) in the continuum theory representing the IR CFT, each operator ϕ_i^{IR} would be represented in some complicated truncation regularisation. If the latter still respects locality it can be modelled in the continuum theory by writing out an expansion of the regulated operators in a series of continuum irrelevant operators with coefficients suppressed by Δ_{max}.

The above arguments along with the numerical data to be considered in the forthcoming sections prompt us to formulate a working hypothesis: the flows beyond are generated by the leading irrelevant perturbation, V_1^{IR}, along which the original RG flow approaches the IR fixed point, with the opposite sign of the coupling. This coupling grows linearly with the original coupling λ in a neighbourhood of some value $\lambda = \lambda^{**}$. Here we also assume that the higher dimension irrelevant operators can be neglected and that some particular truncation scheme is used at the infrared fixed point to model the flows beyond. We will test this working hypothesis in sections 6.3 - 6.4.

Chapter 5

Approach to the IR Fixed Point

In the preceding chapters, we have outlined the relevant background material of (boundary) Conformal Field Theory and the Renormalisation Group and introduced the Truncated Conformal Space Approach, outlining the technical procedure for its numerical implementation. We take this machinery and apply it now, in earnest, in what is the main focus of this thesis.

TCSA has been applied to a variety of models to obtain non-perturbative information of various types matching with good accuracy to analytic results when available. We refer the reader to [61] for a review of the method and results obtained. While TCSA has proven to be largely successful, it would be fair to say there is no good understanding of why the method works so well. The question of error estimates related to the finite truncation level has been addressed in a number of papers (see [53], [55], [58], [59], [60] and references therein). Those papers focus on the regime where the ratio of the characteristic energy scale set by the coupling to the truncation level is small and a perturbative expansion in this ratio is possible. While a good theoretical understanding has been achieved for that regime, that work does not shed much light on a very high coupling regime, in particular the regime where the system approaches an IR point. In this thesis we focus on the TCSA behaviour for very large couplings where analytic control of truncation errors is currently out of reach.

The study takes two main approaches, both in this strong coupling regime:

1. Investigations into the approach to the IR fixed point.
2. Investigations into further flows beyond the IR fixed point.

In our first application of TCSA, we analyse the spectrum of perturbed boundary conformal field theories on approach to the IR fixed point. Perturbed BCFTs provide a useful testing ground for such studies in that they always arrive at non-trivial fixed points containing at least the identity tower in its IR spectrum. We investigate the infrared exponents related to the leading irrelevant operator along which the system enters the fixed point. We describe some general methods of extracting these exponents from numerical data and test them for the examples of boundary flows in the perturbed Ising and tricritical Ising models which are introduced here in detail.
In chapter 6, we discuss our second application of TCSA: Flows beyond the IR fixed point.

5.1 The perturbed Ising model

5.1.1 Ising model with a boundary magnetic field

A particularly simple example amenable to analytic control is the critical Ising model with a boundary magnetic field [62–68]. The critical Ising model in the bulk is described by free massless Majorana fermions ψ, $\bar{\psi}$. On the upper half plane $\{(x, y)|y \geq 0\}$ with complex coordinate $z = x + iy$ the model admits two conformal boundary conditions: $\psi(z) = \bar{\psi}(\bar{z})$, $z = \bar{z}$ that corresponds to having the boundary spin fluctuating freely, and $\psi(z) = -\bar{\psi}(\bar{z})$, $z = \bar{z}$ that describes keeping the boundary spin fixed (up or down). We will use the notation: $(+)$, $(-)$, (f) for the spin up, spin down and free boundary condition respectively.

To describe the doubly degenerate vacuum on the half plane we introduce, following [62], [63], a boundary fermion $a(x)$ with a two point function

$$\langle a(x)a(x')\rangle = \mathrm{sign}(x - x')\,. \tag{5.1}$$

The boundary spin operator $\sigma_{\mathrm{B}}(x)$ is then given by

$$\sigma_{\mathrm{B}}(x) = ia(x)(\psi(x) + \bar{\psi}(x))\,. \tag{5.2}$$

In boundary CFT language this is a primary boundary field of dimension 1/2 that lives on the free boundary condition. We can perturb the latter by this field with a coupling h that gives the value of a boundary magnetic field. The resulting Lagrangian is

$$S = \frac{1}{2\pi}\int_{-\infty}^{\infty} dx \int_{0}^{\infty} dy\ [\psi\bar{\partial}\psi + \bar{\psi}\partial\bar{\psi}] + \int_{-\infty}^{\infty} dx \Big[-\frac{i}{4\pi}\psi\bar{\psi} + \frac{1}{2}a\partial_x a + iha(\psi + \bar{\psi})\Big]. \quad (5.3)$$

To describe this model in TCSA we put it on an infinite strip $\{(\sigma,\tau)|0 \le \sigma \le L\}$ of width L. It is related to the upper half plane by a conformal mapping $w = (L/\pi)\ln z$ where $w = \tau + i\sigma$. We put the free boundary condition on the lower end of the strip: $\sigma = 0$. This is the end we perturb by the boundary magnetic field. For the spectator boundary condition at the other end, at $\sigma = L$, we can choose either the free or fixed boundary condition.

In Hamiltonian quantisation with euclidean time τ, a free spectator corresponds to having Neveu-Schwarz (NS) fermions with mode expansions

$$\psi(w) = \sqrt{\frac{\pi}{L}}\sum_{k=0}^{\infty}\Big[e^{-\frac{(k+1/2)\pi}{L}(\tau+i\sigma)}a_{k+1/2} + e^{\frac{(k+1/2)\pi}{L}(\tau+i\sigma)}a^{\dagger}_{k+1/2}\Big],$$

$$\bar{\psi}(w) = \sqrt{\frac{\pi}{L}}\sum_{k=0}^{\infty}\Big[e^{-\frac{(k+1/2)\pi}{L}(\tau-i\sigma)}a_{k+1/2} + e^{\frac{(k+1/2)\pi}{L}(\tau-i\sigma)}a^{\dagger}_{k+1/2}\Big] \quad (5.4)$$

where $a_{k+1/2}$, $a^{\dagger}_{k+1/2}$ satisfy canonical anti-commutation relations. The boundary fermion field $a(\tau)$ gives rise to a single fermionic mode a satisfying $a^2 = 1$. The corresponding Hamiltonian reads

$$H^{\mathrm{NS}} = \frac{\pi}{L}\Big[\sum_{k=0}^{\infty}(k+1/2)a^{\dagger}_{k+1/2}a_{k+1/2} - \frac{1}{48} + i\alpha\sum_{k=0}^{\infty}(a^{\dagger}_{k+1/2} + a_{k+1/2})a\Big] \quad (5.5)$$

where

$$\alpha = h\sqrt{\frac{\pi}{L}} \quad (5.6)$$

is a dimensionless coupling. The Hamiltonian (5.5) is defined on a physical subspace

of the Fock space spanned by the basis vectors

$$a^\dagger_{k_1+1/2}a^\dagger_{k_2+1/2}\dots a^\dagger_{k_N+1/2}|0\rangle \quad N- \text{ even},\ \ k_1>k_2>\dots>k_N\,,$$

$$a^\dagger_{k_1+1/2}a^\dagger_{k_2+1/2}\dots a^\dagger_{k_N+1/2}|a\rangle \quad N- \text{ odd},\ \ k_1>k_2>\dots>k_N \tag{5.7}$$

where $|0\rangle$ is the Fock space vacuum and $|a\rangle = a|0\rangle$. The physical space contains two irreducible representations of the Virasoro algebra: the identity tower spanned by the states with even numbers of oscillators and the ϵ-tower spanned by the states with odd numbers of oscillators.

Similarly, choosing a fixed spin spectator at $\sigma = L$ gives rise to Ramond fermions with mode expansions

$$\psi(w) = \sqrt{\frac{\pi}{L}}\sum_{n=1}^{\infty}\Big[e^{-\frac{n\pi}{L}(\tau+i\sigma)}b_n + e^{\frac{n\pi}{L}(\tau+i\sigma)}b_n^\dagger + b_0\Big]\,,$$

$$\bar\psi(w) = \sqrt{\frac{\pi}{L}}\sum_{n=1}^{\infty}\Big[e^{-\frac{n\pi}{L}(\tau-i\sigma)}b_n + e^{\frac{n\pi}{L}(\tau-i\sigma)}b_n^\dagger + b_0\Big] \tag{5.8}$$

where b_n, $b_n^\dagger$ satisfy the canonical anti-commutation relations with the zero mode normalised so that $b_0^2 = 1/2$. The Hamiltonian in this case is

$$H^{\rm R} = \frac{\pi}{L}\Big(\sum_{n=1}^{\infty} n b_n^\dagger b_n + \frac{1}{24} + i\alpha[\sum_{n=1}^{\infty}(b_n^\dagger + b_n) + b_0]a\Big) \tag{5.9}$$

and the basis in the physical subspace of the Fock space can be chosen as

$$b^\dagger_{n_1}b^\dagger_{n_2}\dots b^\dagger_{n_M}|\sigma\rangle \quad M- \text{ even},\ \ n_1>n_2>\dots>n_M>0\,,$$

$$b^\dagger_{n_1}b^\dagger_{n_2}\dots b^\dagger_{n_M}|\mu\rangle \quad M- \text{ odd},\ \ n_1>n_2>\dots>n_M>0 \tag{5.10}$$

where $|\sigma\rangle$ is the Fock state vacuum and $|\mu\rangle = -ia|\sigma\rangle$. This space furnishes a single Virasoro tower of the primary state $|\sigma\rangle$ with weight 1/16. The zero mode acts on the vacuum as

$$b_0|\sigma\rangle = \frac{1}{\sqrt{2}}|\mu\rangle\,. \tag{5.11}$$

For each choice of spectator boundary condition the Hamiltonian can be diagonalised

by a Bogolyubov transformation [66], [68][1]. The diagonalising modes $b^\dagger_{\alpha,i}$ carry energies ω_i that are non-negative solutions to a transcendental equation that for the free spectator reads as

$$\tan(\pi\omega) = -\frac{\omega}{2\pi\alpha^2} \tag{5.12}$$

and for a fixed spectator as

$$\tan(\pi\omega) = \frac{2\pi\alpha^2}{\omega}\,. \tag{5.13}$$

The spectral equation (5.12) is plotted for multiple values of the coupling in Fig. 5.1 where the solutions ω_i are the points of intersection. For $\alpha \to \pm\infty$ solutions to (5.12) interpolate between half-integers at $\alpha = 0$ and integers at $\alpha = \pm\infty$. The energy eigenstates are obtained by acting on the perturbed vacuum $|0\rangle_\alpha$ by an even number of raising operators $b^\dagger_i$. At the endpoints $\alpha = \pm\infty$ we thus have the usual physical space of Ramond fermions and the model describes a flow from free to fixed boundary condition in the far infrared. It is completely symmetric under changing the sign of α. The latter specifies the infrared boundary condition to be spin up or down. The boundary fermion a is absorbed into the zero mode $b^\dagger_0$.

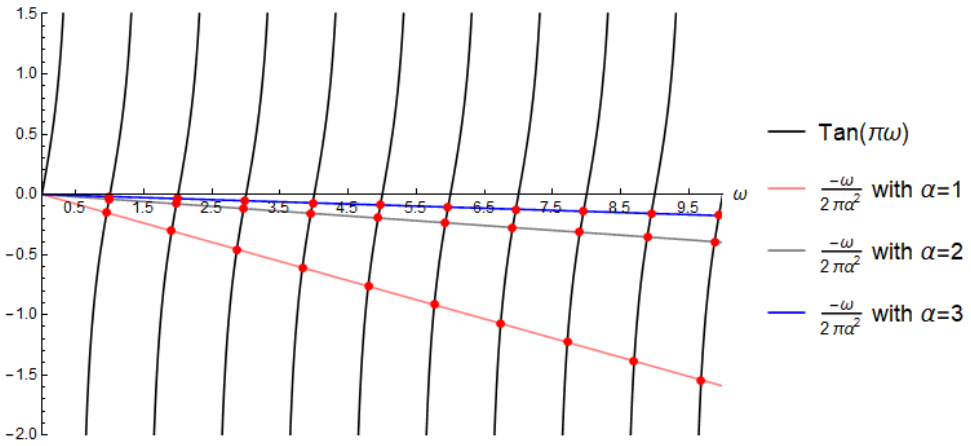

Figure 5.1: NS Sector (free spectator) solutions to spectral equation (5.12) for non-zero positive coupling.

For the fixed spectator the spectral equation (5.13) interpolates between integer solutions at $\alpha = 0$ and the half-integer ones at $\alpha = \pm\infty$. The physical spectrum however depends on the sign of α. For negative α the Fock space vacuum $|0\rangle_\alpha$ with respect to the diagonalising oscillators does not belong to the physical space and thus the physical vacuum is $b^\dagger_{\alpha,1}|0\rangle_\alpha$ where $b^\dagger_{\alpha,1}$ is the creation operator for the lowest

[1]More information on Bogolyubov transformations can be found in section 6.2.

excitation energy ω_1. The physical space for $\alpha \to -\infty$ contains a single Virasoro tower of the ϵ representation and describes the state space with the opposite direction fixed boundary conditions on the two ends of the strip. For positive α the physical vacuum coincides with the Fock space vacuum and in the limit $\alpha \to \infty$ we obtain the Virasoro tower of the identity field that describes the fixed spin boundary condition with the same direction on the two ends.

It was shown in [66] that the perturbed boundary condition approaches the infrared fixed point along the leading irrelevant operator, the stress energy tensor T. More precisely the leading effective Hamiltonian near $\alpha = \infty$ is

$$h_{\text{eff}}^{\text{lead}} = \frac{1}{24} + \sum_{k=1}^{\infty} k\, b_k^\dagger b_k - \frac{g}{2} : \left(\left[\sum_{k=1}^{\infty} (b_k^\dagger + b_k) + b_0 \right] \sum_{l=1}^{\infty} l(b_l^\dagger - b_l) \right) : \tag{5.14}$$

with

$$g = -\frac{1}{2\pi^2\alpha^2}\,. \tag{5.15}$$

The subleading terms in the effective Hamiltonian are discussed in [68]. The leading exponent shows up in the asymptotic behaviour of the perturbed energy levels. From (5.13) we obtain a large α expansion for the fixed spectator

$$\omega_k = (k-1/2)(1 - \frac{1}{2\pi\alpha^2} + \frac{1}{(2\pi\alpha^2)^2} + \frac{1}{(2\pi\alpha^2)^3}[\frac{\pi^2}{3}(k-1/2)^2 - 1] + \dots) \tag{5.16}$$

where the missing terms are of the order $1/\alpha^8$. A similar expansion can be worked out for the excitation energies in the case of a free spectator with the leading correction to integer values being of the order of $1/\alpha^2$.

5.1.2 TCSA in the Ising model. Approach to fixed point.

For the Ising model with a boundary magnetic field, for the case of a fixed spectator (Ramond fermions) there is only one primary tower whereas for the case of the free spectator described by NS-fermions we have two primary fields. The dimensions of the truncated state space for the free and fixed spectators are displayed in the Appendix A.1. Later we will also use modified truncation schemes of the type (3.5) labelled by N^1_{max} and N^ϵ_{max} – the bounds for descendant levels in the identity and the energy density towers.

In this section we concentrate on the approach to the fixed point in the boundary magnetic field model. Below, on Fig. 5.2 , are the plots of the dimensionless energy gaps $e_i - e_0$ for the first 14 excited energy levels.

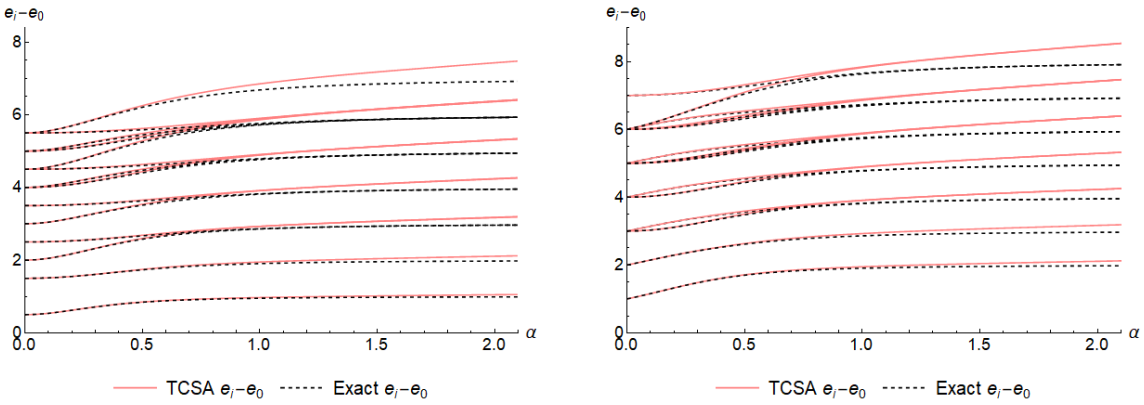

(a) NS Sector (free spectator). $e_i - e_0$ versus α for $\Delta_{\max} = 38$.

(b) Ramond Sector (fixed spectator). $e_i - e_0$ versus α for $\Delta_{\max} = 40$.

Figure 5.2

On these plots we also put the exact solutions (dashed lines). In the first plot we observe that the TCSA energy gaps remain close to the exact solutions until the onset of the asymptotic regime corresponding to the IR fixed point which is marked by levelling of the energy curves and by the change in the multiplicities of the energy levels. Qualitatively, although we do not get the exact degeneration (that in the exact solution also happens only asymptotically at infinite coupling), we clearly see the levels merging giving the degeneracies of the expected IR fixed point described by Ramond fermions. The point at which this merging occurs depends on $\Delta_{\max}$ with larger values of this cutoff corresponding to larger α_*, the best approximation of the coupling value at which the fixed point is reached. The value of α_* can more accurately be determined for a few low lying energy levels, where TCSA is most effective. While the levels initially converge, as we increase the coupling they start diverging from each other and at the same time the TCSA curves start deviating from the exact solutions. The latter have horizontal asymptotes, with the corrections following the expansion (5.16), while the TCSA gaps become, to a good approximation, linear with the coupling with positive slopes. The higher energy level we take the smaller are the values of α at which deviation from the exact solution starts. Similar behaviour is observed in the second plot.

As explained in chapter 4 we expect the energy levels to behave approximately as

$$e_i - e_0 \approx \Delta_i^{\mathrm{IR}} + (\alpha - \alpha_*)A_i^{(-1)} + \frac{A_i^{(2)}}{\alpha^t} + \dots \tag{5.17}$$

where the continuum theory prediction based on (5.14) is $t = 2$. In principle one may expect a more general modification of the form

$$e_i - e_0 \approx \Delta_i^{\mathrm{IR}} + (\alpha - \alpha_*)A_i^{(-1)} + \frac{A_i^{(1)}}{\alpha} + \frac{A_i^{(2)}}{\alpha^2} + \dots \tag{5.18}$$

where the coefficients $A_i^{(-1)}$, $A_i^{(1)}$, $A_i^{(2)}$ depend on $\Delta_{\max}$ and the ellipses stand for the terms suppressed by higher powers of α. To reproduce the continuum results the coefficients $A_i^{(-1)}$, $A_i^{(1)}$ can both be expected to be suppressed by powers of $\Delta_{\max}$ while $A_i^{(2)}$ should be constant up to terms suppressed by powers of $\Delta_{\max}$. It is quite hard to extract next to leading order power corrections from numerical data so we are going to test the simpler ansatz (5.17). If we subtract the linear part in some way then we can estimate t from the numerical data.

As mentioned before, the linear part in (5.17), which ultimately takes the energy levels away from the fixed point, could be related to the domination of the truncated interaction matrix V. Since in TCSA we are dealing with a finite matrix of the form $h = L_0 + \alpha V$, when α is large enough the interaction matrix V dominates and the eigenvalues are well approximated by α times the eigenvalues of V. So that the $\alpha \to \pm\infty$ behaviour is definitely linear. To test this idea we plot on Fig. 5.3 the quantity $e_1 - e_0 - s\alpha$ where s is the difference of the two lowest eigenvalues of V. We note that the two lowest eigenvalues for the free spectator with integer $\Delta_{\max}$ are degenerate and hence, we plot only the unmodified spectrum.

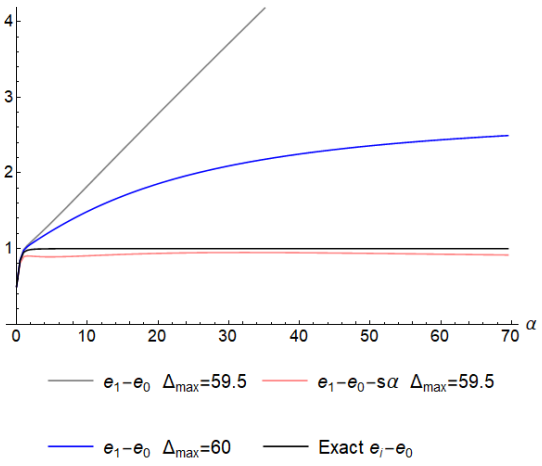

(a) $e_1-e_0-s\alpha$ vs $\alpha > 0$ with s given by the interaction matrix eigenvalues for the free spectator for $\Delta_{\max} = 59.5$ and $\Delta_{\max} = 60$.

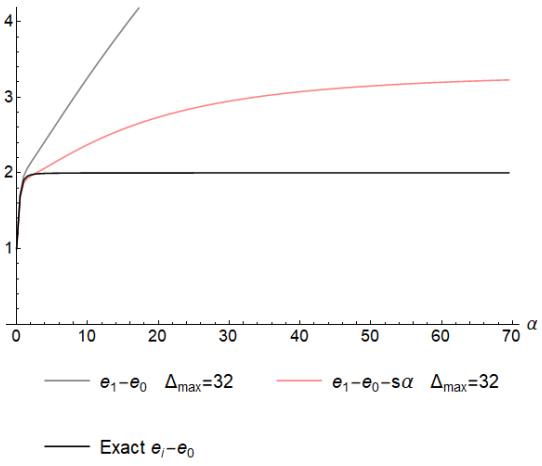

(b) $e_1 - e_0 - s\alpha$ vs $\alpha > 0$ with s given by the interaction matrix eigenvalues for the fixed spectator with $\Delta_{\max} = 32$.

Figure 5.3

The plots show that for larger values of α the energy gap flattens and the interaction matrix dominates as expected. Zooming in to the region near the fixed point, we observe that there is a residual difference between s and the slope of $e_1 - e_0$ near the fixed point. There are thus *two different regimes* in which the energy gaps are approximately linear with the first regime being near the appearance of the physical IR fixed point while the second regime where eigenvalues of V dominate can be related to the flow beyond which we are going to discuss in detail later.

To estimate t from numerical data we use two slightly different procedures. In the first method we calculate numerically

$$\mathcal{D}^1_s(e_1 - e_0) \equiv \alpha \frac{d}{d\alpha} \ln \left(\alpha \frac{d}{d\alpha} [e_1(\alpha) - e_0(\alpha) - s\alpha] \right) \tag{5.19}$$

where $e_i(\alpha)$ are the dimensionless TCSA energy levels and s is a numerically obtained slope of the function $e_1(\alpha) - e_0(\alpha)$ past $\alpha = \alpha_*$. As we do not have a good understanding of the linearity in α of the leading truncation correction we are going to use two different prescriptions for s: taking the difference of the two lowest eigenvalues of the interaction matrix and using a regression analysis for TCSA numerics near the appearance of the IR fixed point.

In the second method we subtract the linear part by applying an additional

differential operator $1 - \alpha d/d\alpha$:

$$\mathcal{D}^2(e_1 - e_0) \equiv \alpha \frac{d}{d\alpha} \ln \left(\alpha \frac{d}{d\alpha} (1 - \alpha \frac{d}{d\alpha})[e_1(\alpha) - e_0(\alpha)] \right) . \tag{5.20}$$

These differential operators are chosen so that substituting into them a function of the form (5.17), we obtain $-t$. In the presence of subleading terms we expect this to be approximately true so that the function changes slowly near the value $-t$.

Using the first method and taking s from the interaction matrix we obtain the plots for each choice of spectator and different truncation levels presented on Fig. 5.4 and Fig. 5.5.

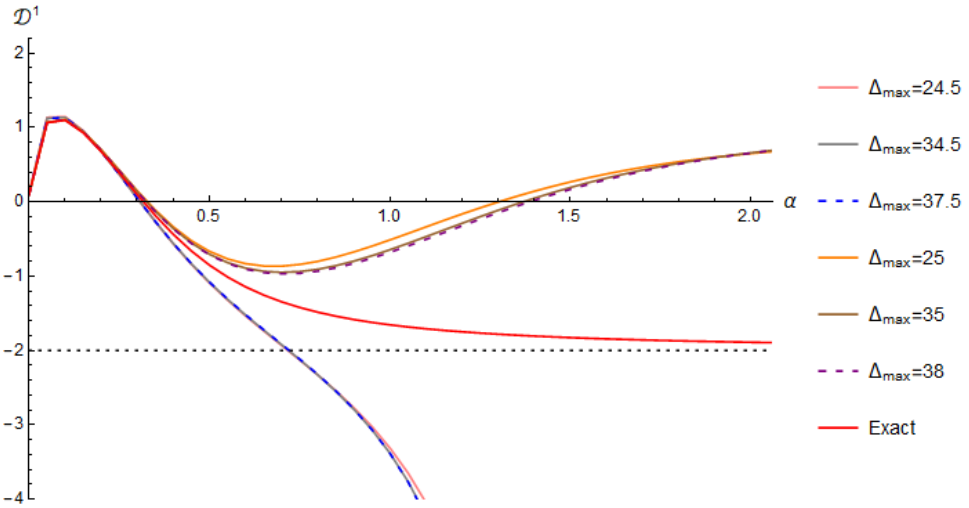

Figure 5.4: $\mathcal{D}^1_s(e_1 - e_0)$ versus $\alpha > 0$ for the free spectator. Linear term removed using interaction matrix eigenvalues.

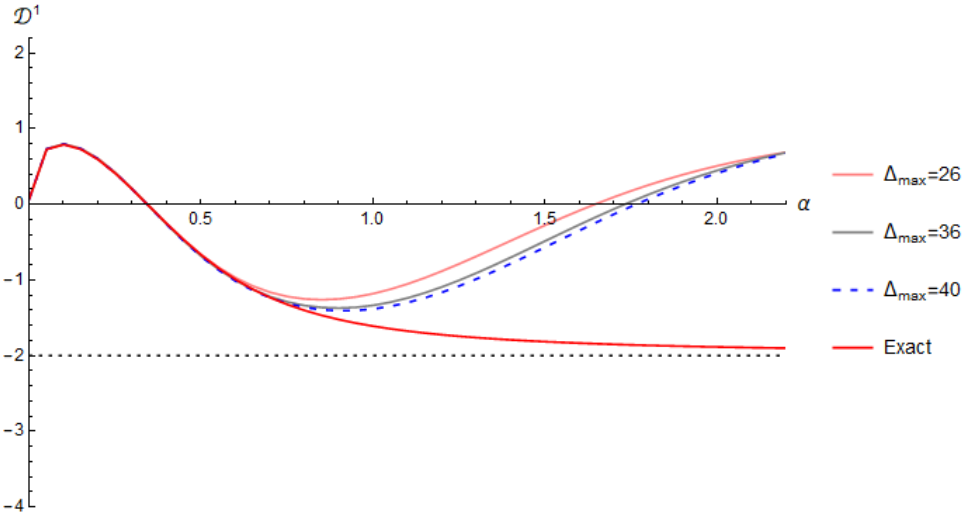

Figure 5.5: $\mathcal{D}^1_s(e_1 - e_0)$ versus $\alpha > 0$ for the fixed spectator. Linear term removed using interaction matrix eigenvalues.

For the fixed spectator and for integer $\Delta_{\max}$ in the free spectator case we see that the curve for $\mathcal{D}_s^1(e_1 - e_0)$ has a minimum descending towards $t = -2$ as we increase $\Delta_{\max}$. For the free spectator the curves for half-integer $\Delta_{\max}$ form a separate band and instead of a minimum they have an inflection point. Increasing the coupling past the minimum or inflection point we arrive to the region approximately between $\alpha = 2$ and $\alpha = 4$ (not displayed in the above plots) where the curve flattens again around the value $t = 1$. The same flattening near the value $t = 1$ also occurs for the fixed spectator and for the free spectator with integer $\Delta_{\max}$. This points to an approximately linear regime past the appearance of the IR fixed point. If we read off the slope numerically (via regression analysis) in that region and use it for the value of s we obtain the plots presented on Fig. 5.6 and 5.7.

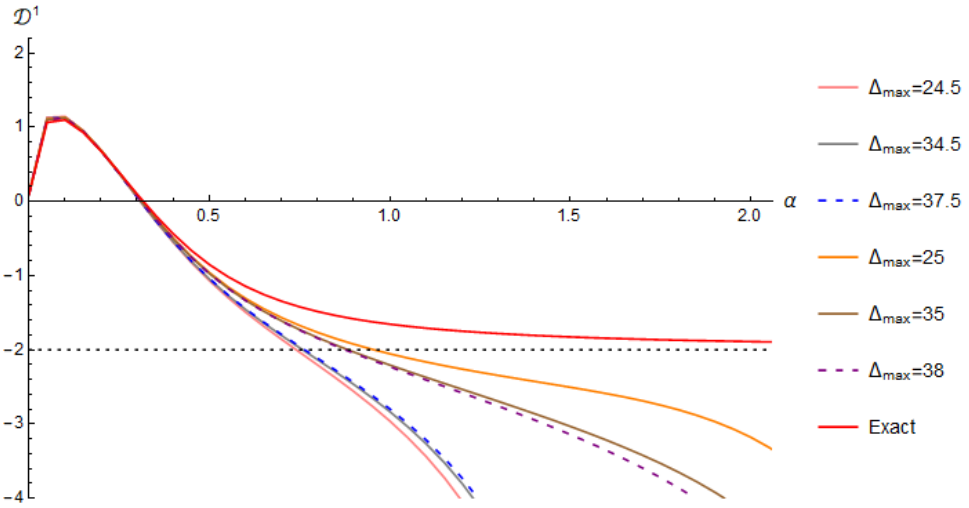

Figure 5.6: $\mathcal{D}_s^1(e_1 - e_0)$ versus $\alpha > 0$ for the free spectator. Linear term removed using regression analysis on the interval $2 < \alpha < 4$.

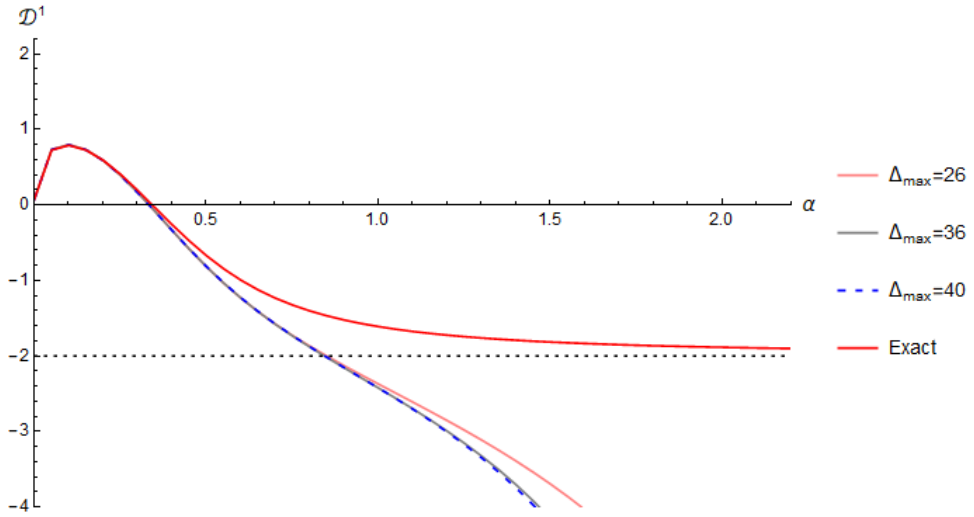

Figure 5.7: $\mathcal{D}_s^1(e_1 - e_0)$ versus $\alpha > 0$ for the fixed spectator. Linear term removed using regression analysis on the interval $2 < \alpha < 4$.

The region where the curve for $\mathcal{D}_s^1(e_1 - e_0)$ flattens now looks like a region near an infection point for both spectators and all truncation levels. These regions are closer to the theoretical value $t = -2$ than with the previous choice of s. In chapter 4 we discussed why such a linear regime occurs past the closest approach to the IR fixed point.

For the second method that uses (5.20) we first present the results for the free spectator on Fig. 5.8.

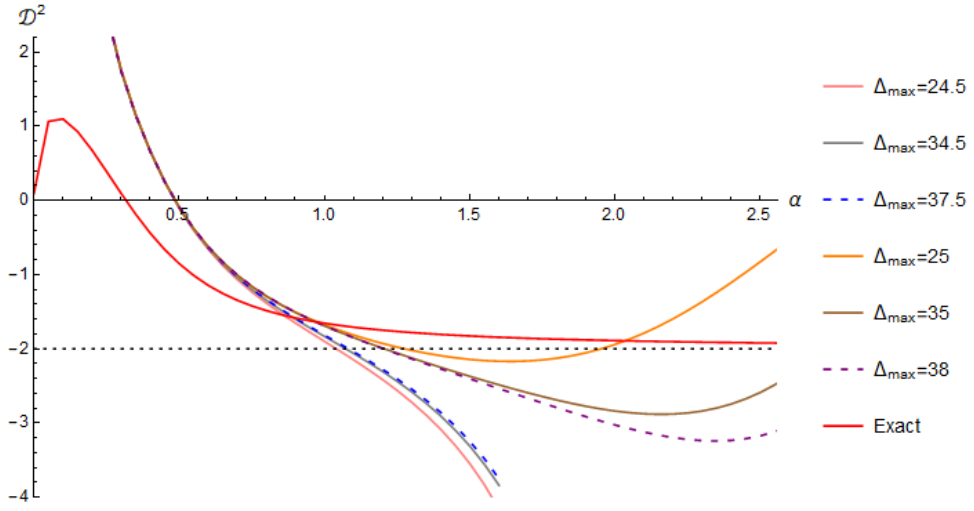

Figure 5.8: $\mathcal{D}^2(e_1 - e_0)$ versus $\alpha > 0$ for the free spectator.

Again we observe a qualitatively different behaviour for integer and non-integer $\Delta_{\max}$. For integer $\Delta_{\max}$ the $\mathcal{D}^2(e_1 - e_0)$ curves have an approximate inflection

point. These inflection points are not easily discerned from the plots but are found numerically and become more pronounced on increasing the truncation. Also they have a minimum for larger values of α. It is interesting to note that such qualitative differences are not visible when looking at the $e_i - e_0$ curves.

For the fixed spectator the plot is presented on Fig. 5.9.

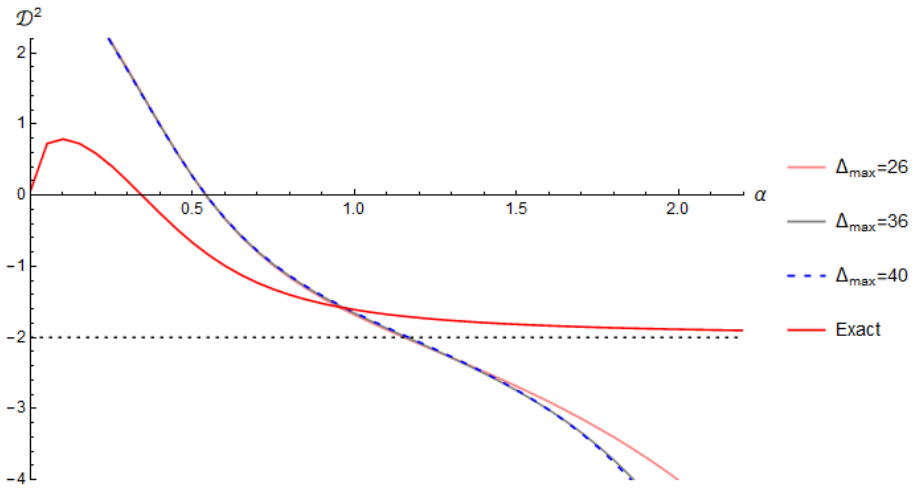

Figure 5.9: $\mathcal{D}^2(e_1 - e_0)$ versus $\alpha > 0$ for the fixed spectator.

For all three methods we observe a flattening of the "treated gaps" $\mathcal{D}^1_s(e_1 - e_0)$ and $\mathcal{D}^2(e_1 - e_0)$ at around $\alpha \approx 1$. Finding the values at the minima or the inflection points we obtain best fits to the value of the leading infrared exponent. These best fits are tabulated below for each choice of spectator, method and a sample of truncations[2].

	$\Delta_{\max}$					
method	24.5	34.5	37.5	25	35	38
$\mathcal{D}^1_s$ with s from interaction matrix eigenvalues	(0.65,-1.76)	(0.64,-1.68)	(0.64,-1.68)	(0.65,-0.86)	(0.68,-0.96)	(0.68,1.00)
$\mathcal{D}^1_s$ with s from regression analysis	(0.713,-1.89)	(0.727,-1.89)	(0.73,-1.89)	(1.361,-2.41)	(1.133,-2.43)	(1.07,-2.36)
$\mathcal{D}^2$	(0.95,-1.8)	(0.965,-1.78)	(0.97,-1.75)	(1.61,-2.2)	(1.38,-2.24)	(1.44,-2.33)

Table 5.1: Best fits (α, t) for the leading IR exponent t, for the free spectator.

We see that $\mathcal{D}^1_s$ with locally determined slope s gives most accurate estimates of t. As we increase $\Delta_{\max}$ the estimates behave monotonically but do not always get closer to the theoretical values. The errors of these approximations can be attributed

[2]The best fit for $\mathcal{D}^2$ for the free spectator with $\Delta_{\max} = 25$ was calculated using the location of the minimum. For the higher truncation levels, the location of the inflection point was used.

	$\Delta_{\max}$		
method	26	36	40
$\mathcal{D}^1_s$ with s from interaction matrix eigenvalues	(0.825,-1.25)	(0.868,-1.35)	(0.88,-1.4)
$\mathcal{D}^1_s$ with s from regression analysis	(0.988,-2.34)	(0.89,-2.17)	(0.88,-2.12)
$\mathcal{D}^2$	(1.2,-2.15)	(1.129,-1.94)	(1.118,-1.92)

Table 5.2: Best fits (α, t) for the leading IR exponent t, for the fixed spectator.

to truncation effects as well as to the deficiencies of the method which in particular include not knowing the coefficient $A^{(1)}_1$ in (5.18) which, given the results, we may expect to be small.

For the free spectator we also tried more general $(N^1_{\max}, N^\epsilon_{\max})$–truncation schemes. For small differences $|N^1_{\max} - N^\epsilon_{\max}|$ the results are roughly in the same ball park as for the standard truncation scheme. We will discuss the effects of these truncation schemes further in section 6.4.

5.2 The perturbed tricritical Ising model

5.2.1 Boundary flows in tricritical Ising model

The space of boundary flows that start out from Cardy boundary conditions in the tricritical Ising model is well known in the literature [53],[71] and is depicted on Figure 5.10. The blue lines on the picture represent the perturbations by ψ_{13} that we will consider in this thesis. The red lines going from (d) to $(+)$ and $(-)$ boundary conditions correspond to the RG flows given by ψ_{12} perturbations and the dashed lines stand for component flows from the $(+) \oplus (-)$ superposition of two boundary conditions. The black lines correspond to two flows from (d) to (-0) and $(0+)$ generated by a particular linear combination of ψ_{12} and ψ_{13} which so far have not been found numerically but should be there for continuity reasons.

Some of the flows depicted on Figure 5.10 are related by the action of topological defects by virtue of the Graham-Watts theorem [72]. Topological defects X_i in a Virasoro minimal model are labelled by a primary state label i. They act on Cardy

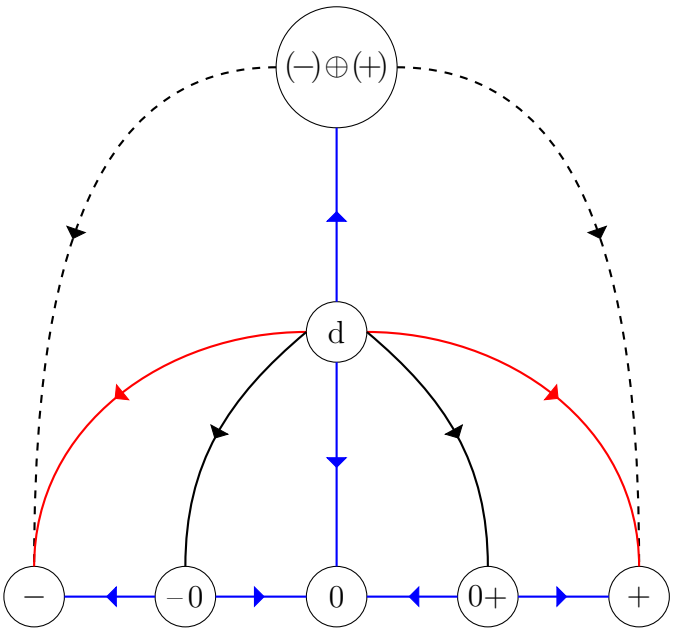

Figure 5.10: The space of boundary flows in the Tricritical Ising Model.

boundary states $|j\rangle\!\rangle$ by means of fusion rules coefficients $\mathcal{N}_{ij}^{k}$ so that

$$X_i|j\rangle\!\rangle = \sum_k \mathcal{N}_{ij}^{k}|k\rangle\!\rangle\,. \tag{5.21}$$

In particular for the tricritical Ising model the defect $X_{\epsilon''}$ is the spin-reversal defect. Its action reflects the flows on Figure 5.10 about the vertical line, exchanging the $+$ and $-$ labels of the boundary conditions. Another useful defect is $X_{\sigma'}$ which maps the horizontal pair of flows from $(0+)$ to $(+)$ and to (0) into the vertical pair of flows from (d) to (0) and to $(+)\oplus(-)$. Thus to describe ψ_{13}-flows we can focus on the pair of flows that starts from $(0+)$:

$$(0) \longleftarrow (0+) \longrightarrow (+)\,. \tag{5.22}$$

For these flows the dimensionless Hamiltonian on a strip is given by

$$h = (L_0 - c/24) + \mu L \psi_{13}(0,0) \tag{5.23}$$

where μ is the dimensionful coupling and $\psi_{13}(0,0)$ stands for the primary field inserted on the strip at $(\tau,\sigma) = (0,0)$. The matrix elements of the perturbing operator can be calculated using the conformal mapping from the upper half plane

to the strip: $w = \frac{L}{\pi}\ln z$. Here $w = \tau + i\sigma$ is the complex coordinate on the strip and $z = x + iy$ is the complex coordinate on the upper half plane: $y \geq 0$. Using this we rewrite (5.23) as

$$h = (L_0 - c/24) + \lambda\pi^{-0.4}\psi_{13}(1) \tag{5.24}$$

where $\lambda = \mu L^{0.4}$ is the dimensionless coupling [3] and $\psi_{13}(1)$ stands for the operator inserted on the boundary of the upper half plane. The matrix elements of the perturbing operator can be computed using radial quantisation.

We assume that on the bottom edge of the strip we have the (0+) boundary condition while on the top edge we have a choice of 6 spectator boundary conditions. Choosing a spectator with label s gives us a Hilbert space that can be decomposed into Virasoro irreducible representations as in (3.1). The dimensions of the truncated state space for the tricritical Ising model with (d) spectator are displayed in the Appendix A.2. The matrix elements are calculated by sandwiching the Hamiltonian (5.24) between states (3.3) and using commutation relations between the Virasoro generators and $\psi_{13}(1)$ to express them in terms of boundary three point functions which we calculate here as per [69].

5.2.2 Structure constants

As discussed earlier, a change in boundary conditions from a to b on the UHP can be described in the boundary operator language, as the insertion of a boundary changing field which we label $\psi^{(ab)}$. When the boundary conditions a and b are the same, it is less common to think of this as a field which changes the boundary condition a to boundary condition a, rather to consider this as a degree of freedom on the a-boundary. This difference is in interpretation only.

We can calculate the short distance expansion of two such boundary fields at points x,y with x>y

$$\psi_i^{(ab)}(x)\psi_j^{(bc)}(y) = \sum_k C_{ij}^{(abc)k}(x-y)^{h_k-h_i-h_j}(\psi_k^{(ac)}(y) + c_1(x-y)(L_{-1}\psi_k^{(ac)}) + \cdots) \tag{5.25}$$

[3] Throughout this thesis, we also use λ to represent a model independent coupling in a more general setting. It should be clear from the context which coupling is being referred to.

thus defining the boundary structure constants $C_{ij}^{(abc)k}$. The three point function can be calculated using this OPE as follows (for $x > y > z$):

$$\begin{aligned} < \psi_i^{(ab)}(x)\psi_j^{(bc)}(y)\psi_k^{(ca)}(z) > &= \sum_p C_{ij}^{(abc)p}(x-y)^{h_p-h_i-h_j} < \psi_p^{(ac)}(y)\psi_k^{(ca)}(z) > \\ &= \sum_p C_{ij}^{(abc)p}(x-y)^{h_p-h_i-h_j} C_{pp}^{(aca)1}(y-z)^{-2h_p} < 1 >^a \delta_{p,k} \\ &= C_{ij}^{(abc)k} C_{kk}^{(aca)1}(x-y)^{h_k-h_i-h_j}(y-z)^{-2h_k} < 1 >^a \end{aligned} \tag{5.26}$$

where we have used $\langle \psi_i^{(ab)}(x)\psi_j^{(ba)}(y)\rangle^a = C_{ii}^{(aba)1}(x-y)^{-2h_i} < 1 >^a \delta_{i,j}$. We can then write down the normalised structure constants:

$$\begin{aligned} \tilde{C}_{ijk}^{(abc)} &= \frac{< \psi_i^{(ab)}(x)\psi_j^{(bc)}(y)\psi_k^{(ca)}(z) >}{||\psi_i^{(ab)}||\ ||\psi_k^{(ac)}||\sqrt{C_{jj}^{(bcb)1}}} \\ &= C_{ij}^{(abc)k}\left(\frac{C_{kk}^{(aca)1}}{C_{ii}^{(aba)1}C_{jj}^{(bcb)1}}\right)^{1/2} \end{aligned} \tag{5.27}$$

where we choose a normalisation for our fields such that $||\psi_i^{(ab)}||^2 = C_{ii}^{(aba)1} < 1 >^a$. There is still an overall unknown normalisation here residing in the one point function of the identity operator, $< 1 >^a$, however, this cancels in the ratio (5.27).

5.2.3 Recurrence relation for fusion matrices

It is shown in [69] that there is a relation between the so-called *fusion* or *F-matrices* and the constants which appear in the three point function defined above:

$$F_{bk}\begin{bmatrix} a & c \\ i & j \end{bmatrix} = C_{ij}^{(abc)k} \tag{5.28}$$

The F-matrices arise in the calculation of conformal blocks. Their meaning can be conveniently captured diagrammatically as shown in figure 5.11. External lines represent the fields in the conformal block and intermediary states are represented by internal lines. The OPE is taken at the vertex, obeying the fusion rules of the

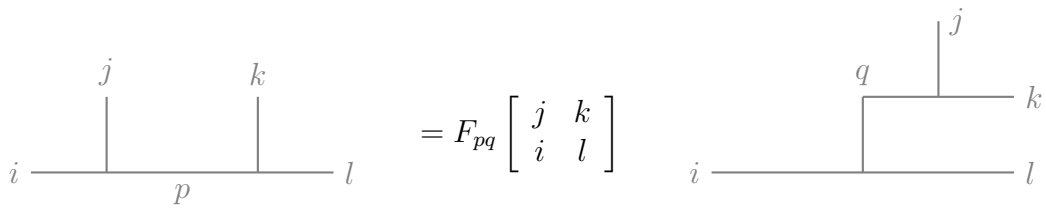

Figure 5.11: Diagrammatic representation of the fusion matrices.

associated field (see Appendix B.1) and giving rise to the intermediate state. The fusion rules must be satisfied whatever way the diagram is 'read'. Here and in the below calculation, Latin letters such as i,j,k,... and Δ all represent fields in the four point function.

We use the Recurrence relation outlined in [69] to calculate these Fusion matrices and hence the normalised structure constants. The recursive formula for the calculation of the F Matrices is:

$$F_{pq}\begin{bmatrix} j & k+\Delta \\ i & l \end{bmatrix} = \sum_{r,s} F_{k+\Delta,r}\begin{bmatrix} l & \Delta \\ p & k \end{bmatrix} \cdot F_{ps}\begin{bmatrix} j & k \\ i & r \end{bmatrix} \cdot F_{rq}\begin{bmatrix} s & \Delta \\ i & l \end{bmatrix} \cdot F_{s,k+\Delta}\begin{bmatrix} \Delta & k \\ q & j \end{bmatrix} \tag{5.29}$$

where $\Delta = (12)$ or (21) and if j stands for (r,s), then j$\pm\Delta$ is (r,s$\pm$1),(r$\pm$1,s) respectively. Commas in the above are used merely to separate the relevant matrix indices. There are restrictions on the allowed values of r and s based on the fusion rules. In particular $N^r_{pk} \cdot N^r_{l\Delta} \neq 0$, $N^s_{jk} \cdot N^s_{q\Delta} \neq 0$ and $N^i_{rs} \neq 0$ with the maximal range of r and s given by r=l$\pm\Delta$ and s=q$\pm\Delta$.

The formula is used recursively until all terms are of the form (ie the expression contains a single term as per the below or a product of such terms):

$$F\begin{bmatrix} j & \Delta \\ i & l \end{bmatrix} = F_{pq}\begin{bmatrix} j & \Delta \\ i & l \end{bmatrix} = \begin{pmatrix} F_{l-\Delta,j-\Delta} & F_{l-\Delta,j+\Delta} \\ F_{l+\Delta,j-\Delta} & F_{l+\Delta,j+\Delta} \end{pmatrix} \tag{5.30}$$

At this point, we use direct substitution to calculate each term as a product of Γ functions given by the following:

For $\Delta = (2,1)$:

$$F_{pq} = \begin{pmatrix} \frac{\Gamma(d_j)\Gamma(1-d_l)}{\Gamma(\frac{1}{2}(1-d_i+d_j-d_l))\Gamma(\frac{1}{2}(1+d_i+d_j-d_l))} & \frac{\Gamma(-d_j)\Gamma(1-d_l)}{\Gamma(\frac{1}{2}(1-d_i-d_j-d_l))\Gamma(\frac{1}{2}(1+d_i-d_j-d_l))} \\ \frac{\Gamma(d_j)\Gamma(1+d_l)}{\Gamma(\frac{1}{2}(1-d_i+d_j+d_l))\Gamma(\frac{1}{2}(1+d_i+d_j+d_l))} & \frac{\Gamma(-d_j)\Gamma(1+d_l)}{\Gamma(\frac{1}{2}(1-d_i-d_j+d_l))\Gamma(\frac{1}{2}(1+d_i-d_j+d_l))} \end{pmatrix} \tag{5.31}$$

For $\Delta = (1,2)$:

$$F_{pq} = \begin{pmatrix} \frac{\Gamma(-\frac{1}{t}d_j)\Gamma(\frac{1}{t}(t+d_l))}{\Gamma(\frac{1}{2t}(t+d_i-d_j+d_l))\Gamma(\frac{1}{2t}(t-d_i-d_j+d_l))} & \frac{\Gamma(\frac{1}{t}d_j)\Gamma(\frac{1}{t}(t+d_l))}{\Gamma(\frac{1}{2t}(t+d_i+d_j+d_l))\Gamma(\frac{1}{2t}(t-d_i+d_j+d_l))} \\ \frac{\Gamma(-\frac{1}{t}d_j)\Gamma(\frac{1}{t}(t-d_l))}{\Gamma(\frac{1}{2t}(t+d_i-d_j-d_l))\Gamma(\frac{1}{2t}(t-d_i-d_j-d_l))} & \frac{\Gamma(\frac{1}{t}d_j)\Gamma(\frac{1}{t}(t-d_l))}{\Gamma(\frac{1}{2t}(t+d_i+d_j-d_l))\Gamma(\frac{1}{2t}(t-d_i+d_j-d_l))} \end{pmatrix} \tag{5.32}$$

The normalised structure constants for the tricritical Ising model are quoted in Appendix B.2 and we note that some helpful identities for their calculation are contained in [69].

5.2.4 TCSA in the tricritical Ising model. Approach to fixed point.

We would like to focus here on reading off the leading asymptotic exponent for the energy gap on approach to the infrared fixed points for the two flows in (5.22).

These flows were analysed in TCSA in [53] where the numerics were also compared against the TBA results. As expected, the approach to the IR fixed point was found to be independent of the choice of spectator boundary condition. Our numeric computations for the energy levels, which were performed with truncated state spaces with dimension of the order 2,500 [4] agree with the results of [53].
For a positive coupling λ the flow $(0+) \to (+)$ is observed whilst for negative coupling the $(0+) \to (0)$ flow is realised. The boundary spectrum of the $(+)$ boundary condition contains only the identity tower and the end of the flow is believed to be dominated by the stress-energy tensor. For the negative coupling the approach to the IR fixed point (0) is believed to be dominated by the irrelevant field $\psi_{31} \equiv \epsilon''$

[4] The dimension is spectator dependent: the results were obtained for various levels, each corresponding to a dimension of the order 2,500 for the chosen spectator.

of dimension $3/2$[5]. Using (4.3) with $\Delta^{UV} = 3/5$ for the $\psi_{13} \equiv \epsilon'$ field and $\Delta^{IR}_{(+)} = 2$ and $\Delta^{IR}_{(0)} = 3/2$ for the stress energy tensor and ψ_{31} field we find

$$t_T^{\text{TIM}} = \frac{5}{2}\,, \qquad t_{\psi_{31}}^{\text{TIM}} = \frac{5}{4}\,. \tag{5.33}$$

To find numerical approximations to these theoretical values we use the same methodology [6] as section 5.1.2 with numerical best fits for the (d) spectator displayed in Table 5.3 below.

	Positive Coupling			*Negative Coupling*		
method \ $\Delta_{\max}$	16	18	20	16	18	20
$\mathcal{D}^1_s$ with s from interaction matrix eigenvalues	(0.641,-1.05)	(0.644,-1.11)	(0.65,-1.17)	(0.208,-1.37)	(0.211,-1.43)	(0.214,-1.55)
$\mathcal{D}^1_s$ with s from regression analysis	(0.704,-2.54)	(0.697,-2.54)	(0.69,-2.54)	(0.54,-1.63)	(0.53,-1.57)	(0.52,-1.55)
$\mathcal{D}^2$	(0.975,-2.62)	(0.946,-2.56)	(0.925,-2.5)	(0.702,-1.43)	(0.7,-1.37)	(0.69,-1.31)

Table 5.3: Best fits (λ, t) for the leading IR exponent t for positive and negative coupling.

On Figure 5.12 we present the plots for the third method based on (5.20). For brevity we present only the results for the spectator boundary condition given by the Cardy state $|\sigma\rangle\!\rangle$. We see similar behaviour near the fixed point as in the Ising model where we have an inflection point in similar plots. Increasing the truncation weight improves the approximation of the leading power bringing it closer to the theoretical value (5/2 for positive coupling and 5/4 for negative coupling).

[5]This claim is substantiated by the fact that for large central charge the boundary ψ_{13} flows become perturbative in the negative coupling direction and the dimension of the leading irrelevant operator in the IR can be shown to be that of ψ_{31}.

[6]The analysis is applied to the second excited state E_2 as this state merges with the third excited state enabling us to better predict when the fixed point is reached. The linear regression for the operator $\mathcal{D}^1_s$ was performed in the region $1 < \lambda < 2$.

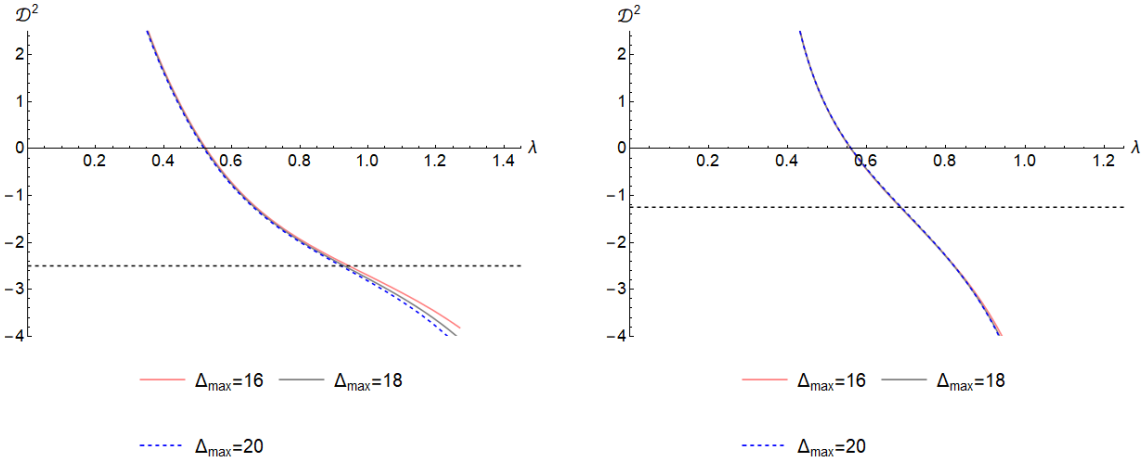

(a) $\mathcal{D}^2(e_2 - e_0)$ versus $\lambda > 0$ in the TIM with (d) spectator boundary condition.

(b) $\mathcal{D}^2(e_2 - e_0)$ versus $\lambda < 0$ in the TIM with (d) spectator boundary condition.

Figure 5.12

We note that similar behaviour is observed for the other spectators.

5.3 Concluding Remarks

In this section we provide a brief review of the work conducted in this chapter.

In chapter 4, we argued that the energy levels in the TCSA spectrum may behave approximately as in eqn (5.17) where α_* is the point of best approximation to the IR fixed point, which is dependent on the value of the truncation Δ_{max}. Naively, one may expect that the linear term here is due to the asymptotic domination of the interaction matrix. In fact, there is a numerically observed linear regime on approach to the fixed point which is not accounted for by the domination of the interaction matrix. This was verified numerically by subtracting a linear term using the eigenvalues of the interaction matrix and calculating the leading power of the TCSA spectrum around the fixed point. That there are multiple linear regimes in the spectrum is a surprising feature of TCSA. Physically, we expect that any linear term in this region is suppressed by truncation as it is not present in the continuum theory. However, it is clearly dominant at the truncation levels we have probed. Subtracting this term from the TCSA spectrum, we can use TCSA to more accurately describe the spectrum of the perturbed CFT.

We have described three methods for removing this linear term and how the leading power may be isolated on approach to the fixed point. We applied this technology to the boundary Ising and Tricritical Ising models where our numeric predictions on the leading power match well with expected analytic values.

Chapter 6

Flows Beyond the IR Fixed Point

In TCSA the closest approach to an IR fixed point emerges at a finite value of the coupling. A well-known and surprising feature of the TCSA spectrum is the presence of further flows beyond this point. In the case of boundary flows, it has been observed [53] that upon increasing the coupling to larger values, the low lying spectrum rearranges itself to approximate that of another fixed point.

This is the subject of our second application of TCSA as referenced in chapter 5. These "flows beyond" take many qualitatively different forms, with some models containing single flows beyond whilst others pass through a sequence of several fixed points. There are examples of reverse physical RG flows whilst in some models, despite seemingly 'deliberate' flows towards a stable regime, the spectrum does not reach a fixed point identifiable with any local boundary condition.

Whilst these flows have been observed numerically, they lack a theoretical understanding. Working in the examples of the boundary Ising and tricritical Ising models, we analyse them numerically, using analytic techniques where possible to elucidate the effects further. We provide supporting evidence for our 'working hypothesis' explaining their appearance in TCSA, outlined in chapter 4, where the spectrum is driven away from the fixed point by the irrelevant operator by which it approached with opposite sign of the coupling.

In general, we find that the flows beyond the first fixed point are very sensitive to modifications of the truncation scheme. We discuss two exactly solvable models in a 'mode truncated' scheme which adds to our understanding of the picture outlined in chapter 4 and consider perturbations of IR fixed points by irrelevant operators in

an effort to understand the large coupling behaviour of the spectrum. Supplementing this, in an effort to model possible infrared regularisation schemes, we consider modified truncation types and investigate their effect on the spectrum.

6.1 Examples

In the examples discussed in the chapter 5 as we increase the coupling past the IR fixed point we observe a rearrangement of multiplicities characteristic of a different fixed point. We call these "flows beyond the IR fixed point", or just "flows beyond". They were observed and discussed in [66],[52], [53].

The simplest case of a flow beyond appears to be the boundary magnetic field flow in the Ising model with a fixed spin spectator (c.f. eqn (5.9)). If we are to plot the energy gaps $e_i - e_0$ versus the coupling we will see that past the fixed point they settle asymptotically into a linear regime[1]. We can interpret this linearity as due to energy rescalings stemming from truncation effects. Such rescalings have been discussed in the perturbative regime in [53]. Looking instead at the normalised energy gaps,

$$\Delta e_i^{\mathrm{n}} = \frac{e_i - e_0}{e_1 - e_0}\,, \tag{6.1}$$

we remove the energy rescalings and can observe the asymptotic multiplicities rearranging themselves (here for simplicity we assume that the vacuum does not become asymptotically degenerate). The normalised gaps for the flow at hand are presented on Figure 6.1 using the logarithmic scale $\ln|\alpha|$ for ease of visualisation.

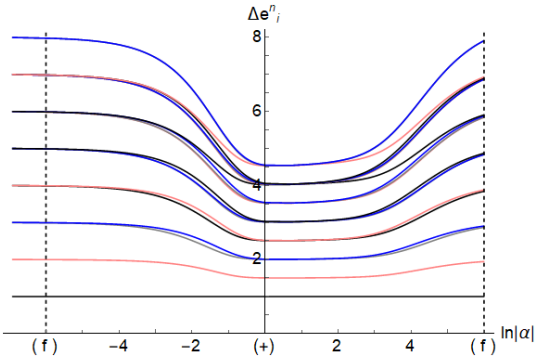

(a) Δe_i^{n} versus $\ln|\alpha|$ for $\alpha > 0$, $\Delta_{\max} = 34$ for the fixed spectator.

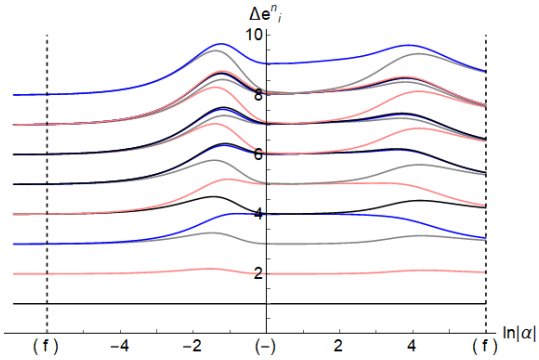

(b) Δe_i^{n} versus $\ln|\alpha|$ for $\alpha < 0$, $\Delta_{\max} = 34$ for the fixed spectator.

Figure 6.1

[1]This is the second linear regime past the $\lambda = \lambda^{**}$ threshold discussed in chapter 4.

These plots show that for very large absolute values of the coupling the multiplicities rearrange back to those of the original UV fixed point so that the flow beyond looks like the reverse of the physical flow from the UV free boundary condition to the IR fixed boundary condition. In the plots we have marked with dashed lines approximate regions representing the vicinities of fixed points (the IR fixed point occurs approximately along the $\alpha = 0$ axis). Of course the flow beyond is not physical in that it violates the g-theorem[74, 75]. It does not happen in the continuum theory and is entirely an artefact of the truncation. However, we find this phenomenon interesting in that it does arise in a variety of situations when using TCSA, especially for boundary perturbations, and understanding the mechanism behind it must tell us something about how TCSA works at large couplings.

In general, in TCSA we are dealing with a Hamiltonian of the form

$$h = L_0^{\mathrm{UV}} + \lambda V^{\mathrm{UV}} \tag{6.2}$$

where L_0^{UV} and V^{UV} are finite matrices. Asymptotically, possibly after a number of different intermediate regimes, the interaction matrix is bound to dominate over the L_0^{UV} matrix and the energy gaps will be given by the difference of the eigenvalues v_i of the interaction matrix V^{UV} times the coupling. More precisely, assuming the eigenvalues v_i are non-degenerate and $v_{\min}$ is the smallest eigenvalue and $v_{\max}$ is the largest eigenvalue we have

$$e_i - e_0 \sim \lambda(v_i - v_{\min}) \text{ when } \lambda \to \infty\,, \tag{6.3}$$

$$e_i - e_0 \sim \lambda(v_i - v_{\max}) \text{ when } \lambda \to -\infty\,. \tag{6.4}$$

For the normalised gaps we then get an asymptotic approach to constant values:

$$\Delta e_i^{\mathrm{n}} \sim \frac{v_i - v_{\min}}{v_1 - v_{\min}} \text{ when } \lambda \to \infty \tag{6.5}$$

and similarly for $\lambda \to -\infty$. For degenerate eigenvalues of V^{UV} the situation is a bit more interesting. If e_i and e_j are two eigenvalues of h that asymptotically tend to the same degenerate eigenvalue, v_k, then their difference will be given asymptotically by the leading correction, which is equal to an eigenvalue of the operator L_0^{UV} reduced

to the eigenspace for $\vec{v}_k$, the associated eigenvector. This will affect the asymptotic behaviour (6.5) when the smallest (or largest) eigenvalue of V^{UV} is degenerate.

Coming back to the boundary magnetic field flow, we checked that the smallest and largest eigenvalues of V^{UV}, which differ only by the sign, are non-degenerate for the fixed spin spectator. The asymptotic behaviour (6.5) holds numerically to good accuracy. The flow beyond is simply described (asymptotically) as the dominance of the interaction matrix. However the multiplicities for low lying eigenvalues of V^{UV} turn out to be the same as those of L_0^{UV}. For a fixed number of low lying states it is essential to take large enough $\Delta_{\max}$ to observe this as for small $\Delta_{\max}$ the multiplicities still deviate. We have no simple explanation of this coincidence.

Although, to avoid clutter, in Fig 6.1 we present only the normalised gaps obtained for a particular value of $\Delta_{\max}$ we have made a comparison for a number of different values of $\Delta_{\max}$ and observed that the value of α at which we enter the asymptotic regime with the UV BCFT multiplicities increases as we increase $\Delta_{\max}$. Physically this supports the intuition that flows beyond constitute a truncation effect and are absent in the continuum theory. Qualitatively this also ties in with the domination of αV^{UV} matrix that would set in for larger values of α because the largest eigenvalue of L_0^{UV} grows linearly with $\Delta_{\max}$ while it is observed numerically that of V^{UV} only grows as a square root of $\Delta_{\max}$.

The phenomenon of flows beyond is even more spectacular for the boundary $\psi_{1,3}$ flows in the TIM. As explained in section 5.2.1 due to the Graham-Watts theorem we can focus on the ψ_{13}-flows originating from the (0+) boundary condition. While for positive values of the coupling we find a physical RG flow to the (+) boundary condition and no flow beyond, for negative coupling we find a cascade of flows beyond that can be summarised by the following diagram

$$(0+) \to (0) \to (-0) \to (-) \tag{6.6}$$

as discerned from the changes in multiplicities of the normalised energy gaps plotted on Figure 6.2.

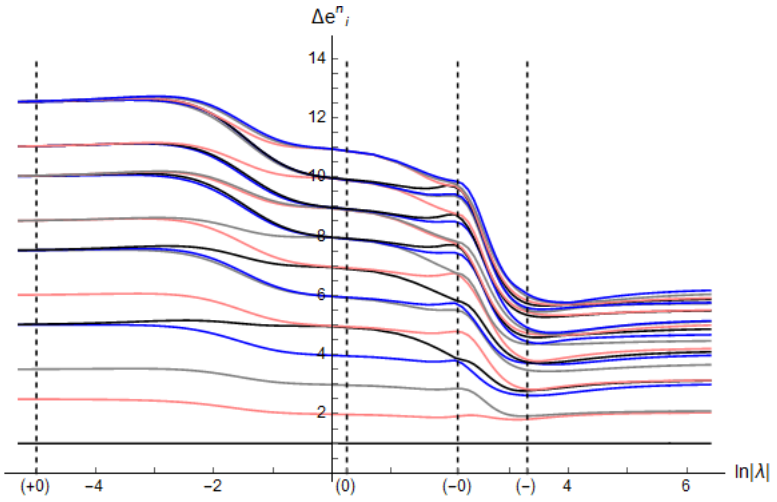

Figure 6.2: Δe_i versus $\ln|\lambda|$ in the TIM with (d)-spectator and $\lambda < 0$ with $\Delta_{\max} = 20$.

In these plots we chose the disordered boundary condition (d) as a spectator but, remarkably, the cascade of multiplicity changes is the same for any choice of 6 spectator boundary conditions. These flows beyond were first investigated in [53]. While the far end of the cascade can be still described by the dominance of the interaction matrix V^{UV} within a degree of numerical accuracy, particularly in the low lying spectrum, the intermediate linear regimes with rearranged multiplicities cannot be described so simply. The independence from the spectator boundary condition suggests some local description in the space of effective Hamiltonians of the type discussed in chapter 4. In that description the flows beyond are described by perturbations of IR fixed points by irrelevant operators with flipped sign. Crucially, to determine where the bounce flow is headed next depends on the truncation scheme at the IR fixed point. In the next section we describe two exactly solvable models of truncated perturbations that offer further insights supporting the picture outlined in chapter 4.

6.2 Two exactly solvable models

6.2.1 Canonical transformations in Quantum Field Theory

In the following section, to supplement our numeric studies, we provide the details of two analytically solvable truncated Quantum Field Theories. Both theories are quadratic (more precisely, bilinear) in the creation and annihilation operators

and are therefore, diagonalisable. One method of solving such theories is via the Bogolyubov transformation, a canonical transformation between the creation and annihilation operators. We recall some generalities of canonical transformations.

Given a set of fermionic[2] creation and annihilation operators $a, a^\dagger$ satisfying the usual anti-commutation relations

$$\{a_i, a_j^\dagger\} = \delta_{ij}, \qquad \{a_i, a_j\} = \{a_i^\dagger, a_j^\dagger\} = 0, \tag{6.7}$$

a canonical transformation is a set of operators $b_i, b_j^\dagger$ defined as

$$b_i = \sum_m (\Phi_{im} a_m + \Psi_{im} a_m^\dagger), \qquad b_j^\dagger = \sum_n (\Phi_{jn}^* a_n^\dagger + \Psi_{jn}^* a_n) \tag{6.8}$$

satisfying the same anti-commutation relations:

$$\{b_i, b_j^\dagger\} = \delta_{ij}, \qquad \{b_i, b_j\} = \{b_i^\dagger, b_j^\dagger\} = 0. \tag{6.9}$$

If such a map is both linear and unitary (sometimes referred to as *proper* or *unitarily equivalent*), it constitutes a Bogolyubov transformation.

Plugging equations (6.8) into (6.9) and using equations (6.7), we can find relations between Φ and Ψ.
For example,

$$\begin{aligned} \{b_i, b_j^\dagger\} = &\sum_{m,n} \Phi_{im} \Phi_{jn}^* \{a_m, a_n^\dagger\} + \sum_{m,n} \Phi_{im} \Psi_{jn}^* \{a_m, a_n\} \\ &+ \sum_{m,n} \Psi_{im} \Phi_{jn}^* \{a_m^\dagger, a_n^\dagger\} + \sum_{m,n} \Psi_{im} \Psi_{jn}^* \{a_m^\dagger, a_n\}. \end{aligned} \tag{6.10}$$

[2]The below can readily be adapted to bosonic operators. See, for example [21].

Using (6.7) and summing over n, we can write

$$\begin{aligned}\delta_{ij} = \{b_i, b_j^\dagger\} &= \sum_m (\Phi_{im}\Phi_{jm}^* + \Psi_{im}\Psi_{jm}^*) \\ &= \sum_m (\Phi_{im}(\Phi_{mj}^*)' + \Psi_{im}(\Psi_{mj}^*)')\end{aligned} \tag{6.11}$$

where Φ' is the transpose of Φ. Then the following relations hold:

$$\begin{aligned}\Phi\Phi^\dagger + \Psi\Psi^\dagger &= \mathbb{I}, \\ \Phi^*\Phi' + \Psi^*\Psi' &= \mathbb{I}.\end{aligned} \tag{6.12}$$

The second equation comes from taking the complex conjugate of the first equation whilst noting that $(\Phi^\dagger)^* = \Phi'$. Similarly, considering the anti-commutators $\{b_i, b_j\} = \{b_i^\dagger, b_j^\dagger\} = 0$ we find the following relations:

$$\begin{aligned}\Phi\Psi' + \Psi\Phi' &= 0, \\ \Phi^*\Psi^\dagger + \Psi^*\Phi^\dagger &= 0.\end{aligned} \tag{6.13}$$

Equations (6.8) may be represented in matrix form as

$$\begin{pmatrix} b \\ b^\dagger \end{pmatrix} = \begin{pmatrix} \Phi & \Psi \\ \Phi^* & \Psi^* \end{pmatrix} \begin{pmatrix} a \\ a^\dagger \end{pmatrix}, \tag{6.14}$$

where we define

$$A = \begin{pmatrix} \Phi & \Psi \\ \Phi^* & \Psi^* \end{pmatrix} \tag{6.15}$$

as the matrix of the canonical transformation.

It is clear from equations (6.12) and (6.13) then, that A has right inverse

$$A^{-1} = \begin{pmatrix} \Phi^\dagger & \Psi' \\ \Phi^\dagger & \Psi' \end{pmatrix}. \tag{6.16}$$

By definition, the canonical transformation is reversible and hence, has a left inverse also. If an operator has both left and right inverse, then these inverses coincide. Then

(6.16) is also the left inverse for A from which we can find the additional relations

$$\begin{aligned} \Phi^\dagger\Psi + \Psi'\Phi^* = 0, \qquad & \Psi^\dagger\Phi + \Phi'\Psi^* = 0, \\ \Phi^\dagger\Phi + \Psi'\Psi^* = \mathbb{I}, \qquad & \Phi'\Phi^* + \Psi^\dagger\Psi = \mathbb{I}. \end{aligned} \tag{6.17}$$

We can see that successive compositions of canonical transformations are realised via matrix multiplication. That the matrix of a canonical transformation has a two sided inverse allows us to conclude that the linear canonical transformations form a group.

The transformation (6.8), (6.9) is unitary if there exists some unitary operator $\hat{U}$ such that

$$b^\dagger = \hat{U}a^\dagger\hat{U}^{-1}, \qquad b = \hat{U}a\hat{U}^{-1}. \tag{6.18}$$

It can be shown [21] that such an operator exists if and only if the operator Ψ is Hilbert-Schmidt and that every canonical transformation is unitary if there are a finite number of degrees of freedom. In infinite dimensional systems (such as a general Quantum Field Theory), we can readily find improper canonical transformations which do not produce unitarily equivalent descriptions of physics. In what follows, we work on a truncated space with finite degrees of freedom and therefore all transformations are unitarily equivalent.

Using this technology, we now present the solution for two Quantum Field Theories within the same truncation scheme: the boundary magnetic field flow in the Ising model and the perturbation of the Ising model by the stress-energy tensor restricted to the boundary.

6.2.2 Model I

In this section, we consider two analytically solvable models with the same truncation scheme. The first example shows that by using an alternative scheme to TCSA, there may be no flow beyond the IR fixed point. The second is an example of a theory with a bounce flow – flowing first to a new fixed point, then returning back to the original one.

In the first example we use a mode truncation scheme for the boundary magnetic field flow in the Ising model where we leave the spin to fluctuate freely on the spectator boundary. The mode truncation scheme for this flow was first considered in [66] where it was noted that there is no flow beyond.

For the free spectator the Hamiltonian in the mode truncation scheme, written in the notation of section 5.1.1 is

$$H^{\rm NS}_{\rm mod} = \frac{\pi}{L}\Big[\sum_{k=0}^{n_c}(k+1/2)a^\dagger_{k+1/2}a_{k+1/2} - \frac{1}{48} + i\alpha\sum_{k=0}^{n_c}(a^\dagger_{k+1/2}+a_{k+1/2})a\Big] \tag{6.19}$$

restricted to the subspace of the physical space spanned by the states of the form (5.7) built with operators $a^\dagger_{i+1/2}$, $i=0,\dots,n_c$. The integer n_c is the mode truncation parameter. The dimension of the truncated state space is 2^{n_c+1}.
We introduce the dimensionless Hamiltonian

$$h^{\rm NS}_{\rm mod} = \frac{L}{\pi}H^{\rm NS}_{\rm mod}. \tag{6.20}$$

This may be diagonalised by means of a Bogolyubov transformation. To find the latter we write an ansatz for the diagonalising modes:

$$b_\omega = \sum_{k=0}^{n_c}(A_{\omega,k}a^\dagger_{k+1/2} + B_{\omega,k}a_{k+1/2}) + af(\omega)\,, \tag{6.21}$$

and require that it satisfies

$$[h^{\rm NS}_{\rm mod}, b_\omega] = \omega b_\omega\,. \tag{6.22}$$

Calculating (6.22), we find

$$[h^{\rm NS}_{\rm mod}, b_\omega] = \sum_{k=0}^{n_c}A_{\omega,k}[h^{\rm NS}_{\rm mod}, a^\dagger_{k+1/2}] + \sum_{k=0}^{n_c}B_{\omega,k}[h^{\rm NS}_{\rm mod}, a_{k+1/2}] + f(\omega)[h^{\rm NS}_{\rm mod}, a], \tag{6.23}$$

at which point, we calculate separately

$$\begin{aligned}
[h^{\mathrm{NS}}_{\mathrm{mod}}, a] &= 2i\alpha \sum_{k=0}^{n_c} (a^\dagger_{k+1/2} + a_{k+1/2}), \\
[h^{\mathrm{NS}}_{\mathrm{mod}}, a^\dagger_{k+1/2}] &= (k+1/2) a^\dagger_{k+1/2} - i\alpha a, \\
[h^{\mathrm{NS}}_{\mathrm{mod}}, a_{k+1/2}] &= -(k+1/2) a_{k+1/2} - i\alpha a.
\end{aligned} \tag{6.24}$$

Equation (6.22) can now be solved for the respective coefficients of the creation and annihilation operators. Solving for a single $a^\dagger_i$ we find

$$A_{\omega,k} = -\frac{2i\alpha f(\omega)}{(k+1/2) - \omega} \tag{6.25}$$

and for a single a_i

$$B_{\omega,k} = \frac{2i\alpha f(\omega)}{(k+1/2) + \omega}. \tag{6.26}$$

Solving for the boundary fermion gives

$$\sum_{k=0}^{n_c} (A_{\omega,k} + B_{\omega,k}) = -\frac{\omega f(\omega)}{i\alpha}. \tag{6.27}$$

Substituting equations (6.25) and (6.26) into (6.27), we find the following spectral equation for the frequencies ω:

$$\sum_{k=0}^{n_c} \frac{2\omega^2}{(k+1/2)^2 - \omega^2} = -\frac{\omega^2}{2\alpha^2}\,. \tag{6.28}$$

The solutions to equation (6.28), ω_i, are shown as the intersection points in Fig. 6.3[3].

[3]The solutions for zero coupling are not shown.

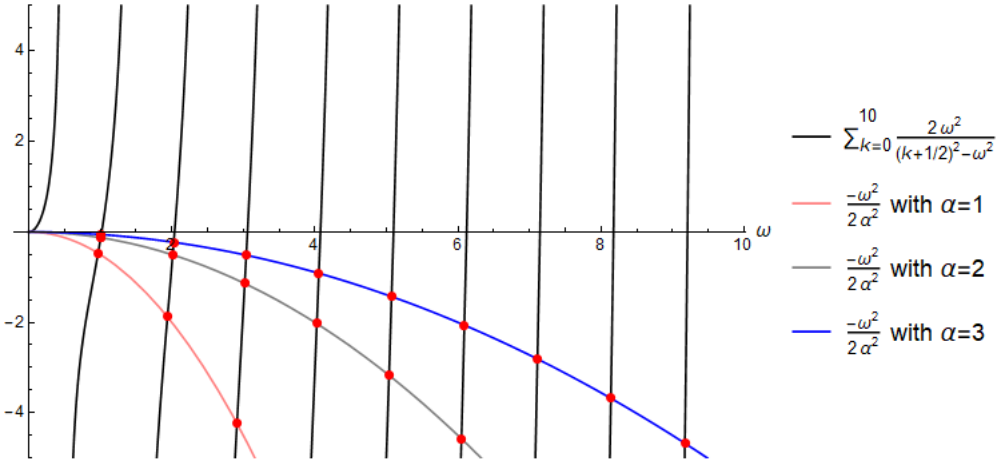

Figure 6.3: NS Sector (free spectator) solutions to the mode truncated spectral equation (6.28) for non-zero coupling.

This equation has $n_c + 1$ bounded modes which include zero and n_c solutions $\omega = \pm\tilde{\omega}_n$, $\tilde{\omega}_n > 0$ that remain bounded as $\alpha \to \infty$. It also has one heavy mode solution $\omega = \Omega_\alpha$ where

$$\Omega_\alpha \sim 2|\alpha|\sqrt{n_c + 1} \quad \text{as } \alpha \to \pm\infty\,. \tag{6.29}$$

The state space then splits neatly into two subspaces: the one with light states that is built using $b^\dagger_{\tilde{\omega}_n}$ and the one with heavy states built using $b^\dagger_{\Omega_\alpha}$ and other oscillators. In the heavy states subspace the energy gaps diverge linearly as $\alpha \to \pm\infty$. Focusing on the light states one has

$$\lim_{\alpha\to\pm\infty} \tilde{\omega}_n = n + \mathcal{O}\left(\frac{1}{n_c}\right)\,, \quad n = 1, \ldots, n_c \tag{6.30}$$

so that up to errors suppressed by the truncation parameter we obtain the spectrum of the fixed spin boundary condition describing the IR fixed point. The vacuum energy also diverges linearly in α due to the Ω_α mode contribution. In the energy gaps $e_i - e_0$ this divergence cancels for the light states. We can interpret this asymptotic behaviour in terms of the dominance of the interaction matrix V. The latter has only two eigenvalues: $\sqrt{n_c + 1}$ and $-\sqrt{n_c + 1}$, with equal dimensions. The light states including the vacuum are, asymptotically, perturbations of the states in the $-\sqrt{n_c + 1}$-subspace for $\alpha \to \infty$ and of the $\sqrt{n_c + 1}$-subspace for $\alpha \to -\infty$. While the states in the heavy states subspace all decouple, the light states give the

approximate spectrum of the IR fixed point due to the first perturbative correction. In a bit more detail we write

$$L_0^{\mathrm{UV}} + \alpha V^{\mathrm{UV}} = \alpha(V^{\mathrm{UV}} + \frac{1}{\alpha} L_0^{\mathrm{UV}}) \tag{6.31}$$

and treat $\frac{1}{\alpha} L_0^{\mathrm{UV}}$ as a perturbation. In the energy gaps, the leading terms from the appropriate eigenvectors of V^{UV} cancel each other while the first order correction from the perturbation gives rise to constant terms in the $\alpha \to \pm\infty$ limit. The numerical values according to the secular equation are the eigenvalues of L_0^{UV} restricted to the appropriate eigensubspace of V^{UV}. It is remarkable that up to corrections suppressed by $1/n_c$ this gives the correct spectrum of L_0^{IR}. We are not aware at present of any simple explanation of this fact.

For the fixed spectator the story is very much similar. The mode truncated Hamiltonian reads

$$H^{\mathrm{R}}_{\mathrm{mod}} = \frac{\pi}{L}\Big(\sum_{n=1}^{n_c} n b_n^\dagger b_n + \frac{1}{24} + i\alpha[\sum_{n=1}^{n_c}(b_n^\dagger + b_n) + b_0]a\Big) \tag{6.32}$$

and the spectral equation (6.28) is replaced by

$$\sum_{k=1}^{n_c} \frac{2\omega^2}{k^2 - \omega^2} - 1 = -\frac{\omega^2}{2\alpha^2}\,. \tag{6.33}$$

As we increase the coupling, the elementary low lying spectrum changes from integers to approximately half-integers, with corrections suppressed by n_c. No flow beyond takes place.

6.2.3 Model II

Our second model is the boundary perturbation of the Ising model by the stress-energy tensor restricted to the boundary: $T = -\frac{L}{2\pi} :\psi\partial_\tau\psi:(0,0)$ with a coupling g. We note that we are perturbing the fixed boundary condition here. Choosing the fixed spin spectator and using the mode truncation scheme this model can be

described by the following dimensionless Hamiltonian

$$h_g^{n_c} = -\frac{1}{48} + \sum_{k=0}^{n_c}(k+\frac{1}{2})a^\dagger_{k+1/2}a_{k+1/2} \\ -\frac{g}{2}:\left(\sum_{k=0}^{n_c}\sum_{l=0}^{n_c}(a^\dagger_{k+1/2}+a_{k+1/2})(l+1/2)(a^\dagger_{l+1/2}-a_{l+1/2})\right): . \quad (6.34)$$

As above, we solve the system by Bogolyubov transformation. We write the diagonalising modes

$$b_\omega = \sum_{k=0}^{n_c} A_{\omega,k}a^\dagger_{k+1/2} + B_{\omega,k}a_{k+1/2} \quad (6.35)$$

such that they solve

$$[h_g^{n_c}, b_\omega] = \omega b_\omega. \quad (6.36)$$

The left hand side of equation (6.36) is equivalent to

$$[h_g^{n_c}, b_\omega] = \sum_{k=0}^{n_c} A_{\omega,k}[h_g^{n_c}, a^\dagger_{k+1/2}] + \sum_{k=0}^{n_c} B_{\omega,k}[h_g^{n_c}, a_{k+1/2}]. \quad (6.37)$$

We calculate separately

$$[h_g^{n_c}, a^\dagger_{k+1/2}] = (k+1/2)a^\dagger_{k+1/2} + \frac{g}{2}\sum_{n=0}^{n_c}\left[(k+1/2)a_{n+1/2} - (n+1/2)a_{n+1/2}\right] \\ + \frac{g}{2}\sum_{n=0}^{n_c}\{(n+1/2)+(k+1/2)\}a^\dagger_{n+1/2} \quad (6.38)$$

and

$$[h_g^{n_c}, a_{k+1/2}] = -(k+1/2)a_{k+1/2} - \frac{g}{2}\sum_{n=0}^{n_c}\left[(k+1/2)a^\dagger_{n+1/2} - (n+1/2)a^\dagger_{n+1/2}\right] \\ - \frac{g}{2}\sum_{n=0}^{n_c}\{(n+1/2)+(k+1/2)\}a_{n+1/2}. \quad (6.39)$$

Equation (6.36) may now be solved for the coefficients of the creation and annihilation operators respectively. We find that this equation amounts to the following

constraints on the coefficients $A_{\omega,k}, B_{\omega,k}$:

$$\begin{aligned} A_{\omega,k} &= -\frac{g/2}{(k+1/2)-\omega}((k+1/2)A_\omega + A'_\omega + (k+1/2)B_\omega - B'_\omega), \\ B_{\omega,k} &= -\frac{g/2}{(k+1/2)+\omega}((k+1/2)B_\omega + B'_\omega + (k+1/2)A_\omega - A'_\omega). \end{aligned} \tag{6.40}$$

where we define

$$\begin{aligned} A_\omega &= \sum_{k=0}^{n_c} A_{\omega,k}, & A'_\omega &= \sum_{k=0}^{n_c}(k+1/2)A_{\omega,k}, \\ B_\omega &= \sum_{k=0}^{n_c} B_{\omega,k}, & B'_\omega &= \sum_{k=0}^{n_c}(k+1/2)B_{\omega,k}. \end{aligned} \tag{6.41}$$

Defining

$$F_+ = \sum_{k=0}^{n_c} \frac{1}{k+1/2+\omega}, \qquad F_- = \sum_{k=0}^{n_c} \frac{1}{k+1/2-\omega} \tag{6.42}$$

we have the following

$$\begin{aligned} \sum_{k=0}^{n_c} \frac{k+1/2}{k+1/2+\omega} &= (n_c+1) - \omega F_+ \,, \\ \sum_{k=0}^{n_c} \frac{k+1/2}{k+1/2-\omega} &= (n_c+1) + \omega F_- \,, \\ \sum_{k=0}^{n_c} \frac{(k+1/2)^2}{k+1/2+\omega} &= \frac{n_c(n_c+1)}{2} + (1/2-\omega)(n_c+1) + \omega^2 F_+ \,, \\ \sum_{k=0}^{n_c} \frac{(k+1/2)^2}{k+1/2-\omega} &= \frac{n_c(n_c+1)}{2} + (1/2+\omega)(n_c+1) + \omega^2 F_- \,. \end{aligned} \tag{6.43}$$

We can now sum equations (6.40) over k and write

$$\begin{aligned} A_\omega &= -\frac{g}{2}((n_c+1)+\omega F_-)(A_\omega + B_\omega) - \frac{g}{2}F_-(A'_\omega - B'_\omega), \\ B_\omega &= -\frac{g}{2}((n_c+1)-\omega F_+)(A_\omega + B_\omega) - \frac{g}{2}F_+(B'_\omega - A'_\omega). \end{aligned} \tag{6.44}$$

Similarly, we multiply equations (6.40) by (k+1/2) and then sum over k to give

$$\begin{aligned} A'_\omega &= -\frac{g}{2}\frac{n_c(n_c+1)}{2} + (1/2+\omega)(n_c+1) + \omega^2 F_-](A_\omega + B_\omega) \\ &- \frac{g}{2}((n_c+1)+\omega F_-)(A'_\omega - B'_\omega), \\ B'_\omega &= -\frac{g}{2}\frac{n_c(n_c+1)}{2} + (1/2-\omega)(n_c+1) + \omega^2 F_+](A_\omega + B_\omega) \\ &- \frac{g}{2}((n_c+1)-\omega F_+)(B'_\omega - A'_\omega). \end{aligned} \tag{6.45}$$

Defining $X = A'_\omega - B'_\omega, Y = A_\omega + B_\omega$ and writing $\Delta = (F_- - F_+)$ and $\xi = 2(n_c+1) + \omega\Delta$ we can write equations (6.44) and (6.45) as a system of two linear equations

$$\begin{pmatrix} \frac{g}{2}\Delta & (1+\frac{g}{2}\xi) \\ (1+\frac{g}{2}\xi) & \frac{g}{2}\omega\xi \end{pmatrix} \begin{pmatrix} X \\ Y \end{pmatrix} = 0 \tag{6.46}$$

which is satisfied provided the determinant is 0 and therefore, that the following transcendental equation is satisfied

$$\omega\Delta = -\frac{(1+g(n_c+1))^2}{g(1+g/2(n_c+1))}. \tag{6.47}$$

Recalling that $\Delta = F_- - F_+ = \sum_{k=0}^{n_c} \frac{2\omega}{(k+1/2)^2-\omega^2}$, the spectral equation is

$$\sum_{k=0}^{n_c} \frac{2\omega^2}{(k+1/2)^2-\omega^2} = -\frac{(1+g(n_c+1))^2}{g(1+\frac{g}{2}(n_c+1))}. \tag{6.48}$$

Being an irrelevant coupling, g goes to zero along the RG flow. If however we investigate the spectrum as we change g from zero to plus or minus infinity, thus going backwards along the flow, we observe a curious pattern. For positive values of g, solutions to (6.48) are comprised of light frequencies with values $\omega_k \approx k + 1/2$ and a single heavy frequency Ω_g that for large g is given by

$$\Omega_g \approx |g| \left(\frac{n_c+1}{\sum_{k=0}^{n_c}(k+1/2)^2}\right)^{1/2}. \tag{6.49}$$

The large g low lying spectrum is described by the equation

$$\sum_{k=0}^{n_c} \frac{2\omega^2}{(k+1/2)^2-\omega^2} = -2(n_c+1) \tag{6.50}$$

that up to corrections of order $1/n_c$ is given by half-integers. This means that the excitation spectrum is changed by terms suppressed by n_c. The low lying spectrum practically does not flow.

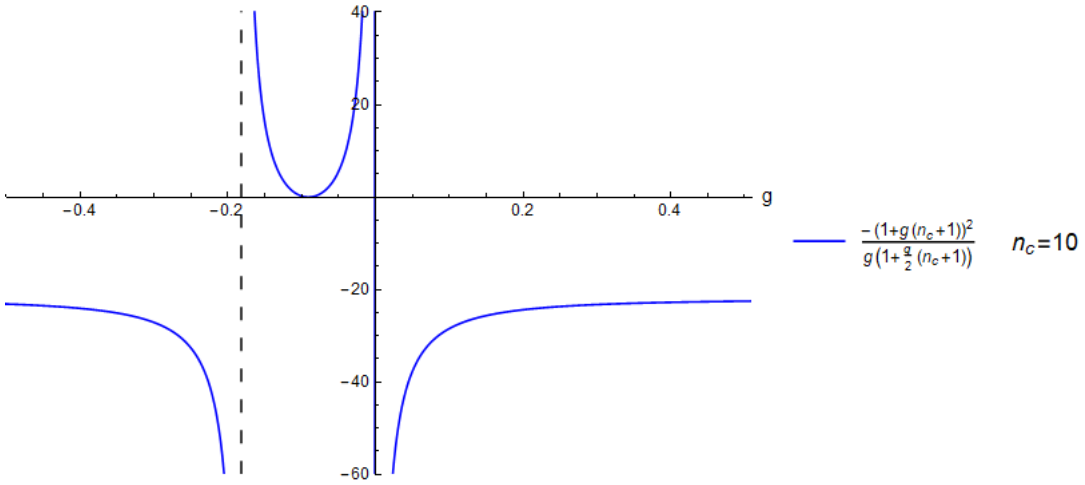

Figure 6.4: Plotting the RHS of the spectral equation (6.48) for positive and negative coupling g.

On Fig. 6.4 we see that for negative values of g we pass through a zero of the function on the right hand side of (6.48) at $g = -1/(n_c+1)$ and then a pole at $g = -2/(n_c+1)$ (shown as a dashed line on Fig. 6.4). Increasing g in absolute value we thus first arrive at a point with low lying spectrum described in terms of integer modes and then back to the same spectrum of the starting point $g = 0$. This actually fits nicely with the absence of flow beyond in the boundary magnetic field perturbation regulated the same way (with a fixed spectator). We know in that flow that we approach the infrared fixed point along the T-perturbation with a negative coupling. Following the empirical rule that near the infrared fixed point the incoming flows get reflected, we depart the (continuum) infrared fixed point along the T-perturbation with a positive coupling. But, as we have seen before, this inflicts only minor corrections to the IR spectrum which are suppressed by n_c. Note that to observe the asymptotic multiplicities of the flows beyond we do not need to resort to the normalised gaps Δe_i^{n} as no energy rescaling seems to be generated by this

truncation scheme. For the first model considered in this section, this was noted in [66].

For the free spectator the mode truncated T-perturbation is described by

$$\tilde{h}_g^{n_c} = \frac{1}{24} + \sum_{k=1}^{n_c} k\, b_k^\dagger b_k - \frac{g}{2} : \left(\left[\sum_{k=1}^{n_c} (b_k^\dagger + b_k) + b_0 \right] \sum_{l=1}^{n_c} l(b_l^\dagger - b_l) \right) : \,. \tag{6.51}$$

In a similar way, we proceed with the solution via Bogolybuov transformation, with the following ansatz for the diagonalising modes:

$$b_\omega = \sum_{n=1}^{n_c} (A_{\omega,n} a_n^\dagger + B_{\omega,n} a_n) + f_\omega a_0 \tag{6.52}$$

Solving the equivalent of equation (6.36) we find the following equations for the coefficients $A_{\omega,n}, B_{\omega,n}$:

$$\begin{aligned} &A_{\omega,n} n + g(nA_\omega + A'_\omega) - g(B'_\omega - nB_\omega) + ngf_\omega = \omega A_{\omega,n}\,, \\ &-B_{\omega,n} n + g(A'_\omega - nA_\omega) - g(nB_\omega + B'_\omega) - ngf_\omega = \omega B_{\omega,n}\,, \\ &g(A'_\omega - B'_\omega) = \omega f_\omega. \end{aligned} \tag{6.53}$$

where

$$\begin{aligned} A_\omega &= \sum_{n=1}^{n_c} A_{\omega,n}, & A'_\omega &= \sum_{n=1}^{n_c} nA_{\omega,n}, \\ B_\omega &= \sum_{n=1}^{n_c} B_{\omega,n}, & B'_\omega &= \sum_{n=1}^{n_c} nB_{\omega,n}. \end{aligned} \tag{6.54}$$

Taking the sum of the first two equations in (6.53) and summing over n we obtain

$$X(1 + 2gn_c) = \omega Y \tag{6.55}$$

where we recall that $X = A'_\omega - B'_\omega, Y = A_\omega + B_\omega$. From (6.53) we also obtain

$$A_{\omega,n} = -\frac{g}{n-\omega}(n(A_\omega + B_\omega + f_\omega) + A'_\omega - B'_\omega)\,,$$
$$B_{\omega,n} = -\frac{g}{n+\omega}(n(A_\omega + B_\omega + f_\omega) - (A'_\omega - B'_\omega)). \tag{6.56}$$

Summing both sides over n we obtain

$$A_\omega = -g[(A_\omega + B_\omega + f_\omega)(n_c + \omega F_-) + (A'_\omega - B'_\omega)F_-]\,,$$
$$B_\omega = -g[(A_\omega + B_\omega + f_\omega)(n_c - \omega F_+) - (A'_\omega - B'_\omega)F_+]. \tag{6.57}$$

We define F_+ and F_- in a similar manner as for the fixed spectator:

$$F_+ = \sum_{n=1}^{n_c} \frac{1}{n+\omega}, \qquad F_- = \sum_{n=1}^{n_c} \frac{1}{n-\omega}. \tag{6.58}$$

Taking the sum of these equations we obtain (recalling that $\Delta = F_- - F_+$)

$$Y = -g[(Y + f_\omega)(2n_c + \omega\Delta) + X\Delta]. \tag{6.59}$$

For $\omega \neq 0$ we can also use the third equation in (6.53) to express

$$f_\omega = \frac{g}{\omega}X\,, \quad \omega \neq 0 \tag{6.60}$$

Substituting this into (6.59) we obtain, together with (6.55) the following system of linear equations:

$$X(1 + 2gn_c) - \omega Y = 0\,,$$
$$Xg\left(\frac{2gn_c}{\omega} + (g+1)\Delta\right) + Y(g(2n_c + \omega\Delta) + 1) = 0 \tag{6.61}$$

These equations have a solution provided the following spectral equation is satisfied

$$\sum_{n=1}^{n_c} \frac{2\omega^2}{n^2 - \omega^2} - 1 = -\frac{(1 + \frac{g}{2}(1 + 2n_c))^2}{g(1 + g(1 + 2n_c)/4)}\,. \tag{6.62}$$

For small ω and large n_c, we have an approximate spectral equation:

$$\omega \cot(\pi\omega) \approx \frac{(1+\frac{g}{2}(1+2n_c))^2}{g(1+g(1+2n_c)/4)} \tag{6.63}$$

where we have used that

$$\sum_{n=1}^{n_c} \frac{2\omega^2}{n^2-\omega^2} \approx \sum_{n=1}^{\infty} \frac{2\omega}{n^2-\omega^2} = 1 - \pi\omega\cot(\pi\omega). \tag{6.64}$$

These spectral equations are valid for $\omega \neq 0$. They have the same qualitative features as (6.48) with a bounce flow in the negative g direction, passing first through a zero at $g = \frac{-2}{(1+2n_c)}$ describing NS fermions with half-integer modes, followed by a pole at $g = \frac{-4}{(1+2n_c)}$, describing integer modes and Ramond fermions. We have a "no flow" in the positive g direction.

We must consider whether the zero mode exists as it is instrumental in ensuring that we reproduce both towers of the NS spectrum at the intermediary fixed point where the towers are built on an even and odd number of modes respectively.

Firstly, we note that at $\omega = 0$ the third equation in (6.53) implies that

$$A_0' = B_0'. \tag{6.65}$$

Next, taking the sum of the first two equations in (6.53) implies that

$$A_{0,n} = B_{0,n} \tag{6.66}$$

whilst taking their difference gives the following equation:

$$A_{0,n} + 2gA_0 + 2gf_0 = 0. \tag{6.67}$$

Taking the sum over n of (6.67) we can write A_0 as

$$A_0 = \frac{-gn_cf_0}{(1+2gn_c)}. \tag{6.68}$$

It is clear from this equation that a coupling value of $g = \frac{-1}{2n_c}$ must be considered separately. We return to this case shortly.
Continuing, therefore, for $g \neq -\frac{1}{2n_c}$ we may substitute (6.68) into equation (6.67) which gives the following (by virtue of (6.66)):

$$A_{0,n} = B_{0,n} = -\frac{gf_0}{1+2n_c}. \tag{6.69}$$

If now we consider a coupling $g = -\frac{1}{2n_c}$, equation (6.68) implies that

$$f_0 = 0. \tag{6.70}$$

Finally then, we may solve (6.67) once more to find that

$$A_{0,n} = B_{0,n} = \frac{A_0}{n_c}, \tag{6.71}$$

which is constant. Therefore, the zero mode indeed always exists.

It is worth mentioning that in the continuum theory perturbations by T have a very different character depending on the sign of the coupling. The operator T restricted to a conformal boundary is proportional to the displacement operator. Perturbing with a negative coupling is equivalent to displacing the boundary outwards, away from the bulk while perturbing with a positive coupling is equivalent to displacing the boundary inwards. Consider the partition function on a cylinder of length L and circumference R with the perturbed boundary condition imposed on both ends, we have two possible quantisations which in string theory are usually referred to as the closed and the open string channels[4]. In the open string channel we represent the partition function in terms of the boundary (strip) spectrum while in the closed string channel we use a representation of the boundaries in terms of boundary states $|\alpha\rangle$:

$$\mathcal{Z} = \langle\alpha| \, e^{-LH^{\sigma}_{\text{cyl}}} \, |\alpha\rangle \tag{6.72}$$

[4]These were discussed previously, in section 2.2.

where

$$H^{\sigma}_{\rm cyl} = \frac{2\pi}{R}(L^{\sigma}_0 - c/24) \tag{6.73}$$

is the Hamiltonian on the cylinder generating translations in the σ direction. The boundary state $|\alpha\rangle$, written as the T-perturbation of, say, the fixed boundary condition, reads

$$|\alpha\rangle = e^{\frac{2\pi\tilde{g}}{R}L^{\sigma}_0}|+\rangle\rangle \tag{6.74}$$

where $\tilde{g}$ is the dimensionful coupling. For a positive T-perturbation, when the boundaries move towards each other we obtain a singularity in the partition function at the value of dimensionless coupling

$$g_{\rm crit} = \frac{\tilde{g}_{\rm crit}}{L} = \frac{1}{2} \tag{6.75}$$

when the unperturbed boundaries sit on top of each other. This clearly signals a pathology of the boundary spectrum at this value of the coupling.

For negative values of the coupling the two ends of the cylinder are shifted away from each other and there is no singularity. This behaviour is qualitatively similar to the $T\bar{T}$ perturbation of the bulk theories discussed in [76], [77].

We should emphasise that in considering the T-perturbation in this section we solve the truncated version of the theory, not adding any counter terms which would be needed in a continuum limit. Such regulated theories should then be very sensitive to the method of regularisation. In the next section we take up the T-perturbation in TCSA. It shows a qualitatively different behaviour from the mode truncated case for positive couplings.

6.3 Perturbations by irrelevant operators in TCSA

As discussed in chapter 4 we assume that the TCSA Hamiltonian in the vicinity of an IR fixed point can be described by a continuum theory with a tower of irrelevant operators switched on. Under certain assumptions the flow towards a fixed point gets reflected in the irrelevant operators space of couplings. In the models we studied numerically the flows beyond eventually terminate with a "no flow" (that is, small changes to the spectrum are suppressed as we increase $\Delta_{\rm max}$). Presumably this can

also be modelled as some particular perturbation of the fixed point by irrelevant operators. The exactly solvable case of the T-perturbation in the mode truncation scheme shows this. We would like to model this situation using TCSA numerics, that is, find particular perturbations by irrelevant operators that in TCSA demonstrate approximately no flow.

6.3.1 T-perturbations

We first consider, in the Ising model, the case when the IR fixed point is described in terms of Ramond fermions. This corresponds to having a fixed boundary condition on the flowing end of the strip and a free one on the spectator end. The leading irrelevant operator along which the boundary magnetic field flows terminate is the stress-energy tensor, T. The corresponding perturbed Hamiltonian is

$$h^{IR} = \frac{1}{24} + \sum_{k=1}^{\infty} k\, b_k^\dagger b_k - \frac{g}{2} : \left(\left[\sum_{k=1}^{\infty} (b_k^\dagger + b_k) + b_0 \right] \sum_{l=1}^{\infty} l(b_l^\dagger - b_l) \right) : \tag{6.76}$$

with a coupling constant g which we allow to vary freely. Taking a negative g and increasing it in magnitude corresponds to flowing backwards along the boundary magnetic field flow. For large enough $|g|$ the higher dimensional irrelevant operators will become important. We will neglect these in the initial analysis. Plots of the normalised energy gaps for both signs of the coupling g are presented below on Fig. 6.5 against $\ln|g|$.

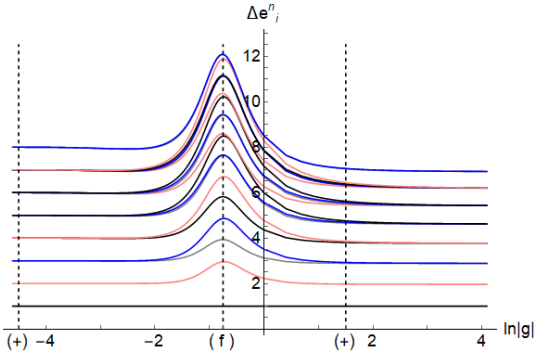

(a) T perturbation of the Ramond Fixed point with positive coupling with $\Delta_{\max} = 26$.

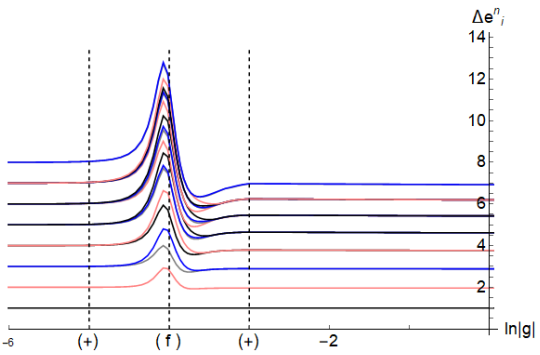

(b) T perturbation of the Ramond Fixed point with negative coupling with $\Delta_{\max} = 26$.

Figure 6.5

We see that going in the negative g direction the spectrum describes a loop in the

theory space when we first 'reverse' the flow from the UV fixed point given by the free boundary condition and then flow back into the $g = 0$ fixed point. Interestingly the same loop is observed when flowing into the unphysical positive g direction. The only difference between the two directions is that for positive g the vicinity of the UV fixed point is reached later than for the negative coupling. This is in contrast with the exact solution for the mode truncated T-perturbation discussed in section 6.2 where there is a "no flow" for positive g perturbation.

We next consider the T-perturbation of the IR fixed point that corresponds to having fixed boundary conditions on both ends. The perturbed Hamiltonian is

$$\begin{aligned} h^{IR} = &- \frac{1}{48} + \sum_{k=0}^{\infty} (k + 1/2)\, b^{\dagger}_{k+1/2} b_{k+1/2} \\ &- \frac{g}{2} : \left(\sum_{k=0}^{\infty} (b^{\dagger}_{k+1/2} + b_{k+1/2}) \sum_{l=0}^{\infty} (l + 1/2)(b^{\dagger}_{l+1/2} - b_{l+1/2}) \right) : . \end{aligned} \tag{6.77}$$

This is described by a single primary tower in the NS fermions Fock space. We choose the boundary conditions below to have the fixed up boundary condition on the top end of the strip and the fixed down one on the bottom end with representation built on the Virasoro ϵ-tower. The numerical values for normalised energy gaps are plotted on Fig. 6.6 against $\ln|g|$ for $\Delta_{\max} = 27.5$ corresponding to a basis of 957 states.

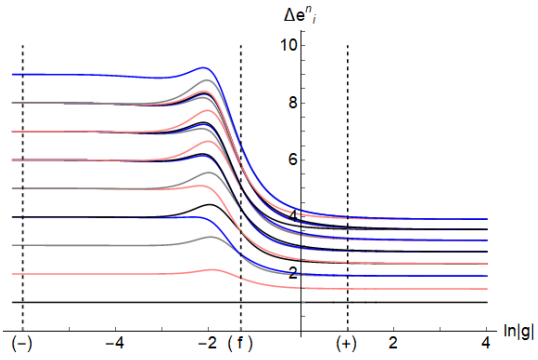

(a) Perturbation of NS fermions (ϵ representation) by T with positive coupling.

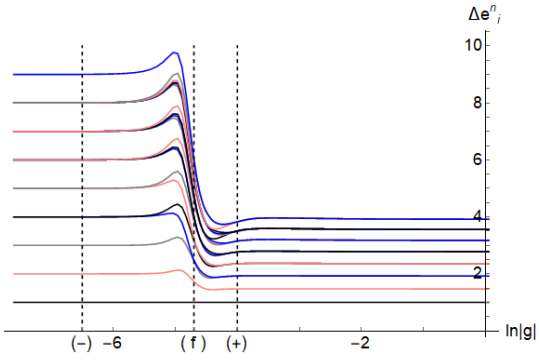

(b) Perturbation of NS fermions (ϵ representation) by T with negative coupling.

Figure 6.6

The flow generated by this perturbation is described by the following diagram

$$(-) \to (f) \to (+)\,. \tag{6.78}$$

The spectrum interpolates between the two NS primary towers (the identity and ϵ) with an intermediary fixed point describing the free boundary condition with a fixed spectator. The fact that we flow beyond the (f) boundary condition towards the reversed spin fixed boundary condition suggests that the relevant coupling of ψ_{13} near (f) gets reflected, which seems to be the pattern with the flows beyond. The spin reversal on the flowing end was not visible with the free spectator due to the spin reversal symmetry. The reversal of spin in (6.78) also means that the T-perturbation of the IR fixed point does not give the same loop as the flow beyond starting from the UV fixed point (which we observed for the fixed spectator in section 6.1).

We also note that, as with the free spectator, the behaviour is qualitatively different from that of the mode truncation scheme with both directions of the flow containing a further flow beyond the fixed point. The flow is realised much earlier for negative coupling as was also seen in the previous example.

We have also looked into the T-perturbation of the (+) boundary condition in the tricritical Ising model. This is a stable infrared fixed point for the ψ_{13} flow originating from the (0+) boundary condition under positive coupling discussed in section 6.1. This is also the end point of the cascade of ψ_{13} flows from (-0) which are equivalent, by spin reversal, to flows from (0+) with negative coupling ending at (-), also discussed in 6.1.
The Hamiltonian describing this perturbation is

$$h^{\mathrm{IR}} = L_0^{\mathrm{IR}} + gT(0). \tag{6.79}$$

On Figure 6.7 we present plots of the normalised energy gaps against $\ln|g|$.

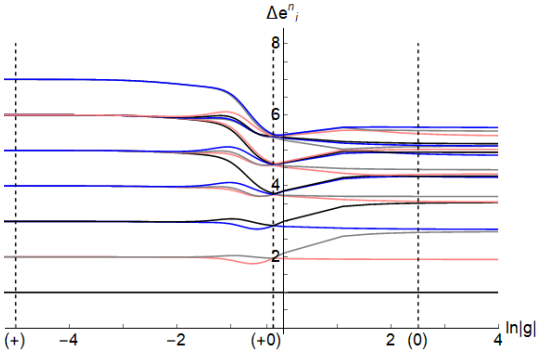

(a) T-perturbation of the (+) boundary condition with the identity spectator in TIM, positive coupling $\Delta_{\max} = 25$.

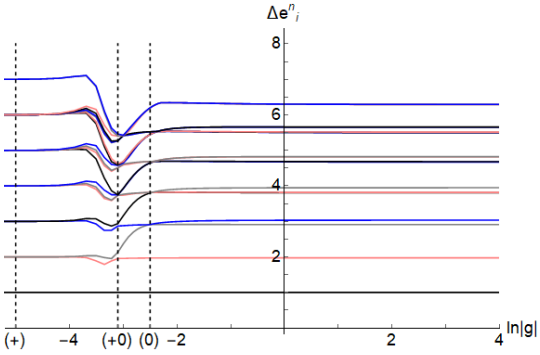

(b) T-perturbation of the (+) boundary condition with the identity spectator in TIM, negative coupling $\Delta_{\max} = 25$.

Figure 6.7

We observe that for both positive and negative coupling we move backwards along the cascade of flows beyond discussed in section 6.1. Thus, the T-perturbation alone does not quite describe the end of the cascade, generating instead, as in the above examples, a flow back to the nearest UV fixed point first, followed by further flows beyond before stopping. In the next section we discuss how higher dimension irrelevant operators added to T can qualitatively change the T-perturbation spectrum for large positive coupling in the Ising model.

6.3.2 Higher order irrelevant perturbations in the Ising model

We would like to modify the irrelevant perturbation of the IR fixed point by adding higher dimension operators to T. In doing so we try to find a situation of a 'no flow' in the reflected direction (positive coupling of T). The higher dimension operators we add are supposed to model, in the IR theory, the truncation effects of the UV theory as well as the subleading irrelevant operators present in the continuum theory on approach to the IR fixed point. The first operator of dimension higher than T is $:\psi\partial_\tau^3\psi:$. We have experimented adding it to the T-perturbation with different relative signs and found significant changes in the asymptotic spectrum sensitive to the relative sign. However we did not see a "no flow" situation. Adding other fermionic bilinears does not change the situation drastically. It should be noted that all fermion bilinears are closed under OPE and thus keep the perturbed continuum theory within a certain subspace under the RG action. The smallest dimension

operator that is not bilinear in the fermions is the operator

$$\mathcal{O}_4 =: \psi \partial_\tau \psi \partial_\tau^2 \psi \partial_\tau^3 \psi : \tag{6.80}$$

which is quartic in the free fermion field and has dimension 8.

Beginning at the IR point, we add a perturbation by the quartic term to see if this can model the flows beyond near the IR fixed point. We consider perturbations of the form:

$$h^{\mathrm{IR}} = L_0^{\mathrm{IR}} + g(T(0) \pm \eta \mathcal{O}_4(0)) \tag{6.81}$$

where η is some fixed constant. The operator $\mathcal{O}_4$ has very large matrix elements. To observe changes in the energy levels we found it convenient to set $\eta = 5e^{-19}$. Looking at the quartic interaction only, i.e. perturbing by $\eta g \mathcal{O}_4(0)$ only, we get the following remarkably ordered picture (Fig. 6.8) in which the energy gaps $e_i - e_0$ are presented against g.

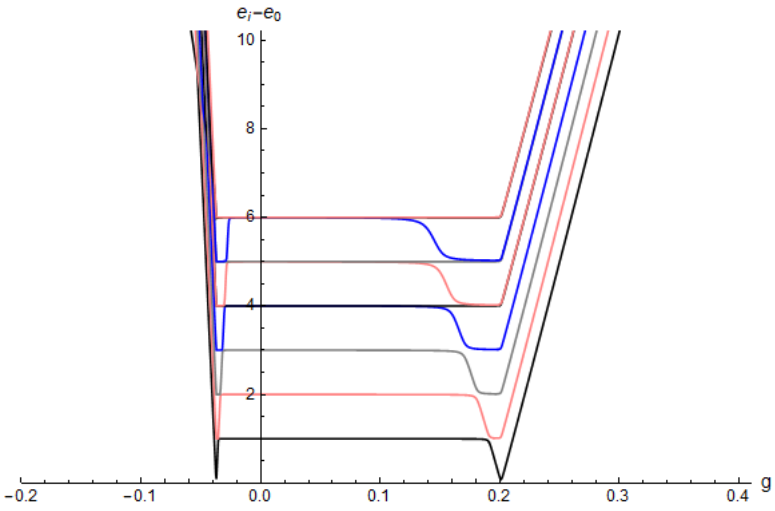

Figure 6.8: Perturbation of NS (13) fermions by the quartic term for both positive and negative coupling with $\Delta_{\max} = 25.5$.

The behaviour is peculiar with almost all states dropping by one level at a very distinct value of the coupling, which is then followed by an almost uniform linear regime.

Next, in Fig. 6.9 we look at the normalised energy gaps Δe_i^n for different choices of sign in (6.81) with $\Delta_{\max} = 25.5$ corresponding to a state space of dimension 688. Here the spectator boundary condition is (+) and the initial flowing boundary

condition is $(-)$.

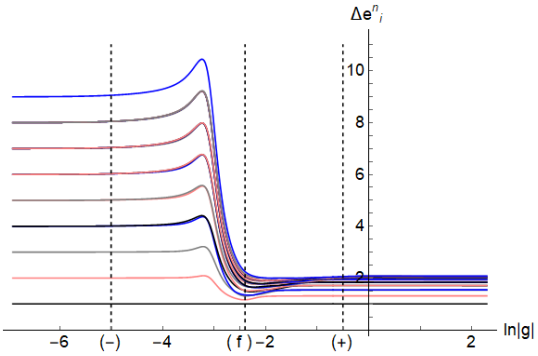

(a) Perturbation of NS fermions by T and the quartic operator with positive g and $+\eta$ chosen in (6.81).

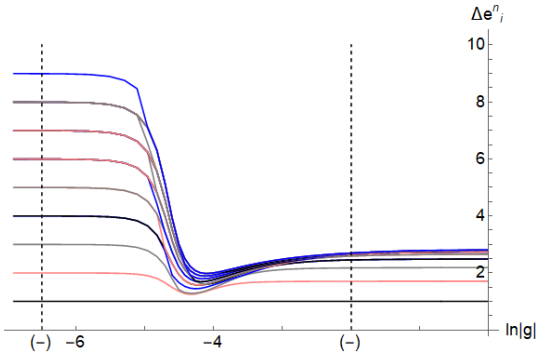

(b) Perturbation of NS fermions by T and the quartic operator with positive g and $-\eta$ chosen in (6.81).

Figure 6.9

The intermediate and the final multiplicities are different when we change the sign in front of η. For positive η we indeed reach the UV fixed point describing Ramond fermions as one might expect. For negative η it is difficult to discern what happens to the multiplicities in this intermediate regime where it does not look as though the UV fixed point is reached. The asymptotic multiplicities, however, are easy to read off in both cases. With the plus sign in front of η starting with the $(-)$ boundary condition we arrive at the $(+)$ one that corresponds to the end point of the T-perturbation flow (6.78). For the minus sign in front of η the end multiplicities are the same as at the starting boundary condition. We get the same result for choosing the spectator to be $(-)$ that is the same as the initial boundary condition. Hence we see that this particular irrelevant perturbation, given by (6.81) with the minus sign, behaves like the end of the flow we observed in the flows beyond examples discussed above[5].

6.4 A maverick: Ising model with free spectator

In section 6.1 we reviewed a number of examples of flows beyond the fixed point. Locality would imply that the qualitative behaviour of these flows is independent of the choice of spectator boundary condition and indeed this is the case in the tricritical Ising model. In the Ising model the reverse flows are observed in the

[5]The results are also similar whether we take positive or negative g.

Ramond sector. For the free spectator we start with two primary towers present in the UV theory: the identity and the ϵ-tower described by NS fermions. The multiplicities for low lying states up to level 8 are shown in Table 6.1.

Δ	0	1/2	1	3/2	2	5/2	3	7/2	4	9/2	5	11/2	6	13/2	7	15/2	8
$\mathbb{I}$ - tower	1	0	0	0	1	0	1	0	2	0	2	0	3	0	3	0	5
ϵ - tower	0	1	0	1	0	1	0	1	0	2	0	2	0	3	0	4	0
$\mathbb{I}+\epsilon$ towers	1	1	0	1	1	1	1	1	2	2	2	2	3	3	3	4	5

Table 6.1: Multiplicities of NS fermions.

For a reversed flow we would expect the asymptotic multiplicities to be the same as the starting ones – given by both Virasoro towers. The numerical results plotted on Figure 6.10 do not show this. Whilst we see that the IR fixed point is reached, with the correct multiplicities, there is a further rearrangement of the spectrum in the asymptotic regime where the multiplicities do not correspond to a Cardy boundary condition.

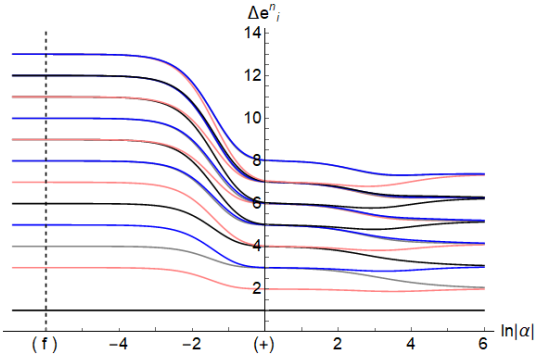

(a) NS Sector. TCSA normalised energy gaps with $\Delta_{\max} = 31.5$ against $\ln|\alpha|$.

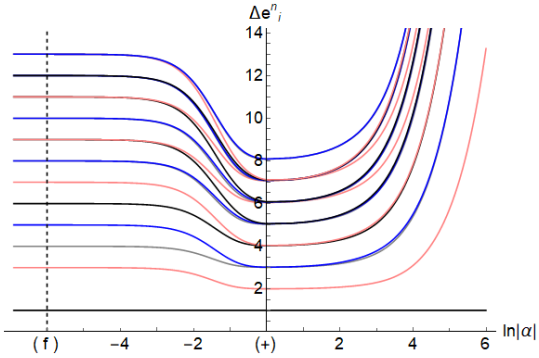

(b) NS Sector. TCSA normalised energy gaps with $\Delta_{\max} = 32$ against $\ln|\alpha|$.

Figure 6.10

Moreover the asymptotic spectra depend on the truncation scheme, falling into two distinct patterns depending on whether $\Delta_{\max}$ is integer or half-integer. In particular the asymptotic vacuum state becomes doubly degenerate for integer $\Delta_{\max}$ while it is unique for half-integer $\Delta_{\max}$. The flow certainly looks 'deliberate' and we investigate this behaviour more closely now.

The low lying asymptotic spectrum, although not described by a fixed point, can

still be described in terms of the NS Virasoro towers[6]. For half-integer $\Delta_{\max}$ one should shift the weights in the ϵ-tower by 1/2 and add this to the identity tower. For integer $\Delta_{\max}$ the asymptotic multiplicities can be obtained by shifting the weights in the ϵ-tower by -1/2 and adding it to the identity tower. The resulting multiplicities are illustrated in the two tables below.

Δ	0	1	2	3	4	5	6	7	8
$\mathbb{I}$ - tower	1	0	1	1	2	2	3	3	5
ϵ - tower with weights shifted by +1/2	0	1	1	1	1	2	2	3	4
TCSA asymptotic multiplicities	1	1	2	2	3	4	5	6	9

Table 6.2: Observed multiplicities of the large coupling fixed point with half-integer $\Delta_{\max}$.

Δ	0	1	2	3	4	5	6	7	8
$\mathbb{I}$ - tower	1	0	1	1	2	2	3	3	5
ϵ - tower with weights shifted by -1/2	1	1	1	1	2	2	3	4	5
TCSA asymptotic multiplicities	2	1	2	2	4	4	6	7	10

Table 6.3: Observed multiplicities of the large coupling fixed point with integer $\Delta_{\max}$.

This pattern of shifted towers leads us to think that the important characteristic of the truncation scheme is the difference between $\Delta^1_{\max}$ – the maximal conformal weight in the truncated identity tower, and $\Delta^\epsilon_{\max}$ – the maximal conformal weight in the truncated ϵ- tower. The difference $\Delta^\epsilon_{\max} - \Delta^1_{\max}$ is $-1/2$ when $\Delta_{\max}$ is integer and $+1/2$ when $\Delta_{\max}$ is half integer. We test this pattern further using generalised truncation schemes (3.5) in which we use arbitrary positive integers $N^1_{\max}$, $N^\epsilon_{\max}$ to truncate the descendants in each tower. For such schemes we introduce a parameter

$$d = |\Delta^\epsilon_{\max} - \Delta^1_{\max}| = |1/2 + N^\epsilon_{\max} - N^1_{\max}|\,. \tag{6.82}$$

Using schemes with different values of d we checked numerically that the asymptotic spectrum is described by shifting the weights of the tower with the larger value of

[6]We are grateful to G. Watts for this observation.

$\Delta^i_{\max}$ by d units up. For illustration in Table 6.4 we give the asymptotic weights corresponding to the scheme with $N^1_{\max} = 30$ and $N^\epsilon_{\max} = 31$ that has $d = 3/2$.

Δ	0	1	2	3	4	5	6	7	8
$\mathbb{I}$ - tower	1	0	1	1	2	2	3	3	5
ϵ - tower with weights shifted by +3/2	0	0	1	1	1	1	2	2	3
TCSA asymptotic multiplicities	1	0	2	2	3	3	5	5	8

Table 6.4: observed multiplicities of the large coupling fixed point with $\Delta_{\max} = 31.5$, $\Delta^1 = 30$, $\Delta^\epsilon = 31.5$ and $d = 3/2$.

For large values of the splitting parameter d the two towers become completely decoupled (as far as the low energy states are concerned). The plot on Fig. 6.11 shows the normalised energy gaps for the scheme with $N^1_{\max} = 7$ and $N^\epsilon_{\max} = 21$ with $d = 14.5$.

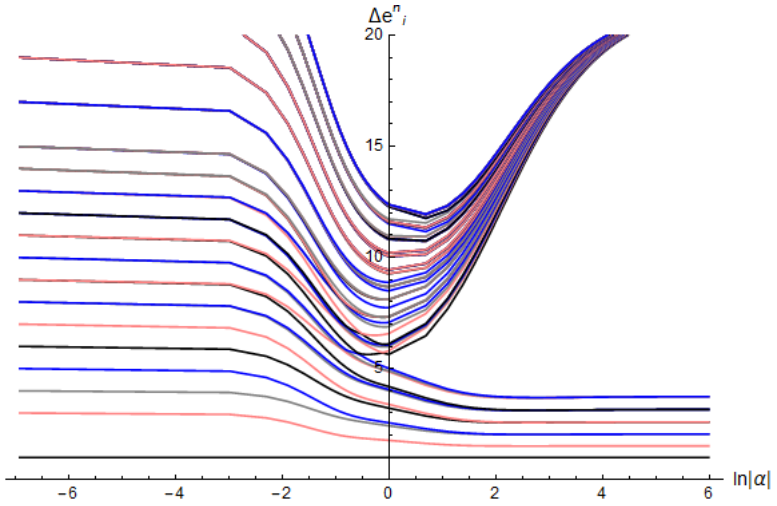

Figure 6.11: Δe^n_i against $\ln|\alpha|$ for free spectator, positive coupling and $N^1_{\max} = 7$, $N^\epsilon_{\max} = 21$.

In the asymptotic regime the flow is dominated by the interaction matrix. The perturbing term in (5.5) has a block structure with interacting terms coming only from the mixing of states between the two towers. Increasing the split between the two towers, we remove matrix elements from the interaction. The multiplicities of the low lying spectrum match those of the smallest tower. The second tower is essentially decoupled from this low lying spectrum. The tight band of levels that are lifted in the asymptotic regime visible on the plot above corresponds to the zero eigenvalue of the interaction matrix. Its multiplicity is given by the difference between the dimensions of the two truncated towers.

The split in energies between the two towers can be expected based on Renormalisation Group analysis of truncation effects introduced in [53]. As shown in [53] whenever a self-coupling is present perturbatively, via a non-vanishing three-point function of the perturbing operator, as is the case in TIM, it gives the dominant truncation effect in the form of a coupling constant running with $\Delta_{\max}$. In the Ising model such a self-coupling is absent and it was shown in [54] that the leading truncation effect can be described via a coupling to a non-local operator, $(-1)^N$, where N is the free fermion number[7]

$$N = \sum_{n=0}^{\infty} a^{\dagger}_{n+1/2} a_{n+1/2} \,. \tag{6.83}$$

As yet, there is no clear explanation for the quantisation that we have detailed previously. Looking at higher orders in perturbation theory may give some indication as to why the scaling is bounded and the energy levels are shifted by precisely 1/2.

It appears to be important to understand in general when the non-local operators are important for TCSA truncation effects. We hope to return to this question in future work.

6.4.1 A maverick: dual description

There is a dual description of this model which we may consider[8]. Starting with the fixed up boundary condition on the upper boundary and a superposition of fixed up and fixed down on the lower, we can add a boundary changing field perturbation to the lower boundary. The Hilbert space in the UV is $\mathcal{H}(0) + \mathcal{H}(1/2)$ and the boundary changing field on the lower boundary has weight h=1/2. That the models are dual (at least up to extra identity fields) can be easily seen by pulling a σ topological defect off the top boundary of the previous picture and moving it to the bottom boundary. The superposition of fixed up and fixed down boundary conditions is realised according to the fusion rules.

[7]For the fixed spectator, the coupling to $(-1)^F$ cancels, explaining why we do not see these shifted flows in this sector.

[8]We thank Gerard Watts for bringing this to our attention.

This dual description contains an additional local operator, the identity, which we can switch on. Adding $\mathbb{I}_0$ or $\mathbb{I}_{1/2}$ fields on the component boundaries on the bottom edge into the action, or equivalently adding projectors onto the $\mathcal{H}(0)$ and $\mathcal{H}(1/2)$ parts of the Hilbert space into the Hamiltonian, we can control the initial representation in the UV in such a way as to realise reverse flows beginning and ending at the 'maverick' fixed points discussed above. Indeed, if in our initial picture, we add $\pm 1/2\mathbb{I}_0$ or $\pm 1/2\mathbb{I}_{1/2}$ to the free Hamiltonian in the UV, we begin the flow from one of the two 'maverick' endpoints.

The plots on Fig. 6.12 below show the results of adding the identity operator in the UV with the following Hamiltonian:

$$H = H_0 \pm \frac{1}{2}\mathbb{I}_0 + \alpha\psi_{13}$$

The first plot shows results for positive coupling to the identity. We see the flow beginning at the large coupling fixed point in the previous picture with integer truncation and proceeding as before.

Shown in the second plot are the negative coupling results beginning at the large coupling fixed point of the half-integer truncation picture, this time with a further 'reverse flow beyond' similar to the sequence seen in the Ramond sector ψ_{13} perturbation.

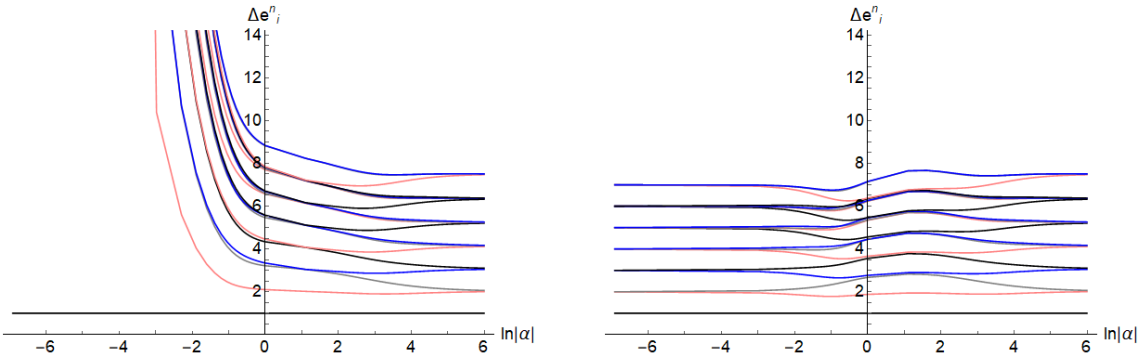

(a) NS: H = H_0+1/2$\mathbb{I}_0$ + $\alpha\psi_{13}$ for $\Delta_{\max}$ = 25.

(b) NS: H = H_0-1/2$\mathbb{I}_0$ + $\alpha\psi_{13}$ for $\Delta_{\max}$ = 25.

Figure 6.12

Adding a term proportional to $\mathbb{I}_{1/2}$ to the UV allows us to control the initial

fixed point in a similar way. We also note that the effect on the UV multiplicities for half-integer $\Delta_{\max}$ is similar.

More work is needed to understand this picture more clearly. It is certainly curious that the additional local operators can produce the same 'maverick' multiplicities, now in the UV. However, many questions remain. The origin of the precise value of the couplings is, as yet, unclear. Additionally, if we are to work in this picture, it is desirable to understand how these operators behave under RG by running the coupling.

6.5 Different truncation methods for TIM

Whenever we have more than one primary tower in the UV spectrum we can apply the truncation schemes (3.5). In the tricritical Ising model for the UV boundary condition (0+) and the spectator (d), the state space contains two Virasoro towers corresponding to the primaries σ and σ'. For the truncation schemes with $N^{\sigma} = 20$ and $N^{\sigma'} = 18, 19$ we find that for positive coupling the flow gets close to the (+) fixed point and that the flows beyond are susceptible to these changes in truncation scheme, with, in particular, some examples showing rearrangements in the multiplicities which do not correspond to a known fixed point. For negative coupling we obtain a picture qualitatively different from the simple truncation scheme. Past the first IR fixed point (0) we obtain a flow beyond to multiplicities that may not correspond to a known fixed point (see the plot below where the vacuum becomes degenerate). However, past this region the multiplicities rearrange further with the 3 low lying levels being the same as that describing the (−) boundary condition that is the left end of the cascade of TCSA flows. On Figure 6.13 the reader can see a plot of energy gaps normalised by dividing them by $e_2 - e_0$.

The effects of increasing the split in truncation levels between the two towers are similar to the Ising model in the NS sector. However, some important differences do remain. In particular, while for some truncation schemes we pass through a point that cannot be identified as a fixed point, asymptotically we always recover the multiplicities of the (−) fixed point for negative coupling. For positive coupling, the

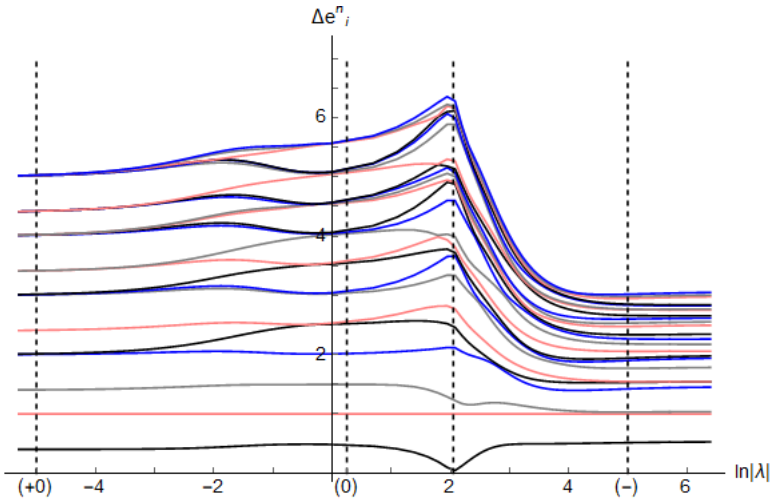

Figure 6.13: Normalised Energies (wrt E_2) in the perturbed TIM with (d) spectator for negative coupling. Respective truncation levels $N^{\sigma} = 20$, $N^{\sigma'} = 18$.

multiplicities of the (+) fixed point are not always reached. For the simple truncation scheme governed by $\Delta_{\max}$ we always flow through identifiable fixed points. The difference with the Ising model can be explained by the absence in the latter of the self-coupling of the ϵ operator that would be responsible for the leading truncation effects [53].

Chapter 7

Conclusions

In this section we attempt to summarise our investigations.

This thesis has been concerned with the application of the Truncated Conformal Space Approach to boundary perturbations of Conformal Field Theories, focusing mainly on two areas of investigation: studying the TCSA spectrum on approach to the IR fixed point and investigating the behaviour of the TCSA spectrum past this point and the 'flows beyond' in particular.

In chapter 3, we introduced the Truncated Conformal Space Approach and detailed a procedure for its technical implementation. This algorithm is for the construction of a basis of states in a (Conformal) Field Theory described by the Virasoro algebra. We have also included a short note on how such a procedure may be carried out in the free fermion picture. Matrix elements of the perturbed Hamiltonian are calculated for boundary perturbations by a primary operator Ψ. We have provided some technical details on constructing the programme in Mathematica and included some helpful principles for optimising the implementation. Associations, new in Mathematica versions 10 and beyond, have been introduced. Incorporating these into the TCSA routine allows for a vast increase in speed of both basis generation and calculation of matrix elements.

In chapter 4 we offered a tentative explanation for why the leading truncation error is linear. It is desirable to understand this better, confirming or disproving that sce-

nario. It would be interesting to understand the subleading corrections and improve upon the numerical accuracy of the method.

In chapter 5 we studied numerically how TCSA behaves near the IR fixed point. We identified the leading truncation error in that region as a certain linear function. We designed two methods that subtract the leading error and extract a numerical approximation to the leading infrared exponent that is the dimension of the leading irrelevant operator along which the RG trajectory approaches the fixed point. It would be interesting to apply this method to other models and determine whether the two linear regimes observed here are present there also.

In chapter 6 we studied the behaviour of TCSA energy levels past the closest approach to the IR fixed point. There we observed, confirming prior work by other people, flows beyond where the energy levels rearrange their multiplicities passing through several discernible regimes. We investigated how these flows depend on the choice of the spectator boundary condition and on the choice of the truncation scheme. We presented examples of 3 types of behaviour: when the flow beyond arrives to a known fixed point, reversing a known RG flow; when the flow beyond arrives to a set of multiplicities not corresponding to any fixed point; when there is no flow beyond at all. We found that one scenario can be replaced by another when we change the truncation scheme and/or the spectator boundary condition.

Our working hypothesis, discussed in section 4, is that the TCSA behaviour near the IR fixed point can be described by the continuum theory with a number of irrelevant *local* operators switched on. Based on this, we described a possible scenario of how the flow beyond may originate, starting at the IR fixed point, via the leading irrelevant perturbation, with the reversed sign of the coupling. The behaviour of the TCSA spectrum past the IR fixed point then depends heavily on the truncation scheme used. We were able to model the qualitative behaviour of TCSA flows beyond by adding higher dimension irrelevant perturbations to the leading one, producing a 'no-flow' situation. This could be used in future to model the end of a sequence of flows in which a variety of irrelevant operators are switched on in the

strong coupling limit of relevant perturbations of UV fixed points.

The assumption of locality of an effective description remains essential in describing flows that pass or end at a physical fixed point. In some cases, like the boundary magnetic field perturbation in the Ising model with a free spectator, we observed a flow to an unphysical set of multiplicities. The fact that this depends on a choice of spectator boundary condition suggests that some non-local operators may be needed to describe TCSA corrections in such cases. This is corroborated by a perturbative calculation in that model [54]. It is important for future progress to understand theoretically in which cases the non-local operators are important and how to take them into account, or how to modify the truncation scheme to suppress their effects. We discussed a dual model of this theory which contains additional local operators in the UV which may be switched on in order to control the UV starting point of our flows. It would be useful to understand the effects of these operators on the IR spectrum under RG flow. This dual model is constructed using a conformal defect and is, therefore, irreversible. It would be interesting to establish an explanation of how these local operators may be mapped to non-local operators in the original description and to understand the relationship between these two descriptions more completely.

Bibliography

[1] E. Noether, *Invariante Variationsprobleme*, Nachr. d. Konig. Gesellsch. d. Wiss. zu Gottingen, Math-phys. Klasse, 235257 (1918).

[2] E. Noether, *Invariant Variation Problems*, M. A. Tavels English translation of Invariante Variationsprobleme, arXiv:physics/0503066.

[3] L. Landau, *On the Theory of Phase Transitions*, Translated and reprinted from Landau L.D. Collected Papers (Nauka, Moscow, 1969), Vol. 1, pp. 234252. Originally published in Zh. Eksp. Teor. Fiz. 7, pp. 1932 (1937)

[4] M. E. Fisher, *Renormalization of Critical Exponents by Hidden Variables*, Physical Review 176: 25772 (1968).

[5] L. P. Kadanoff, Critical Behavior. Universality and Scaling in Proceedings of the International School of Physics Enrico Fermi, Course LI (27 July 8 August 1970). Edited by M. S. Green (1971).

[6] A.A. Belavin, A. M. Polyakov, A. B. Zamolodchikov, *Infinite conformal symmetry in two-dimensional quantum field theory*, Nucl. Phys. **B241** 333 (1984).

[7] V.G. Kacs, *Contravariant form for infinite dimensional Lie algebras and superalgebras*, Lecture notes in physics, vol. 94, Springer-Verlag Berlin (1979).

[8] B.L. Feigin, D.B. Fuchs, *Skew-symmetric differential operators on the line and Verma modules over the Virasoro algebra*, Funct. Anal. and Appl. **17** 114 (1982).

[9] S. Ferrara, A. Grillo, and R. Gatto, *Tensor representations of conformal algebra and conformally covariant operator product expansion*, Annals Phys. 76 (1973) 161188.

[10] A. Polyakov, *Nonhamiltonian approach to conformal quantum field theory*, Zh.Eksp.Teor.Fiz. 66 (1974) 2342.

[11] D. Friedan, Z.-a. Qiu, and S. H. Shenker, *Conformal Invariance, Unitarity and Two-Dimensional Critical Exponents*, Phys.Rev.Lett. 52 (1984) 15751578.

[12] M. Gell-man, F.E. Low, *Quantum Electrodynamics at small distances*, Physical Review. 95 (5): 13001312 (1954).

[13] L.P. Kadanoff, *Scaling laws for Ising models near T_c*, Physics. 2: 263. (1966)

[14] K.G Wilson, *The renormalization group: Critical phenomena and the Kondo problem*, Rev. Mod. Phys. 47 (4): 773 (1975).

[15] K.G Wilson, (1971). *Renormalization group and critical phenomena. I. Renormalization group and the Kadanoff scaling picture*, Physical Review B. 4 (9): 31743183 (1971).

[16] K.G Wilson, *Renormalization group and critical phenomena. II. Phase-space cell analysis of critical behavior*, Physical Review B. 4 (9): 31843205 (1971).

[17] K.G. Wilson, M. Fisher, *Critical exponents in 3.99 dimensions*, Physical Review Letters. 28 (4): 240 (1972).

[18] Ph. Di Francesco, P. Mathieu, D. Senechal. *Conformal Field Theory* , Springer 1998.

[19] S. V. Ketov. *Conformal Field Theory*, World Scientific Publishing, 1995.

[20] R. Blumenhagen, E. Plauschinn. *Introduction to Conformal Field Theory with Applications to String Theory*, Springer, 2009.

[21] F . A. Bezerin. *The Method of Second Quantization*, Academic Press Inc. 1996.

[22] P. Ginsparg, *Applied Conformal Field Theory*, Fields, Strings and Critical Phenomena, (Les Houches, Session XLIX, 1988) ed. by E. Brézin and J. Zinn Justin, 1989; arXiv:hep-th/9108028.

[23] J.L. Cardy, *Conformal Invariance And Statistical Mechanics* , Fields, Strings and Critical Phenomena, (Les Houches, Session XLIX, 1988) ed. by E. Brézin and J. Zinn Justin, 1989.

[24] J. Qualls, *Lectures on Conformal Field Theory*, Lecture notes based on course given at National Taiwan University, National Chiao-Tung University, and National Tsing Hua University 2015; arXiv:hep-th/1511.04074.

[25] E. Verlinde, *Fusion rules and modular transformations in 2D conformal field theory*, Nucl. Phys. **B300** (1988) 300-367.

[26] J. Cardy, *Boundary Conditions, Fusion Rules and the Verlinde Formula*, Nucl. Phys. **B324** (1989) 581-596.

[27] J. Cardy, *Conformal invariance and surface critical behaviour*, Nucl. Phys. **B240** 514 (1984).

[28] N. Ishibashi, *The Boundary and Crosscap States in Conformal Field Theories*, Mod. Phys. Lett. A4 (1989) 251.

[29] V. G. Kac, *Simple graded Lie algebras of finite growth*, Func. Anal. Appl. 1, 328 (1967).

[30] A. M. Polyakov, *Conformal symmetry of critical fluctuations*, JETP Lett. **12**, 381 (1970).

[31] F. Kos, D. Poland, D. Simmons-Duffin, A. Vichi, *Precision islands in the Ising and O(n) models*, JHEP. (2016) 2016: 36.

[32] K. Wilson, *Broken scale invariance and anomalous dimensions*, in *Proceedings of Midwest Conference on Theoretical Physics*, Notre Dame, 1970, pg. 31.

[33] J. Polchinski, *Scale and conformal invariance in Quantum Field Theory*, Nucl.Phys. B303 (1988) 226-236.

[34] M. E. Peskin and D. V. Schroeder, *An Introduction to Quantum Field Theory*, Addison-Wesley, Reading, 1995. 2nd edition, pbk. Westview Press. 2015.

[35] M. D. Schwartz, *Quantum Field Theory and the Standard Model*, Cambridge University Press, 2013.

[36] D. Skinner, *Quantum Field Theory II*, Lecture notes, Part III of the Mathematical Tripos, University of Cambridge.

[37] A. B. Zamolodchikov, *"Irreversibility" of the Flux of the Renormalization Group in a 2D Field Theory*, JETP Lett. 43: 730732 (1986).

[38] J. R. Schrieffer, P.A. Wolff, *Relation between the Anderson and Kondo Hamiltonians*, Phys. Rev. **149** pg 491-492 (1966).

[39] S. Bravyi, D. P. DiVincenzo, D. Loss, *Schrieffer-Wolff transformation for quantum many-body systems*, Ann. Phys. Vol. 326, No. 10, pp. 2793-2826 (2011).

[40] C. G. Callan, *Broken Scale Invariance in Scalar Field Theory*, Phys. Rev. D 2, 1541 (1970).

[41] K. Symanzik, *Small distance behaviour in field theory and power counting*, Commun. Math. Phys. 18, 227 (1970).

[42] V. Yurov and Al. Zamolodchikov, *Truncated Conformal Space Approach To Scaling Lee-yang Model*, Int. J. Mod. Phys. **A5** (1990) 3221-3246.

[43] V. Yurov and Al. Zamolodchikov, *Truncated fermionic space approach to the critical 2-D Ising model with magnetic field*, Int. J. Mod. Phys. **A6** (1991) 4557-4578.

[44] M. Lässig, G. Mussardo, and J.L. Cardy, *The scaling region of the tricritical Ising model in two dimensions*, Nucl. Phys. **B348** (1991) 591.

[45] P. Dorey, A. Pocklington, R. Tateo, and G. Watts, *TBA and TCSA with boundaries and excited states*, Nucl. Phys. **B525** (1998) 641; arXiv:hep-th/9712197.

[46] P. Dorey, I. Runkel, R. Tateo, and G. Watts, *g - function flow in perturbed boundary conformal field theories*, Nucl. Phys. B 578, 85 122 (2000).

[47] P. E. Dorey, M. Pillin, R. Tateo, and G. M. T. Watts, *One-point functions in perturbed boundary conformal field theories*, Nucl. Phys. B 594, 625 659 (2001).

[48] Z Bajnok, L Palla, and G Takács, *Boundary states and finite size effects in sine-gordon model with neumann boundary condition*, Nuclear Physics B 614, 405448 (2001).

[49] M. Kormos, I. Runkel, and G. M. T. Watts, *Defect flows in minimal models*, JHEP 2009, 057 (2009).

[50] P. Dorey, M. Pillin, A. Pocklington, I. Runkel, R. Tateo, and G. M. T. Watts, *Finite size effects in perturbed boundary conformal field theories*, conference proceedings, *Non-perturbative Quantum effects 2000*, hep-th/0010278.

[51] G. Takács and G. M. T. Watts, *Excited state gfunctions from the truncated conformal space*, JHEP 2012, 82 (2012).

[52] G. Feverati, K. Graham, P. A. Pearce, G. Zs. Toth, and G. Watts, *A Renormalisation group for TCSA*, J. Stat. Mech. (2008) P03011; arXiv:hep-th/0612203.

[53] G. Watts, *On the renormalisation group for the boundary Truncated Conformal Space Approach*, Nucl. Phys. **B859** (2012) 177-206; arXiv:1104.0225.

[54] G. Watts, *unpublished*.

[55] P. Giokas and G. Watts, *The renormalisation group for the truncated conformal space approach on the cylinder*, (2011) arXiv:1106.2448.

[56] T. R. Klassen and E. Melzer, *Spectral flow between conformal field theories in (1+1) dimensions*, Nucl.Phys. B370 (1992) 511550.

[57] G. Feverati, F. Ravanini, and G. Takacs, *Truncated conformal space at $c = 1$, nonlinear integral equation and quantization rules for multi-soliton states*, Phys.Lett. B430 (1998) 264273.

[58] M. Hogervorst, S. Rychkov, and B. C. van Rees, *A Cheap Alternative to the Lattice?*, Phys. Rev. **D91** (2015) 025005; arXiv:1409.1581.

[59] S. Rychkov, L. G. Vitale, *Hamiltonian Truncation Study of the Φ^4 Theory in Two Dimensions*, Phys. Rev. **D 91** (2015) 085011; arXiv:1412.3460.

[60] J. Elias-Miro, S. Rychkov, L. G. Vitale, *NLO Renormalization in the Hamiltonian Truncation*, Phys. Rev. **D96** (2017) 065024; arXiv:1706.09929.

[61] A. J. A. James, R. M. Konik, P. Lecheminant, N. J. Robinson, and A. M. Tsvelik, *Non-perturbative methodologies for low-dimensional strongly-correlated systems: From non-abelian bosonization to truncated spectrum methods*, Rep. Prog. Phys. **81** (2018) 046002; arXiv:1703.08421.

[62] S. Ghoshal and A. Zamolodchikov, *Boundary S-Matrix and Boundary State in Two-Dimensional Integrable Quantum Field Theory*, Int. J. Mod. Phys. **A9** (1994) 3841-3886; Erratum-ibid. **A9** (1994) 4353; arXiv:hep-th/9306002.

[63] R. Chatterjee and A. Zamolodchikov, *Local Magnetization in Critical Ising Model with Boundary Magnetic Field*, Mod. Phys. Lett. **A9** (1994) 2227; arXiv:hep-th/9311165.

[64] R. Chatterjee, Exact Partition Function and Boundary State of Critical Ising Model with Boundary Magnetic Field, Mod. Phys. Lett. **A10** (1995) 973; arXiv:hep-th/9412169.

[65] A. Konechny, *Ising model with a boundary magnetic field - an example of a boundary flow*, JHEP **0412** (2004) 058; arXiv:hep-th/0410210.

[66] G. Z. Toth, *A study of truncation effects in boundary flows of the Ising model on a strip*, J. Stat. Mech. 0704 (2007) P04005; arXiv:hep-th/0612256.

[67] G. Z. Toth, *Investigations in Two-Dimensional Quantum Field Theory by the Bootstrap and TCSA Methods*, PhD Thesis, Eötvös University, Budapest, (2006). arXiv:0707.0015.

[68] A. Konechny, *Critical Ising Model with Boundary Magnetic Field: RG Interface and Effective Hamiltonians*, JHEP **04** (2019) 001; arXiv:1811.07599.

[69] I. Runkel, *Boundary structure constants for the A-series Virasoro minimal models*, Nucl.Phys. **B549** (1999) 563; arXiv:hep-th/9811178.

[70] A. Capelli, C. Itzykson, J.-B. Zuber, *Modular invariant partition functions in two dimensions* Nucl. Phys. B280 (1987) 445465.

[71] I. Affleck, *Edge Critical Behaviour of the 2-Dimensional Tri-critical Ising Model*, J. Phys. **A33** (2000) 6473; arXiv:cond-mat/0005286.

[72] K. Graham and G. M. T. Watts, *Defect Lines and Boundary Flows*, JHEP **04** (2004) 019; arXiv:hep-th/0306167.

[73] G. Feverati, E. Quattrini, and F. Ravanini, *Infrared Behaviour of Massless Integrable Flows entering the Minimal Models from* ϕ_{31} , Phys. Lett. **B374** (1996) 64; arXiv:hep-th/9512104.

[74] I. Affleck and A.W.W. Ludwig, *Universal non integer 'ground state degeneracy' in critical quantum systems*, Phys. Rev. Lett **67** (1991) 161.

[75] D. Friedan and A. Konechny, *Boundary entropy of one-dimensional quantum systems at low temperature*, Phys. Rev. Lett. **93** (2004) 030402; arXiv:hep-th/0312197.

[76] F.A. Smirnov, A.B. Zamolodchikov, *On space of integrable quantum field theories*, Nucl. Phys. **B915** (2017) pp. 363-383; arXiv:1608.05499.

[77] A. Cavaglià, S. Negro, I. M. Szécsényi, and R. Tateo, $T\bar{T}$*-deformed 2D Quantum Field Theories*, JHEP **10** (2016) 112; arXiv:1608.05534.

Appendix A

Dimensions of the Truncated Space

A.1 The Ising model

Tables A.1 and A.2 contain the dimensions of the truncated physical space depending on $\Delta_{\max}$ for the fixed spectator and the free spectator respectively.

$\Delta_{\max}$	17	19	21	24	26	29	32	34	36	40
dimension of truncated space	207	307	447	762	1069	1739	2765	3725	4978	8697

Table A.1: Dimensions of truncated spaces of Ramond fermions.

$\Delta_{\max}$	19.5	20	24.5	25	29.5	30	34.5	35	37.5	38
dimension of truncated space with even number of oscillators	214	260	534	632	1217	1426	2611	3019	4020	4629
dimension of truncated space with odd number of oscillators	236	236	581	581	1317	1317	2809	2809	4315	4315
total dimension of truncated space	450	496	1115	1213	2534	2743	5420	5828	8335	8944

Table A.2: Dimensions of truncated spaces of NS fermions.

A.2 The tricritical Ising model

Table A.3 contains the dimensions of truncated physical space depending on $\Delta_{\max}$ for the (d) spectator in TIM.

$\Delta_{\max}$	16	17	18	19	20
dimension of truncated space	848	1082	1373	1731	2170

Table A.3: Dimensions of truncated spaces in the tricritical Ising model with (d) spectator.

Appendix B

Useful Technical Details: the Tricritical Ising Model

B.1 Fusion rules

The non-trivial fusion rules for the tricritical Ising model are as follows:

$$
\begin{aligned}
&\epsilon \times \epsilon = \mathbb{I} + \epsilon' \\
&\epsilon \times \epsilon' = \epsilon + \epsilon'' \\
&\epsilon \times \epsilon'' = \epsilon' \\
&\epsilon \times \sigma = \sigma + \sigma' \\
&\epsilon \times \sigma' = \sigma \\
&\\
&\epsilon' \times \epsilon' = \mathbb{I} + \epsilon' \\
&\epsilon' \times \epsilon'' = \epsilon \\
&\epsilon' \times \sigma = \sigma + \sigma' \\
&\epsilon' \times \sigma' = \sigma \\
&\\
&\epsilon'' \times \sigma = \sigma \\
&\epsilon'' \times \sigma' = \sigma' \\
&\epsilon'' \times \epsilon'' = \mathbb{I} \\
&\\
&\sigma \times \sigma = \mathbb{I} + \epsilon + \epsilon' + \epsilon'' \\
&\sigma \times \sigma' = \epsilon + \epsilon' \\
&\\
&\sigma' \times \sigma' = \mathbb{I} + \epsilon''
\end{aligned}
\tag{B.1}
$$

B.2 Results: normalised structure constants

Definition:

$$\begin{aligned}\tilde{C}_{ijk}^{(abc)} &= \frac{< \psi_i^{(ab)}(x)\psi_j^{(bc)}(y)\psi_k^{(ca)}(z) >}{||\psi_i^{(ab)}||\ ||\psi_k^{(ca)}||\sqrt{C_{jj}^{(bcb)1}}} \\ &= C_{ij}^{(abc)k}\left(\frac{C_{kk}^{(aca)1}}{C_{ii}^{(aba)1}C_{jj}^{(bcb)1}}\right)^{1/2}.\end{aligned} \tag{B.2}$$

As an example calculation, we show:

$$\begin{aligned}\tilde{C}_{\sigma\epsilon'\sigma}^{(\sigma\epsilon'\sigma)} &= \frac{< \psi_\sigma^{(\sigma\epsilon')}\psi_{\epsilon'}^{(\epsilon'\epsilon')}\psi_\sigma^{(\epsilon'\sigma)} >}{||\psi_\sigma^{(\sigma\epsilon')}||\ ||\psi_\sigma^{(\epsilon'\sigma)}||\sqrt{C_{\epsilon'\epsilon'}^{(\epsilon'\epsilon'\epsilon')1}}} \\ &= C_{\sigma\epsilon'}^{(\sigma\epsilon'\epsilon')\sigma}\left(\frac{1}{C_{\epsilon'\epsilon'}^{(\epsilon'\epsilon'\epsilon')1}}\right)^{1/2} \\ &= \frac{1}{4}(1-\sqrt{5})\left(\frac{2\pi\Gamma(4/5)}{3\Gamma^3(3/5)\sin(2\pi/5)}\right)^{1/2}.\end{aligned} \tag{B.3}$$

We now quote the results of the structure constants for the tricritical Ising Model.

σ spectator

$$\begin{aligned}&\bullet\ \tilde{C}_{\sigma\epsilon'\sigma}^{(\sigma\epsilon'\epsilon')} = \frac{1}{4}(1-\sqrt{5})\left(\frac{2\pi\Gamma(4/5)}{3\Gamma^3(3/5)\sin(2\pi/5)}\right)^{1/2}. \\ &\bullet\ \tilde{C}_{\sigma'\epsilon'\sigma'}^{(\sigma\epsilon'\epsilon')} = 0. \\ &\bullet\ \tilde{C}_{\sigma\epsilon'\sigma'}^{(\sigma\epsilon'\epsilon')} = \frac{\sqrt{3}}{2}. \\ &\bullet\ \tilde{C}_{\sigma'\epsilon'\sigma}^{(\sigma\epsilon'\epsilon')} = \frac{\sqrt{3}}{2}.\end{aligned} \tag{B.4}$$

σ' spectator

$$\bullet\ \tilde{C}^{(\sigma'\epsilon'\epsilon')}_{\sigma\epsilon'\sigma} = \frac{1}{2}\left(\frac{2\pi\Gamma(4/5)}{3\Gamma^3(3/5)\sin(2\pi/5)}\right)^{1/2}. \tag{B.5}$$

$\mathbb{I}$ spectator

$$\bullet\ \tilde{C}^{(\mathbb{I}\epsilon'\epsilon')}_{\epsilon'\epsilon'\epsilon'} = \left(\frac{2\pi\Gamma(4/5)}{3\Gamma^3(3/5)\sin(2\pi/5)}\right)^{1/2}. \tag{B.6}$$

ϵ spectator

$$\begin{aligned}
&\bullet\ \tilde{C}^{(\epsilon\epsilon'\epsilon')}_{\epsilon\epsilon'\epsilon} = \frac{1}{2}(-1+\sqrt{5})\left(\frac{2\pi\Gamma(4/5)}{3\Gamma^3(3/5)\sin(2\pi/5)}\right)^{1/2}.\\
&\bullet\ \tilde{C}^{(\epsilon\epsilon'\epsilon')}_{\epsilon''\epsilon'\epsilon''} = 0.\\
&\bullet\ \tilde{C}^{(\epsilon\epsilon'\epsilon')}_{\epsilon\epsilon'\epsilon''} = -\left(\frac{3}{7}\right)^{1/2}.\\
&\bullet\ \tilde{C}^{(\epsilon\epsilon'\epsilon')}_{\epsilon''\epsilon'\epsilon} = -\left(\frac{3}{7}\right)^{1/2}.
\end{aligned} \tag{B.7}$$

ϵ' spectator

$$\begin{aligned}
&\bullet\ \tilde{C}^{(\epsilon'\epsilon'\epsilon')}_{\mathbb{I}\epsilon'\mathbb{I}} = 0.\\
&\bullet\ \tilde{C}^{(\epsilon'\epsilon'\epsilon')}_{\epsilon'\epsilon'\epsilon'} = \frac{1}{2}(1-\sqrt{5})\left(\frac{2\pi\Gamma(4/5)}{3\Gamma^3(3/5)\sin(2\pi/5)}\right)^{1/2}.\\
&\bullet\ \tilde{C}^{(\epsilon'\epsilon'\epsilon')}_{\mathbb{I}\epsilon'\epsilon'} = 1.\\
&\bullet\ \tilde{C}^{(\epsilon'\epsilon'\epsilon')}_{\epsilon'\epsilon'\mathbb{I}} = 1.
\end{aligned} \tag{B.8}$$

ϵ'' spectator

$$\bullet\ \tilde{C}^{(\epsilon''\epsilon'\epsilon')}_{\epsilon\epsilon'\epsilon} = -\left(\frac{2\pi\Gamma(4/5)}{3\Gamma^3(3/5)\sin(2\pi/5)}\right)^{1/2}. \tag{B.9}$$

Appendix C

TCSA Runtimes

The following tables contain information on the runtime of the TCSA algorithm for both the free fermion description of the Ising model with fixed spectator and the Virasoro description of the tricritical Ising model with (d) spectator. Runtimes are displayed for a number of different Δ_{max}.

All times were recorded on a HP Pavilion TS 15 Notebook PC with Intel(R) Core(TM) i5-4200U CPU @ 1.60GHz 2.30GHz processor, 8 GB RAM (7.78 useable) and 676 GB of storage.

Table C.1 contains the runtime in seconds for the constituent parts of the TCSA algorithim in the free fermion basis of the Ising model with fixed spectator.

Δ_{max}	21	26	36
Basis Construction	1.56	8.82	248.51
Construction of Hamiltonian Matrix	2.11	11.18	270.45
Calculation of spectrum (100 points)	12.17	87.36	3079.94

Table C.1: Runtime in seconds for TCSA algorithm in the Ising model with fixed spectator in the free fermion basis.

Table C.2 contains the runtime in seconds for the constituent parts of the TCSA algorithim in the Virasoro basis of the tricritical Ising model with (d) spectator.

Δ_{max}	14	17	20
Basis Construction	28.03	240.92	2053
Calculation of OPE coefficients	55.3	498.14	4672.69
Construction of Hamiltonian Matrices	28.19	215.61	1596.89
Calculation of spectrum (100 points)	23.48	115.61	737.38

Table C.2: Runtime in seconds for TCSA algorithm in the tricritical Ising model with (d) spectator in the Virasoro basis.